

## STATUS OF THESIS

Title of thesis

STRESS ANALYSIS USING FINITE ELEMENT METHOD ON  
SIALON/AISI 430 FERRITIC STAINLESS STEEL JOINT

I CIK SUHANA BINTI HASSAN

hereby allow my thesis to be placed at the Information Resource Center (IRC) of  
Universiti Teknologi PETRONAS (UTP) with the following conditions:

1. The thesis becomes the property of UTP
2. The IRC of UTP may make copies of the thesis for academic purposes only.
3. This thesis is classified as

Confidential

Non-confidential

If this thesis is confidential, please state the reason:

---

---

The contents of the thesis will remain confidential for \_\_\_\_\_ years.

Remarks on disclosure:

---

---

Endorsed by

---

Signature of Author

---

Signature of Supervisor

Permanent address:

Name of Supervisor

NO.42, FELDA SELANCAR 03  
26700 MUADZAM SHAH,  
PAHANG DARUL MAKMUR.

ASSOC. PROF. DR. PATTHI HUSSAIN

Date: \_\_\_\_\_

Date: \_\_\_\_\_

UNIVERSITI TEKNOLOGI PETRONAS

STRESS ANALYSIS USING FINITE ELEMENT METHOD ON SIALON/AISI  
430 FERRITIC STAINLESS STEEL JOINT

by

CIK SUHANA BINTI HASSAN

The undersigned certify that they have read, and recommend to the Postgraduate Studies Programme for acceptance this thesis for the fulfilment of the requirements for the degree stated.

Signature: \_\_\_\_\_

Main Supervisor: ASSOC. PROF. DR. PATTHI HUSSAIN

Signature: \_\_\_\_\_

Co-Supervisor: DR. MOKHTAR AWANG

Signature: \_\_\_\_\_

Head of Department: ASSOC. PROF. DR. AHMAD MAJDI ABDUL RANI

Date: \_\_\_\_\_

STRESS ANALYSIS USING FINITE ELEMENT METHOD ON SIALON/AISI  
430 FERRITIC STAINLESS STEEL JOINT

by

CIK SUHANA BINTI HASSAN

A Thesis

Submitted to the Postgraduate Studies Programme

as a Requirement for the Degree of

MASTER OF SCIENCE

MECHANICAL ENGINEERING DEPARTMENT

UNIVERSITI TEKNOLOGI PETRONAS

BANDAR SERI ISKANDAR,

PERAK

JANUARY 2011

DECLARATION OF THESIS

Title of thesis

STRESS ANALYSIS USING FINITE ELEMENT METHOD ON  
SIALON/AISI 430 FERRITIC STAINLESS STEEL JOINT

I CIK SUHANA BINTI HASSAN

hereby declare that the thesis is based on my original work except for quotations and citations which have been duly acknowledged. I also declare that it has not been previously or concurrently submitted for any other degree at UTP or other institutions.

Witnessed by

\_\_\_\_\_  
Signature of Author

\_\_\_\_\_  
Signature of Supervisor

Permanent address:

Name of Supervisor

NO.42, FELDA SELANCAR 03  
26700 MUADZAM SHAH,  
PAHANG DARUL MAKMUR.

ASSOC. PROF. DR. PATTHI HUSSAIN

Date: \_\_\_\_\_

Date: \_\_\_\_\_

*Dedicated to my beloved husband, parent, family and friends.*

*I love you all!*

## ACKNOWLEDGEMENT

Alhamdulillah praises to The Almighty Allah for blessing me with the strength and health towards completing this project. It is a pleasure to thank the many people who made this thesis possible.

First and foremost, I would like to express my deepest appreciation to my supervisor, Assoc. Prof. Dr. Patthi Bin Hussain whom had contributed and extended his assistance throughout the completion of this project. This thesis would not have been possible without his guidance.

My heartfelt gratitude also goes out to my co-supervisor, Dr. Mokhtar Bin Awang. His knowledge, enthusiastic support, suggestions and constructive criticisms helped me greatly in understanding the project.

I gratefully acknowledge Universiti Teknologi PETRONAS (UTP) for providing facilities which enables the completion of the analytical work for this project.

Special thanks to Mr. Hudiyo Firmanto for providing guidance and sharing his knowledge. I am extremely grateful for the greatest support in brainstorming and for the great help in difficult times.

My keen appreciation also goes to postgraduate office staffs whom deeply involved in providing guidelines and scheduling in order to make this project successful.

I would like to express my heartiest thanks to all my friends whom immensely helped me by giving me encouragement and friendship. The love, support and precious time together has made this journey more meaningful.

My utmost appreciation goes to my family for the continuous love and advices. I am forever indebted to the overflowing love.

Thank you to my wonderful husband, Adi Akmal Nasrul Hisham, for his patience, support, love and encouragement.

Last but not least, many thanks to all who had involved either directly or indirectly in completing this project.

## ABSTRACT

Ceramic has many good characteristics for high temperature applications such as in heat exchangers. In the actual application of the ceramic to the structures, a ceramic-to-metal joint is unavoidable. This makes joining of ceramic to metal a critically important technology in advanced engineering. However, the fundamental problem in joining of metals and ceramics is the development of residual stresses which originated from the property mismatch between the ceramic and metal.

A finite element analysis (FEA) using ANSYS was used to evaluate the residual stresses in the joints. In this analysis, stress analyses were conducted on sialon/AISI 430 joint. The joint was assumed to be perfectly bonded at the interface at 1200°C and stresses developed during cooling down to room temperature. Sequential coupled-field analysis was performed with PLANE55 and PLANE42. Model was simplified to two dimensional (2-D) problems, since its rotation about the axis of symmetry will generate the complete volume of the cylinder.

It was found that the maximum tensile stress occur at the edge of sialon, close to the joint interface. The influence of thickness of sialon, diameter and joint design on the generation of stress in sialon was analyzed. Analyses were made to study the effect of each parameter on stress by varying it, for example, thickness of sialon, while fixing the other parameters. It was found that increasing thickness of sialon and diameter of the joint has resulted in increasing magnitude of tensile stress. The stresses can be reduced by employing symmetrical design joint and incorporating interlayer. The verification of the model was carried out by analytical calculation and comparison with literature review. The results of simulated stresses are in good agreement with the analytical method and literature review.



## ABSTRAK

Seramik dilengkapi dengan pelbagai ciri-ciri yang bersesuaian untuk aplikasi yang memerlukan suhu yang tinggi. Penggunaan seramik dalam aplikasi industri sering melibatkan seramik dihubungkan dengan keluli. Ini menyebabkan sambungan seramik dan keluli sangat penting. Namun, masalah yang sering timbul dalam menghubungkan seramik dan keluli ialah penghasilan tegangan sisa (residual stress) yang terjadi akibat daripada perbezaan dalam sifat kedua-dua bahan tersebut.

Kajian ke atas tegangan sisa di dalam sambungan seramik dan keluli telah dijalankan menggunakan ANSYS. Dalam analisis ini, sialon seramik telah dihubungkan dengan keluli tahan karat gred AISI 430. Sambungan tersebut dijangka telah berhubung dengan sempurna pada suhu 1200°C dan tegangan sisa hanya terhasil sewaktu sambungan tersebut disejukkan ke suhu bilik. Analisis dijalankan dalam dua langkah, menggunakan PLANE55 dan PLANE42. Model sambungan tersebut diringkaskan menjadi dua-dimensi (2-D) kerana putaran pada paksi simetri akan menghasilkan satu silinder.

Maksima magnitud tegangan sisa telah dijumpai di permukaan sialon, berdekatan dengan ruang perhubungan (interface) seramik dan keluli. Pengaruh ketebalan sialon, diameter dan desain sambungan ke atas magnitud tegangan sisa dikaji. Analisis dijalankan dengan mempelbagaikan faktor yang ingin dikaji dan menetapkan faktor-faktor lain. Kajian mendapati penambahan ketebalan sialon dan diameter akan menyebabkan magnitud tegangan sisa yang terhasil lebih tinggi. Magnitud tegangan sisa tersebut boleh dikurangkan dengan menggunakan desain simetri dan meletakkan lapisan (bahan lain) di antara seramik dan keluli yang dihubungkan. Hasil analisis dibandingkan dengan hasil yang diperolehi daripada pengiraan dan tinjauan literatur. Keputusan analisis menunjukkan hasil yang diperolehi menggunakan ANSYS adalah selari dengan keputusan pengiraan dan tinjauan literatur.

In compliance with the terms of the Copyright Act 1987 and the IP Policy of the university, the copyright of this thesis has been reassigned by the author to the legal entity of the university,

Institute of Technology PETRONAS Sdn Bhd.

Due acknowledgement shall always be made of the use of any material contained in, or derived from, this thesis.

© Cik Suhana Binti Hassan, 2011  
Institute of Technology PETRONAS Sdn Bhd  
All rights reserved.

## TABLE OF CONTENTS

STATUS OF THESIS .....	i
APPROVAL PAGE .....	ii
TITLE PAGE .....	iii
DECLARATION OF THESIS .....	iv
DEDICATION .....	v
ACKNOWLEDGEMENT .....	vi
ABSTRACT.....	viii
ABSTRAK .....	ix
COPYRIGHT PAGE .....	x
TABLE OF CONTENTS.....	xi
LIST OF TABLES .....	xv
LIST OF FIGURES .....	xvi
CHAPTER 1 INTRODUCTION .....	1
1.1 Chapter Overview .....	1
1.2 Background of Study.....	1
1.3 Problem Statement .....	4
1.4 Research Objectives.....	5
1.5 Scope of Work.....	6

1.6	Organization of the Thesis .....	6
1.7	Chapter Summary.....	7
CHAPTER 2 THEORY AND LITERATURE REVIEW .....		9
2.1	Chapter Overview .....	9
2.2	Ceramic .....	10
2.2.1	Sialon.....	11
2.3	Stainless Steel.....	12
2.3.1	Ferritic Stainless Steel .....	13
2.4	Benefits of Ceramic/Metal Joint .....	14
2.5	Development of Ceramic/Metal Joining .....	15
2.5.1	Indirect Joining of Ceramic and Metal: Brazing.....	16
2.5.2	Direct Joining of Ceramic and Metal: Diffusion Bonding.....	19
2.6	Ceramic/Metal Joining Problems .....	21
2.6.1	Residual Stress in Ceramic/Metal Joint .....	22
2.6.1.1	Methods of Reducing the Residual Stress .....	26
2.6.1.2	Evaluation of the Residual Stress.....	32
2.7	Finite Element Method (FEM).....	35
2.7.1	Review on Past Research Works of FEM in Ceramic/Metal Joint..	40
2.8	Chapter Summary.....	44
CHAPTER 3 MATERIALS AND METHODOLOGY.....		47
3.1	Chapter Overview .....	47

3.2	Research Procedure .....	47
3.3	Materials.....	48
3.3.1	Sialon .....	48
3.3.2	Ferritic Stainless Steel.....	50
3.4	Finite Element Modelling.....	51
3.4.1	Assumptions.....	51
3.4.2	Geometry of the sialon/AISI 430 ferritic stainless steel joint.....	52
3.4.3	Selection of element type.....	53
3.4.4	Meshing of the model .....	55
3.4.5	Modelling the sialon/AISI 430 ferritic stainless steel joint .....	55
3.4.6	Modelling the effect of geometrical parameters .....	56
3.5	Verification of the FEM analysis on the residual stress generated in the sialon/AISI 430 ferritic stainless steel joint.....	60
3.5.1	Verification by using stress equation.....	60
3.5.2	Verification by using literature review .....	60
3.5.3	Error analysis .....	63
3.6	Chapter Summary.....	64
CHAPTER 4 RESULT AND DISCUSSION .....		65
4.1	Chapter Overview .....	65
4.2	Preliminary analysis .....	66
4.2.1	FEM vs stress equation .....	66

4.2.1.1	Result obtained by using FEM.....	66
4.2.1.2	Result obtained by using stress equation .....	68
4.2.1.3	Comparison between FEM and stress equation .....	69
4.1.2	Past model vs present model.....	70
4.3	Elasto-Plastic Analysis .....	73
4.3.1	Magnitude and Distribution of Residual Stress .....	73
4.4	Effect of Geometrical Parameters .....	80
4.4.1	Effect of Thickness of Sialon.....	81
4.4.2	Effect of Joint Diameter .....	83
4.4.3	Effect of Joint Design .....	84
4.4.4	Effect of Interlayer .....	88
4.5	Chapter Summary.....	90
CHAPTER 5 CONCLUSION AND RECOMMENDATIONS .....		91
5.1	Chapter Overview .....	91
5.1	Conclusion.....	91
5.2	Recommendations .....	92
5.1	Chapter Summary.....	93
REFERENCES .....		95
LIST OF PUBLICATIONS .....		105

## LIST OF TABLES

Table 2-1 Summary of interlayers for reducing thermal expansion mismatch in ceramic/metal joints. ....	30
Table 3-1 Material properties of the ceramic and metal employed. ....	49
Table 3-2 Temperature-dependent coefficient of thermal expansion of sialon and AISI 430 ferritic stainless steel. ....	49
Table 3-3 Chemical composition of the sialon and AISI 430 ferritic stainless steel. ....	50
Table 3-4 Material properties of the interlayer materials employed in the analysis..	59
Table 3-5 Material properties of the components used in the comparison of present FEM with Travessa et al.'s work .....	61
Table 3-5 Material properties of the components used in the comparison of present FEM with Zhang et al.'s work .....	62
Table 4-1 Comparison of FEM and analytical results. ....	69

## LIST OF FIGURES

Figure 1-1 Example of ceramic turbocharger rotors, one illustrating attachment to a metal shaft.....	2
Figure 1-2 Design of bonding between ceramic rotor and metal shaft.....	3
Figure 1-3 Schematics of factors affecting the reliability of ceramic-metal joint. ....	3
Figure 2-1 Ceramic metal joining process.....	16
Figure 2-2 Typical fracture mechanism of a ceramic/metal assembly. . . . .	23
Figure 2-3 Example of typical fracture occur in ceramic/metal joint. . . . .	23
Figure 2-4 Properties of ceramics and metals. . . . .	24
Figure 2-5 Schematic of residual stresses developed during joining process. . . . .	25
Figure 2-6 Contour map of maximum principal stress calculated by FEM.....	26
Figure 2-7 Thickness dependence on the maximum tensile stress in the silicon nitride/steel joint. . . . .	27
Figure 2-8 Effect of joint shape on the stress level of ceramic/metal joint . . . . .	28
Figure 2-9 Effect of diameter on the magnitude of tensile stress in ceramic/metal joint. . . . .	28
Figure 2-10 Schematic of the layered structure . . . . .	33
Figure 2-11 Axisymmetric formulation of a three-dimensional problem . . . . .	37
Figure 3-1 Schematic representation of the sialon/AISI 430 ferritic stainless steel	



joint. . . . .	52
Figure 3-2 Schematic representation of the model geometry resulted from the geometric simplification, showing the dimensions used in the analysis. . . . .	53
Figure 3-3 PLANE55 geometry . . . . .	54
Figure 3-4 PLANE42 geometry . . . . .	54
Figure 3-5 Details on meshing and constrains employed . . . . .	55
Figure 3-6 Schematic representation of boundary conditions . . . . .	57
Figure 3-7 Schematic representation of symmetrical joint . . . . .	58
Figure 3-8 Schematic representation of the sialon/AISI 430 ferritic stainless steel joint with interlayer. . . . .	59
Figure 3-9 Schematic representation of the Al <sub>2</sub> O <sub>3</sub> /AISI 304 steel joint with Ti interlayer. . . . .	61
Figure 3-10 Schematic representation of the Al <sub>2</sub> O <sub>3</sub> /AISI 304 steel joint with Ti interlayer. . . . .	63
Figure 4-1 Radial stress distribution in fully elastic sialon/AISI 430 ferritic stainless steel joint. . . . .	67
Figure 4-2 Axial residual stress distribution (in MPa) across Al <sub>2</sub> O <sub>3</sub> /AISI 304 steel joint with Ti interlayer. . . . .	71
Figure 4-3 Present result of axial residual stress distribution in Al <sub>2</sub> O <sub>3</sub> /AISI 304 steel joint with Ti interlayer. . . . .	71
Figure 4-4 Axial residual stress distribution (in MPa) across Al <sub>2</sub> O <sub>3</sub> /AISI 304 steel	

joint with Ni interlayer. . . . .	72
Figure 4-5 Plane state of stress . . . . .	73
Figure 4-6 Temperature profile of the cooling process. . . . .	74
Figure 4-7 Von Mises stress distribution across the sialon/AISI 430 ferritic stainless steel joint. . . . .	75
Figure 4-8 Radial stresses distribution across the sialon/AISI 430 ferritic stainless steel joint. . . . .	76
Figure 4-9 Axial stresses distribution across the sialon/AISI 430 ferritic stainless steel joint. . . . .	77
Figure 4-10 Close up view of axial stress distribution, showing the location of maximum tensile stress. . . . .	77
Figure 4-11 Shear stress distribution across the sialon/AISI 430 ferritic stainless steel joint. . . . .	78
Figure 4-12 Close up view of shear stress distribution. . . . .	79
Figure 4-13 Principal stress distribution across the sialon/AISI 430 ferritic stainless steel joint. . . . .	80
Figure 4-14 Effect of increasing the thickness of sialon on the axial stress level of the ceramic . . . . .	82
Figure 4-15 Effect of diameter on the stress level in the ceramic. . . . .	83
Figure 4-16 Effect of joint design on the magnitude of maximum tensile stress developed in the sialon/AISI 430 ferritic stainless steel joint. . . . .	84

Figure 4-17 Radial stress distribution in symmetrical joint . . . . .	86
Figure 4-18 Axial stress distribution in symmetrical joint. . . . .	87
Figure 4-19 Shear stress distribution in symmetrical joint. . . . .	87
Figure 4-20 Effect of interlayer and their thickness on the maximum tensile stress developed during cooling of the sialon/AISI 430 ferritic stainless steel joint . . . . .	89



# CHAPTER 1

## INTRODUCTION

### **1.1 Chapter Overview**

This chapter perform as an introduction to the research work. The chapter entails the background of the study, problem statement, objectives of this research work, the scope of work and thesis organization.

### **1.2 Background of study**

Ceramics have many good properties such as high temperature strength, hardness, lightness, low expansion etc. Due to their superior properties, they have been the material of choice in an increasing number of applications. The applications of ceramics are diverse from brick and tiles to electronic and magnetic compounds [1]. For example, ceramics have been employed in many mechanical applications such as cutting tools, nozzles, valves and ball bearings due to their hardness, wear and corrosion resistance [2].

Although ceramics are well known for their superior properties, they have a major defect of being brittle [3]. The brittleness prevents their introduction as monolithic parts in structural applications, since they are difficult to machine and fabricate into complex shapes on a large scale. In some applications, however, the desirable properties of ceramics are needed not for an entire structure but only in one portion of a structure [4]. Thus, in their applications, ceramics are often required to be joined with another material, most commonly metal. An example of application which utilize ceramic/metal joint is the turbocharger. As can be seen from Figure 1-1, in ceramic turbocharger rotors, each ceramic rotor requires attachment to a metal shaft, as illustrated by one of the rotors [5].

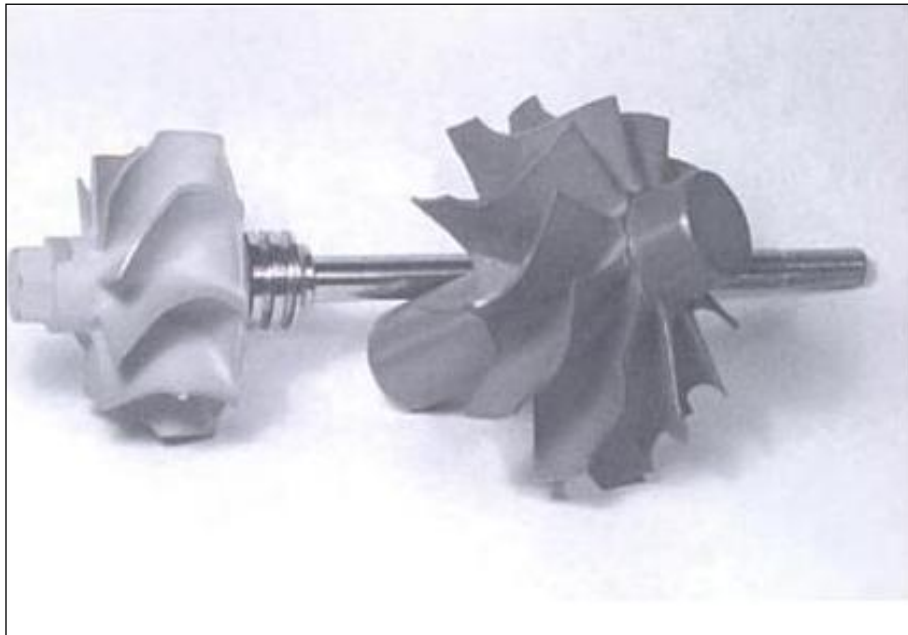


Figure 1-1 Example of ceramic turbocharger rotors, one illustrating attachment to a metal shaft. (Photo by D.W. Richerson) [1].

The automotive industry has profited from the developments in ceramics, fabricating turbochargers and other engine components for service temperatures in excess of  $1000^{\circ}\text{C}$  [6],[7]. Nissan, in its effort to overcome the problem of turbo lag, has been using ceramic to reduce the moment of inertia of the turbocharger rotor [8]. As can be seen in Figure 1-2, silicon nitride was chosen as the rotor material because of its strength, fracture toughness, thermal shock resistance and thermal expansion coefficient [8-10]. The use of the light-weighted silicon nitride reduced rotating inertia by 40% and improved time-to-boost by 30%, delivering 280 hp with nearly instantaneous acceleration [11].

In producing a reliable ceramic metal joint, every factor that affecting the strength of the joint must be studied in details. Figure 1-3 briefly portrayed several factors influencing the reliability of a ceramic-metal joint [12].

Williamson et al. [13] claim that the capability to produce a ceramic-metal joint is determined by two factors which are the chemical factors, comprises of bonding and interface strength, as well as mechanical factors, comprises of stress state and loading. This study has tended to focus on the mechanical factors rather than on the chemical factors. So far, research has been concentrated on the residual stress generated during

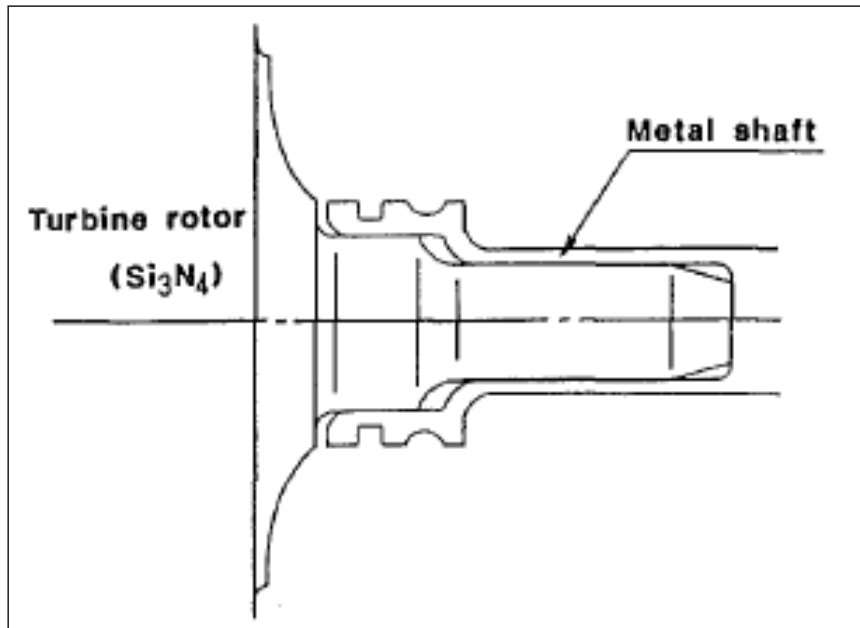


Figure 1-2 Design of bonding between ceramic rotor and metal shaft [6].

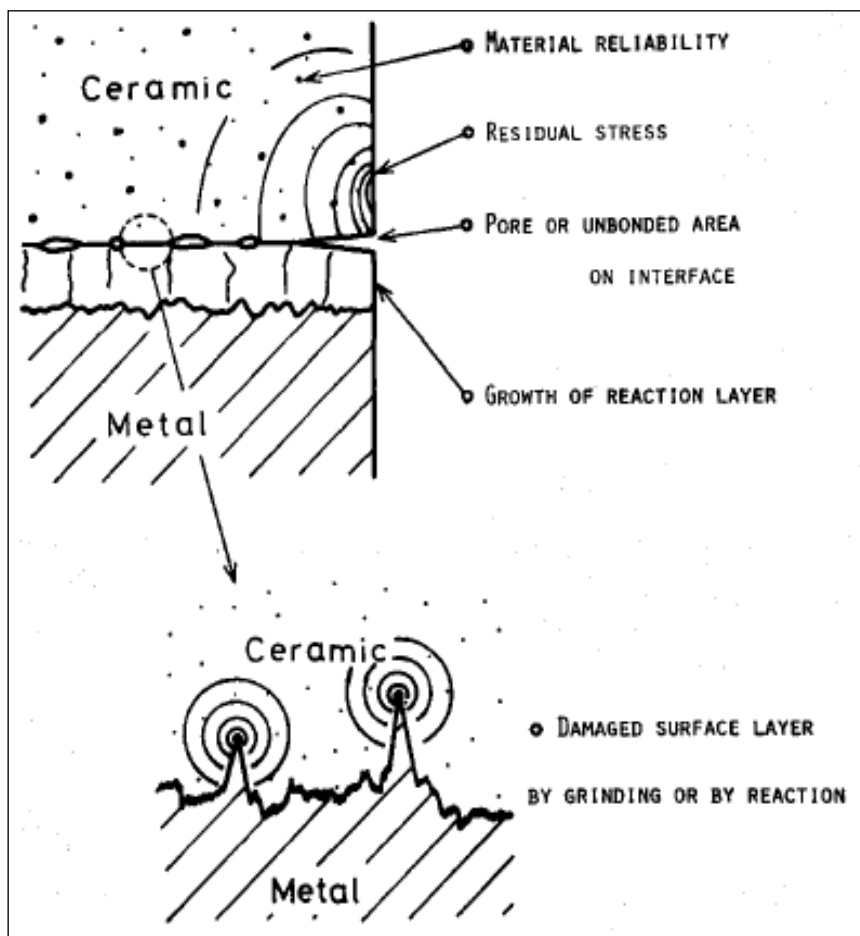


Figure 1-3 Schematics of factors affecting the reliability of ceramic-metal joint [12].

cooling from the extreme fabrication temperature. Obtaining successful ceramic/metal joints are difficult due to the rise of residual stresses in the joint which are due to the mismatches in the coefficient of thermal expansion and elastic modulus of the base materials. Developments of these residual stresses are induced upon cooling down of the joint from the fabrication temperature to room temperature.

In present work, finite element analysis using ANSYS has been used to evaluate the residual stresses in the ceramic-metal joint. However, the investigations have been confined on the residual stresses developed in the sialon-AISI 430 ferritic stainless steel joint. The aim of the present work is to numerically evaluate the magnitude and distribution of residual stresses in sialon-AISI 430 ferritic stainless steel joint by means of finite element method (FEM).

Sialon was chosen as they present excellent mechanical properties at high temperature. However, they cannot in general be used alone due to their brittleness. On the other hand, stainless steel is tough but cannot withstand high temperature and only operates at low temperature. Therefore, it is preferable to join them in order to utilize the strength of both materials.

Maximum tensile stress is expected at the edge of ceramic close to the interface [14] since most commonly ceramic/metal joint fracture initiated on the ceramic surface. FEM results were then compared to the calculation and experimental work and shows good correlation. Results obtained from this analysis can be used as a guideline in the ceramic/metal joint fabrication.

### **1.3 Problem Statement**

The advancement of engineering application sometimes requires components to be constructed from more than one type of material. Joining dissimilar materials has thus become a vital field in research and development. However, joining of any two dissimilar materials may result in thermal residual stresses which can arise due to the change in temperature [15]. The development of the thermal residual stresses in the ceramic/metal joint is due to the large differences in the properties of both material such as coefficient of thermal expansion and Young's modulus. Metal with higher



thermal expansion coefficient than ceramic will contract more during cooling of the joint thus inducing the development of thermal residual stress.

The stresses that constructed during cooling down from fabrication temperature to room temperature will give a strong influence on the strength of the joint. Upon cooling from the relatively high joining temperatures which is the characteristics of usual joining processes, the interface restricts the contraction of the material, concentrating local stresses [16],[17]. Such stresses can cause plastic deformation and cracking and thereby affect the mechanical integrity of the bonded materials [18].

In general, these stresses may deteriorate the strength and operational characteristics of the ceramic/metal joint. In some cases, these stresses exceed the bond strength and causes failure along the interface of the joint. In cases when the bond is strong enough, the fracture will occur in the ceramic. This failure can occur due to the development of tensile stress in the ceramic since ceramic can bear with compressive stress but tend to fracture under the influence of tensile stress.

It is therefore essential to evaluate the magnitude and distribution of residual stresses in the ceramic/metal joint. K. Sukanuma [12], in his review, had stated that it is important to know the actual distribution of the residual stress in a ceramic/metal joint in order to reduce the harmful influence on the mechanical properties especially on strength. Since residual stress strongly affects the mechanical properties of a ceramic/metal joint, it is very essential to ensure its reliability in various applications by quantifying them via experimental and modelling studies.

#### **1.4 Research Objectives**

The main goal of this project is to simulate the residual stresses developed in sialon-AISI 430 ferritic stainless steel joint during cooling down from fabrication temperature to room temperature.

To achieve the main goal, the following objectives need to be attained:

- a) To develop a finite element model of the sialon/AISI 430 ferritic stainless steel joint

- b) To study the effect of thickness, diameter, joint design and interlayer on the magnitude of residual stress developed.

## **1.5 Scope of Work**

The work in this thesis involves computer simulation which focuses on the magnitude and distribution of the thermal residual stresses developed in the sialon-AISI 430 ferritic stainless steel joint.

To investigate the magnitude and distribution of the residual stress in the sialon-AISI 430 ferritic stainless steel joint, FEM using ANSYS was applied in modelling the transient response of the joint. This transient modelling was then followed by simulation of the stresses. The effect of geometrical parameters has also been studied. Preliminary analysis based on calculation and literature review was then performed in order to verify the accuracy of the simulation.

## **1.6 Organization of the Thesis**

The fundamental problem in the ceramic metal joint is the development of residual stresses which originated from the property mismatch between the ceramic and metal. The residual stresses often lead to the fracture of the joint. This thesis purpose is to evaluate the stresses through the use of FEM. The aim of this project is to provide a useful guideline in fabricating ceramic metal joint. The study however only limited to the sialon-AISI 430 ferritic stainless steel joint. This thesis reports on the magnitude and residual stress distribution across the sialon-AISI 430 ferritic stainless steel joint as well as the effect of geometrical parameters on the magnitude of residual stresses developed across the joint. The outline of this thesis is as follow:

Chapter 1 presents a brief introduction to the ceramic metal joining as well as the problems associated with the joining. The objectives and scope of work for the project also discussed. Additionally, this chapter summarizes the objectives and provides a brief overview of this thesis.

In Chapter 2, theory and extensive literature review on the ceramic metal joining was performed. Theoretical background of the materials used in this project and residual stresses discussed here. The governing equations used in the FEM explained in details in this chapter. This chapter also discussed the past work that preceded the development of the ceramic/metal joint, the method used to evaluate the stress in the joint and the achievement so far.

Chapter 3 presents the material properties and methodology or roadmap used in managing this project. Procedures applied in the FEM as well as the assumptions made in the analysis were explained thoroughly in this chapter.

Chapter 4 discussed the results obtained from the analysis. Here, the comparison of the FEM results with calculations and the literature review were reported in details. The geometrical effect i.e., thickness of sialon, diameter of the cylindrical joint, joint design as well as the effect of incorporating interlayer on the residual stresses development also discussed.

Chapter 5 forms the conclusions of this thesis. The discussions on the findings are summarized and five contributions of knowledge engineering for the joint are identified. A few recommendations also presented in this chapter. The recommendations fall into two categories which are continuation of research work via FEM and future research work that can be done through experimental work.

## **1.7 Chapter Summary**

This chapter present the introduction of this project. A brief overview on ceramic/metal joint, their application in industry and factors that influence the joint reliability were served as the background of this study.

The main problem to be tackled was clearly addressed in the problem statement. The criticality of the problem and the need for it to be evaluated also discussed. The chapter then goes on with the presentation of the research objectives, scope of work and thesis organization.

Next chapter will discuss the theory behind the development of the residual stress and the application of FEM to evaluate the problem. Related preceded research works and findings by other authors will also be discussed in the next chapter.

## CHAPTER 2

### THEORY AND LITERATURE REVIEW

It is widely known that there are three basic categories of materials i.e., metals, ceramics and polymers, each carrying different properties. The development of many engineering applications has led to the need of joining dissimilar materials in order to utilize the properties of the constituent materials. Numerous types of applications frequently require ceramics to be joined with metals.

Schwartz has stated that the technology of ceramic to metal joining has progressed steadily since the early 1930s [19]. The evolution of joining process has allowed the joining to be widely used. However, joining the ceramic to metal is not easy to carry out. According to Liu et al. [20], due to differences of thermal and mechanical properties in ceramics and metals, residual stresses develop in regions near the ceramic/metal interfaces during fabrication and under thermal and mechanical loading in service. These stresses affect the performance and the lifetime of the ceramic/metal bonded systems and can cause cracking within ceramic, plastic deformation accompanied by formation and growth of the voids in metal and/or ceramic/metal decohesion [20]. The increasing interest in using ceramic metal joint has heightened the need for evaluating the stresses.

This study focused on the residual stresses developed in the sialon-AISI 430 ferritic stainless steel joint and the effect of the geometrical parameters on the magnitude of the stresses.

#### **2.1 Chapter overview**

This chapter presents the theoretical background and literature review of the research. Readers will be introduced to the materials used in the analysis, the benefits of the ceramic/metal joint, the possible techniques to join the materials and problems

associated with joining. Preceded research works that related to this research also discussed here.

The objective of this chapter is to apply the knowledge presented to help in understanding the problem and effectively simulating the residual stress distribution in the ceramic/metal joint. The discussion in this chapter draws on the lesson learned over the years in the ceramic/metal joint area and introduces the basic knowledge behind the application of the finite element method in analyzing the problem.

## 2.2 Ceramic

The most acknowledged definition of a ceramics is given by Kingery et al. [21]; “A ceramic is a non-metallic, inorganic solid.” The basic difference that sets engineering ceramics apart from conventional ceramics is the origin of both types of ceramics i.e. engineering ceramics such as silicon nitride ( $\text{Si}_3\text{N}_4$ ) are usually products of an artificial process whereas conventional ceramics such as alumina are made of natural minerals [22].

Extensive development in the 1980's resulted in a considerable amount of engineering ceramics which are commonly used in two general areas i.e. [23];

- 1) In the ambient temperature, due to their extreme wear and corrosion resistance, e.g. typical applications in pumps, seals and valves.
- 2) In the high temperature applications, due to their thermal stability, dynamic and static mass reduction as well as hot corrosion/erosion resistance, e.g. in mining, mineral processing and handling as well as in papermaking.

Bengisu [22] has provided several examples of ceramics that have been adopted in the structural applications:

Some examples of structural applications of ceramic materials are bearings, seals, amors, liners, nozzles and cutting tools. Due to their current high cost, ceramic bearings and journals are used only for precision systems. Silicon nitride balls are used in spindle bearings for cutting tools, turbomolecular pumps, dental drills and

speciality instrumentation bearings. Boron carbide and single-crystal sapphire are used in bearings and seals. Silicon nitride and sialons are being considered for gas turbine bearings. Advantages of such ceramics over conventional materials, e.g., steel, are their lower densities, which reduce the centrifugal load on the balls, high resistance to wear and superior high temperature properties. Slide bearings made from siliconized SiC have been mass-produced since 1980s [22].

In this research work, sialon was chosen to be joined with metal as they present excellent mechanical properties at high temperature.

### **2.2.1 Sialon**

Mandal and Thompson stated that sialon ceramics were found almost at the same time which was in late 1971 at Newcastle University and also at the Toyota Research Laboratories in Japan [24]. They are an alloy of silicon nitride and aluminum oxide. Sialon is formed by partially substituting Al and O for Si and N in silicon nitride and generally classed under 'nitrides'[23].The term 'sialon' was chosen to particularize any composition containing elements Si, Al, O and N as major constituents [25-28].

This superior refractory material has the combined properties of silicon nitride, i.e., high strength, fracture toughness and low thermal expansion; and aluminum oxide, i.e., corrosion resistance, chemical inertness, high temperature capabilities and oxidation resistance [29]. Due to its good mechanical properties, sialon finds applications in engine components and other structural applications that involve both high temperatures and wear conditions [30].

Smallman and Bishop [31] in their book of modern physical metallurgy and materials engineering described the use of sialons in the applications that requires their useful properties of being wear resistance and their ability to withstand high temperature:

The strength and wear resistance of sialons led to their use in the metal-working operations of extrusion and tube drawing. In each process, the relative movement of the metal stock through the die aperture should be fast with low friction and

minimal die wear, producing closely dimensioned bar/tube with a smooth and sound surface texture. Sialon die inserts have been successfully used for both ferrous and non-ferrous metals and alloys, challenging the long-established use of tungsten carbide inserts. Sialons have also been used for the plugs (captive or floating) which control bore size during certain tube-drawing operations. It appears that the absence of metallic microconstituents in sialons obviates the risk of momentary adhesion or 'pick up' between dies and/or plugs and the metal being shaped. Sialon tools have made it possible to reduce the problems normally associated with drawing of the difficult alloys such as stainless steel [31].

The endurance of sialons at high temperatures and in the presence on invasive molten metal or slag has led to their use as furnace and crucible refractories. On a smaller scale, sialons have been used for components in electrical machines for welding (e.g. gas shrouds, locating pins for the workpiece). These applications can demand resistance to thermal shock and wear, electrical insulation, great strength as well as immunity to attack by molten metal spatter. Sialons have proved superior to previous materials (alumina, hardened steel) and have greatly extended the service life of these small but vital machine components [31].

Despite the fact that sialons displaying its superior properties even at high temperature, sialons, like any other ceramics are brittle i.e. they experience catastrophic failure before permanent deformation. Due to their brittle nature, monolithic ceramics are sensitive to defects that act as stress concentrators. Therefore, structural applications of monolithic ceramics are limited to parts that are subjected to compressive loading or limited tensile or multiaxial loading [22].

### **2.3 Stainless steel**

Metals have always been the material of choice for joining with ceramics. By virtue of their wide range of mechanical, physical and chemical properties, stainless steel have been widely employed in the joining technology. Kalpakjian and Schmid [32] have described stainless steel as follows:



Stainless steels are characterized primarily by their corrosion resistance, high strength and ductility, and high chromium content. They are called stainless because in the presence of oxygen (air) they develop a thin, hard adherent film of chromium oxide that protects the metal from corrosion (passivation). This protective film builds up again in the event that the surface is scratched. For passivation to occur, the minimum chromium content should be 10% to 12% by weight.

In addition to chromium, the other alloying elements in stainless steel is typically are nickel, molybdenum, copper, titanium, silicon, manganese, columbium, aluminium, nitrogen and sulphur. The L is used to identify low-carbon stainless steel. The higher the carbon content is, the lower is the corrosion resistance of stainless steels. The reason is that the carbon combines with the chromium in the steel and forms chromium carbide; the reduced availability of chromium lowers the passivity of the steel. Still worse, the chromium carbide introduces a second phase and thereby promotes galvanic corrosion.

Developed in the early 1990s, stainless steels are made by using electric furnaces or the basic-oxygen process and then techniques similar to those used in other types of steel making. The level of purity is controlled by various refining techniques.

Stainless steels are generally divided into five types, which are: austenitic, ferritic, martensitic, precipitation hardening and duplex structure.

Ferritic stainless steel was chosen to be joined with sialon in this research work due to their mechanical properties and the fact that they can offer better corrosion resistance in harsh environment.

### **2.3.1 Ferritic stainless steel**

Cardarelli [29] had defined ferritic stainless steel as:

Ferritic stainless steel alloys (i.e., AISI 400 series) exhibit a chromium content ranging from 17 to 30 wt. % but have a lower carbon level, usually less than 0.2 wt. %. Ferritic stainless steels exhibit the following common characteristics:

- i. They exhibit a body-centered cubic ferrite crystal lattice due to the high chromium content;
- ii. They are ferromagnetic and retain their basic microstructure up to the melting point if sufficient Cr and Mo are present;
- iii. They cannot be hardened by heat treatment, and they can be only moderately hardened by cold working; hence they are always used in the annealed condition;
- iv. In the annealed condition, their strength is 50% higher than that of carbon steels;
- v. Like martensitic steels, they have poor weldability.

Ferritic stainless steels are typically used where chloride stress-corrosion cracking (SCC) may be a problem because they have high resistance to this type of corrosion failure.

In the sialon/AISI 430 ferritic stainless steel joint, besides offering its good corrosion resistance at high temperature, AISI 430 is also employed in the hope of utilizing its toughness to make up the defect of sialon which is its brittleness.

## **2.4 Benefits of Ceramic/Metal Joint**

The joining of the ceramic and metal has led to the hope that their combination of superior properties can be utilized in a wide range of applications. This joint will impart great advantages to the applications.

One of the major advantages of incorporating the ceramic-metal joint into structural applications is to provide reliability to the ceramic components by backing up with metal components [33]. Despite the fact that ceramics can withstand extreme

temperature condition, they are very fatal to be introduced into structural applications due to their brittleness. Thus, in adopting ceramics in structural applications, they are often required to be joined with metal. Metals, utilizing their toughness, are used to support ceramic throughout the joint.

As briefly described in Chapter 1, using ceramic-metal turbochargers as opposed to all metal turbochargers in vehicle will contribute marginal advantages to the engines performance. United States Office of Technology Assessment Congress [34] observed:

The primary attraction of the ceramic rotor is the improved performance provided by its low rotational inertia, which enables a quick response by the turbocharger at low engine rpms. The higher weight of metal alloys causes a delayed response called turbo lag. Secondly, there are expected material cost savings to be gained from the use of ceramics, along with overall weight savings (providing additional fuel economy) [34].

Messler [35] has explained a few examples on which the application of ceramic metal joint has generated great advantages described as follows:

In an automobile spark plug, for example, an insulating ceramic must be bonded to a conductive metal electrode for the spark plug to function. Metal might be needed to structurally support a ceramic and provide a degree of toughness by serving to arrest any cracks propagating in the ceramic. Or a ceramic might provide a sink for heat engines, including internal combustion engines and gas turbines, metal may be used instead of ceramics to reduce cost whenever the ceramics are no longer needed for their principal properties (e.g., refractoriness, wear resistance and low density, and, hence, inertia) [35].

## **2.5 Development of Ceramic/Metal Joining**

In order to combine the advantages of ceramics with those of metals, reliable joining methods is necessary. The development of techniques to join ceramics to metals makes this combination possible. Figure 2-1 shows three basic categories of method

to join ceramics and metals. Mechanical joining encompasses simple and cost-efficient processes, while indirect and direct joining refers to the use or not of an intermediate material to promote physical or chemical bonding between counterparts [36].

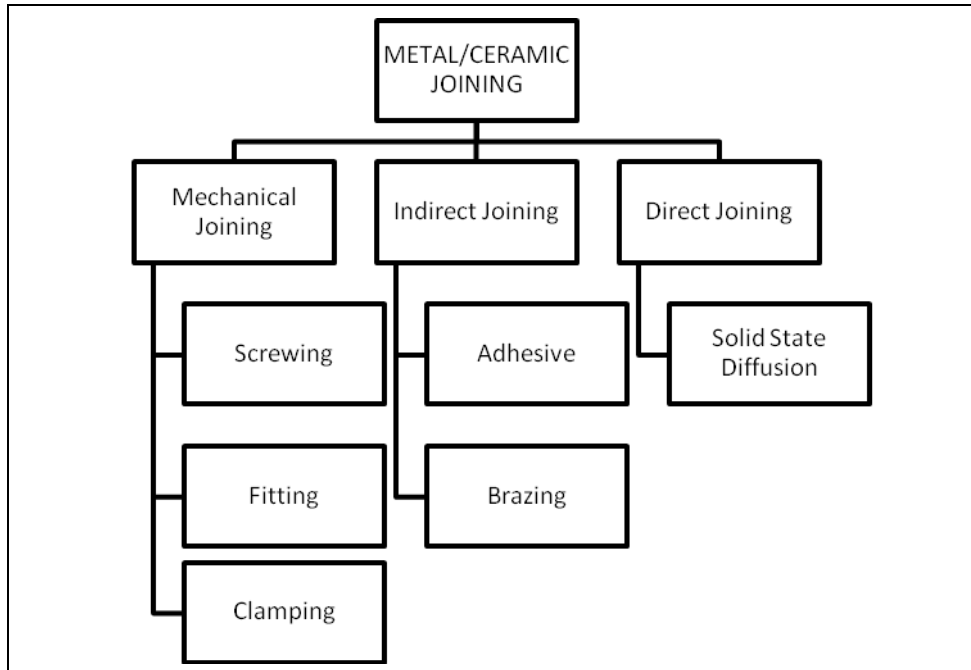


Figure 2-1 Ceramic metal joining process [36]

Among these techniques, the indirect joining brazing and direct joining diffusion bonding are the most suitable [37]. Brazing is used when the ceramic is subjected to working temperature below 700°C. However, higher working temperature requires the use of other joining techniques which are based mainly on diffusion phenomena in the solid state, e.g. diffusion bonding [38]. The next two sections will describe the brazing and diffusion bonding techniques in details.

### 2.5.1 Indirect Joining of Ceramic and Metal: Brazing

Brazing is a method of joining materials by a metallic interlayer [4]. Brazing has been defined by the American Welding Society (AWS) as a joining process that takes place above 450 °C using filler metals or alloys which flows by capillary forces whose

melting temperature is lower than the solidus temperature of the base materials [39]. Meanwhile, Schwartz [40] has described brazing as follow:

Brazing does not involve any melting or plastic state of the base metal. Brazing comprises a group of joining processes in which coalescence is produced by heating to suitable temperatures above 450°C and by using a ferrous and/or nonferrous filler metal that must have a liquidus temperature above 450°C and below the solidus temperature(s) of the base metals(s). The filler metal is distributed between the closely fitted surfaces of the joint by capillary attraction. Brazing is distinguished from soldering in that soldering employs a filler metal having a liquidus below 450°C.

Brazing has four distinct properties which are:

- i. The coalescence, joining, or uniting of an assembly of two or more parts into one structure is achieved by heating the assembly or the region of the parts to be joined to a temperature of 450°C or above.
- ii. Assembled parts and brazing filler metal are heated to a temperature high enough to melt the filler metal but not the parts.
- iii. The molten filler metal spreads into the joint and must wet the base metal surfaces.
- iv. The parts are cooled to freeze the filler metal, which is held in the joint by capillary attraction and anchors the part together.

Since internal stress may developed due to the thermal expansion coefficient disparity, special metals that offer matched coefficients of thermal expansion, and particularly ductile filler metals are selected when brazing ceramics to metals [41]. The basis for selecting suitable brazing alloys are that they must wet or coat the ceramic, must form a chemical bond at the interfaces producing a strong joint and should cause minimal deterioration of the base material [4]. The common adhesion mechanism is not applicable in brazing of ceramics as the material, by definition, is non-metallic. Instead, special filler metals are applied that react with the ceramic due

to alloying elements present in the ceramic such as titanium, zirconium or hafnium. The formation of predominantly ceramic phases allows wetting to occur [41].

According to Tomsia [4], there are also some limitations in the brazing process, most importantly the direct consequence of the presence and action of the reactive metal. The flow of some reactive metal alloys is reported to be sluggish, and as a result, preplacing foils is often necessary. The reactivity of the alloys generally demands that they be used in a vacuum or in an inert atmosphere containing sub-ppm oxygen levels. Tomsia also claimed that the excessive brazing time or the brazing temperature can deteriorate the joint strength.

Elssner and Petzow [42] reported that the brazed components usually show reaction layers of some micrometers thick at the brazed/ceramic interface and if these reaction layers increases in thickness, the bond strength of the joints can be degraded due to the formation of flaws in their microstructure and/or thermal expansion and volume mismatch promoting premature failure by interfacial stresses. In addition, it was also reported that the brazed joints do not withstand prolonged loading at high temperature because reaction of the active metal with the ceramic will proceed.

Brazing has been widely employed in joining of ceramics to metal. Soon-Bok and Jong-Ho [18] had successfully joined silicon nitride to carbon steel by the activation metal vacuum-brazing method. Ti-Ag-Cu alloy was used as the brazing filler metal. As a method of reducing stress, they had incorporated copper sheet as the interlayer and a compressive load was applied during the joining process. Two types of round ceramic/metal joints specimen were made i.e.  $\text{Si}_3\text{N}_4/\text{S45C}$  and  $\text{S45C}/\text{Si}_3\text{N}_4/\text{S45C}$ .

Zhang et al. [43] had obtained  $\text{Al}_2\text{O}_3$ -SS304 joints by partial transient liquid phase (PTLP) brazing. Prior to bonding, the materials were polished to make the surface roughness of the SS304 and alumina reaches 0.03 and 0.23 $\mu\text{m}$  respectively. The materials were then cleaned in an ultrasonic bath with isopropyl alcohol for 1 hour. The bonding was carried out in a vacuum furnace which was kept in the range of  $8 \times 10^{-6}$  to  $2 \times 10^{-5}$  mbar during the process. The temperature was raised to brazing temperature at 4°C/min, maintained at 1150 or 1250°C for 3 hours, and then reduced to room temperature at 1°C/min.

Yoshinori and Kazuo [44] has examined the strength characteristics of the Si<sub>3</sub>N<sub>4</sub>/SUS 304 joint acquired by the active metal method using oxygen-free copper as an interlayer and Ti-Ag-Cu as the brazing filler metal. Thicknesses of the interlayer were varied from 0.1 to 1.0 mm. The maximum joining temperature was 880°C and the holding time at maximum temperature was 10 minutes.

### **2.5.2 Direct Joining of Ceramic and Metal: Diffusion Bonding**

Diffusion bonding requires two nominally flat surfaces e.g., ceramic and metal to be brought into contact at an elevated temperature for a period of time until a strong joint is formed. Generally the temperature is in the region of 0-0.8 T<sub>m</sub> where T<sub>m</sub> is the melting point of the least refractory material i.e., metal in the case of ceramic/metal joint. This solid state bonding usually carried out in a vacuum atmosphere under a low mechanical pressure which can be applied either uniaxially or isostatically.

Diffusion bonding involves the decomposition of the surface of the ceramic by the metallic part and allows diffusion of the active component in the metallic part [45]. Sample preparation is important in diffusion bonding as to minimize surface oxidation. Elssner and Petzow [42] claim that the surfaces need to be cleaned and free from impurity atoms and adhering films.

In their work, Elssner and Petzow [42] also listed the technical advantages of diffusion bonding, which are:

- 1) Low deformation which enables parts to be joined without distortion,
- 2) The ability to join large areas,
- 3) The applicability of diffusion bonded joints at high service temperature and,
- 4) Possibilities for joining materials in nonconventional situations.

According to Ashby and Johnson [46], diffusion bonding can create high quality joint even though it requires high temperature and longer time. However, there are also a few restrictions and disadvantages of diffusion bonding i.e., high cost, only flat specimens can be joined, a vacuum/inert atmosphere is required, and pressure must be

applied. The need to apply pressure during diffusion bonding imposes restrictions on the joint geometry; most joints are of the face seal type and are not well suited for accommodating thermal expansion mismatch [4].

Zhang et al. [47] added that the diffusion joining is unfit for joining thin metal parts and ceramic components. Besides, when the joining temperature is too high, brittle compounds will be formed at the ceramic/metal joint. Consequently, their structure, distribution and thickness will give a big influence on the joint strength.

Stoop and den Ouden [48],[49] in their series of work has proven that the silicon nitride can be joined to austenitic stainless steel either with or without the metallic interlayers, by means of diffusion bonding. The experiments were carried out under vacuum condition of  $10^{-5}$  to  $10^{-3}$  at the temperature, time and pressure varied between  $1000^{\circ}\text{C}$  to  $1225^{\circ}\text{C}$ , up to 1440 minutes and from 0 to 15 MPa, respectively, in the former case and from  $850^{\circ}\text{C}$  to  $1200^{\circ}\text{C}$ , 22.5 minutes to 1440 minutes and 3 MPa to 30 MPa, respectively, in the later case. The ceramic/metal was heated to the required bonding temperature at a rate of  $25^{\circ}\text{C}/\text{min}$ , after which the mechanical pressure was applied. The pressure was released at the start cooling, which occurred at a rate of  $5^{\circ}\text{C}/\text{min}$ .

Polanco et al. [50] have obtained a moderate strength of diffusion bonded silicon nitride-stainless steel joint. The stainless steel foil was set in between two  $\text{Si}_3\text{N}_4$  pieces using a lap configuration while a uniaxial pressure of 4 to 5 MPa was applied to the assembly during the heating cycle. The pressure was removed at the onset of the cooling cycle. The joining was performed under a vacuum atmosphere of about  $1 \times 10^{-4}$  Pa with the joints held for 120 minutes at the maximum temperature of  $1100^{\circ}\text{C}$ . The joints were cooled at  $20^{\circ}\text{C}/\text{hour}$  to minimize thermal residual stresses at the interface.

Several other researches also have successful in joining of ceramic to metal by utilizing diffusion bonding. Krajewski [38] managed to join silicon nitride to wear-resistant steel by direct diffusion bonding. The experiments were performed under vacuum condition with the temperature of  $1200^{\circ}\text{C}$  for 30 minutes. Travessa et al. [51] have employed diffusion bonding to join aluminium oxide to AISI 304 steel by incorporating various stress relief interlayer.



Although active-metal brazing is now widely used, it is limited by low temperature application. Thus for high temperature application, diffusion bonding is preferable [52]. Research work [48],[49] had shown that under specific process conditions, joints can be obtained between silicon nitride and stainless steel, either with or without interlayer, by means of diffusion bonding.

## **2.6 Ceramic/Metal Joining Problems**

Although many methods have been already established for joining ceramics and metals, one has to notice the fact that no ceramic/metal joint structure is stable because of the big gaps both in chemical and physical nature between the two materials [53].

There are numerous obstacles for successful metal–ceramic joining, the most important of which is the relative inertness of the ceramic and the coefficient of thermal expansion (CTE) mismatch [54] which can lead to the development of residual stresses. Residual stresses deteriorate the strength of the ceramic counterpart and causing the failure of the joint at lower strengths [36].

Foley [55] listed four factors that govern the build up of residual stress in a ceramic-metal joint during cooling:

- a) The difference between the temperature at which stress can be transmitted across the joint and ambient temperature.
- b) The difference in the coefficient of thermal expansions of the ceramic and metal
- c) The ability of the materials in the joint to undergo plastic deformation or other forms of distortion thus helping to counteract the effects of differential strain.
- d) The dimensions of the joint being made.

CTE mismatch has become the most serious problem in ceramic metal joining, as metal with higher CTE will shrink more during cooling of the joint from the fabrication temperature. Temperature changes induced during cooling from the

joining temperature and during subsequent service can generate high internal stresses due to the CTE mismatch and lead to poor joint strength or failure [56]. Figure 2-2 shows the typical fracture mechanism that occurs in ceramic metal joint. In the ceramic metal joint, it was observed that the maximum tensile stress developed at the free surface of the ceramic, above the joint interface. When the interface is strong enough, mode I crack initiation occurs in the ceramic at this point. The stress then becomes compressive. However, maximum shear stress values are observed. As a consequence, mode I will rapidly transform to mode II crack propagation. The propagation in the ceramic occurs very near or along the interface [57], [58].

Mechanical attachments invariably result in residual stress concentration which may initiate cracks and cause failure [58],[59]. It must be pointed out that tensile stresses in the ceramic substrate, experimentally observed by X-ray diffraction, are harmful for the joint integrity since ceramic materials cannot withstand high tensile stress [60],[61].

Figure 2-3 shows the “concave/convex” fracture mode that is sometimes observed in a joint with a large thermal expansion mismatch [12]. The distribution of tensile and shear stress in the ceramic, as can be seen in Figure 2-2, clearly depicted the fracture profile. Figure 2-2 shows the typical fracture mechanism of a ceramic/metal assembly. If the joint is strong enough, mode I crack initiation occurs on the lateral surface of the ceramic in the maximum tensile stress area and mode II crack propagation follows in the ceramic along the joint in the maximum shear stress area [57]. Since the stresses developed strongly influence the joint integrity and often lead to fracture, it is therefore essential to evaluate the residual stress state in the joint.

### **2.6.1 Residual Stress in Ceramic/Metal Joint**

Schijve [62] has clearly defined residual stress, in which he claims:

By definition, residual stress refers to a stress distribution, which is present in a structure, component, plate or sheet, without a load being applied. In view of the absence of an external load, the residual stresses are sometimes labelled as internal stresses. The background of the terminology “residual stress” is that a

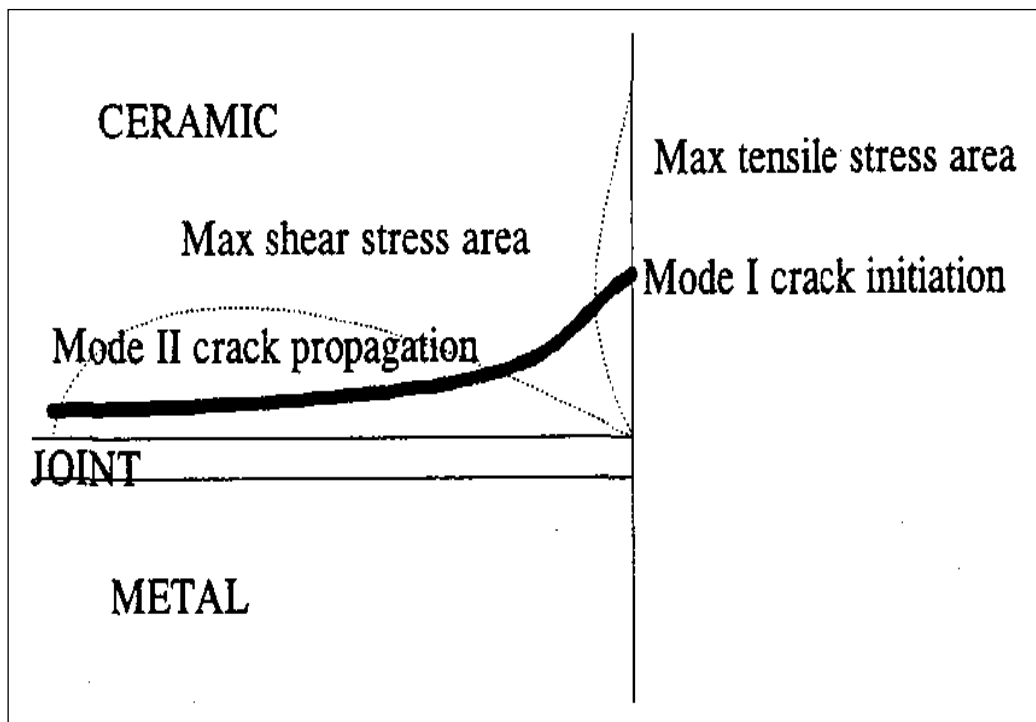


Figure 2-2 Typical fracture mechanism of a ceramic/metal assembly [57].

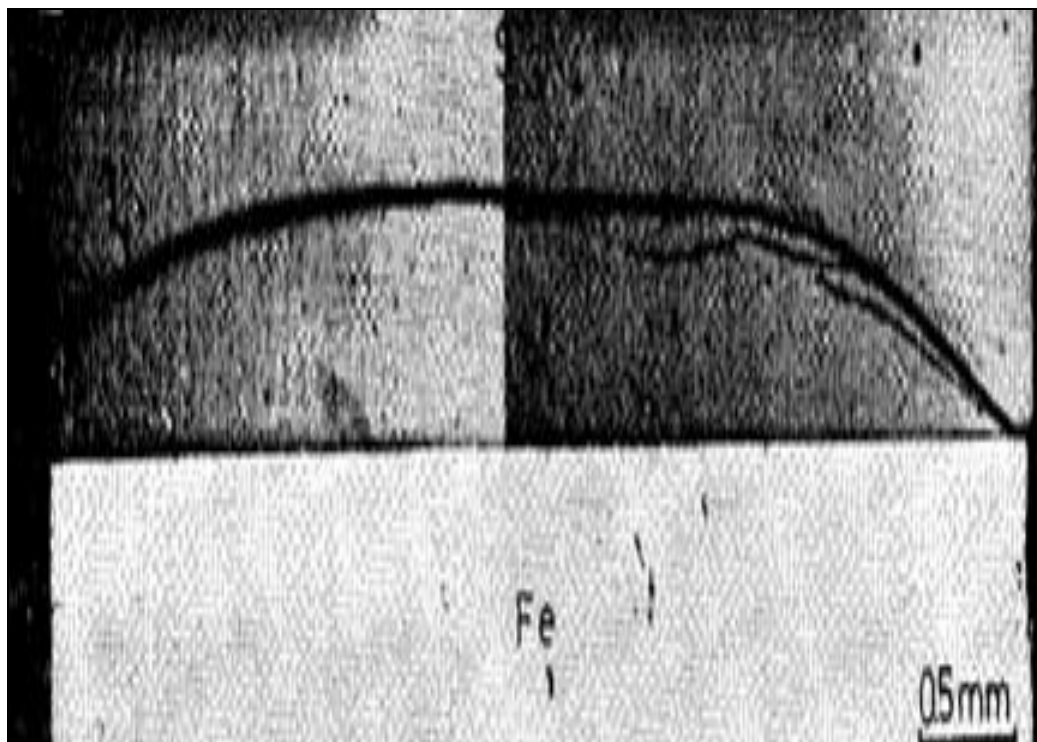


Figure 2-3 Example of typical fracture occur in ceramic/metal joint [12].

residual stress distribution in a material is often left as a residue of inhomogeneous plastic deformation [62].

As discussed earlier, it is widely known that joining of ceramic to metal will generate residual stresses mainly due to the mismatch in properties of both materials. It can be seen from Figure 2-4 [63] that ceramics tend to have lower thermal expansion coefficient and fracture toughness but higher modulus of elasticity as compared to metals. Since metals have higher coefficient of thermal expansion than ceramics, they will contract more during cooling of the ceramic metal joint and inducing the development of residual stress.

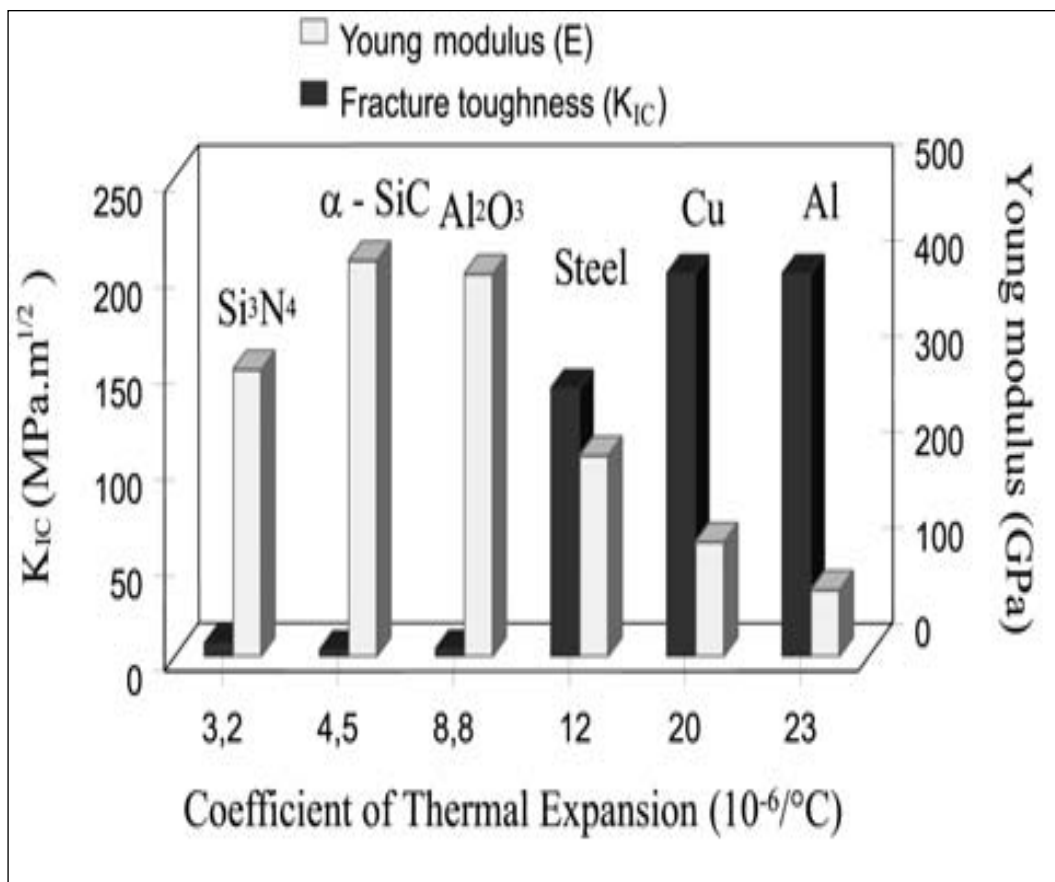


Figure 2-4 Properties of ceramics and metals [63].

Figure 2-5 shows the schematic representation of residual stresses developed during fabrication of ceramic/metal joint. Metals with a relatively low elastic modulus tend to deform under the influence of this stress while ceramics, due to their

brittleness, will have a tendency to fracture. Information from numerous experimental results [18],[64],[65] about the location of crack initiation in the ceramic metal joint are coincide with the location of the maximum tensile residual stress in ceramic as presented by Suganuma [66] in Figure 2-6. The joint is assumed to be cooled from 800°C to room temperature fully elastically. The arrows indicate the position and direction of the maximum tensile stress [66]. Suganuma had shown that maximum tensile stress concentrates on or near the interface and the free surface of the ceramic/metal joint. Durov et al. stated that the maximum tensile residual stress within ceramic/metal joints is usually developed within a ceramic, because a ceramic tends to have a smaller CTE than a metal [67].

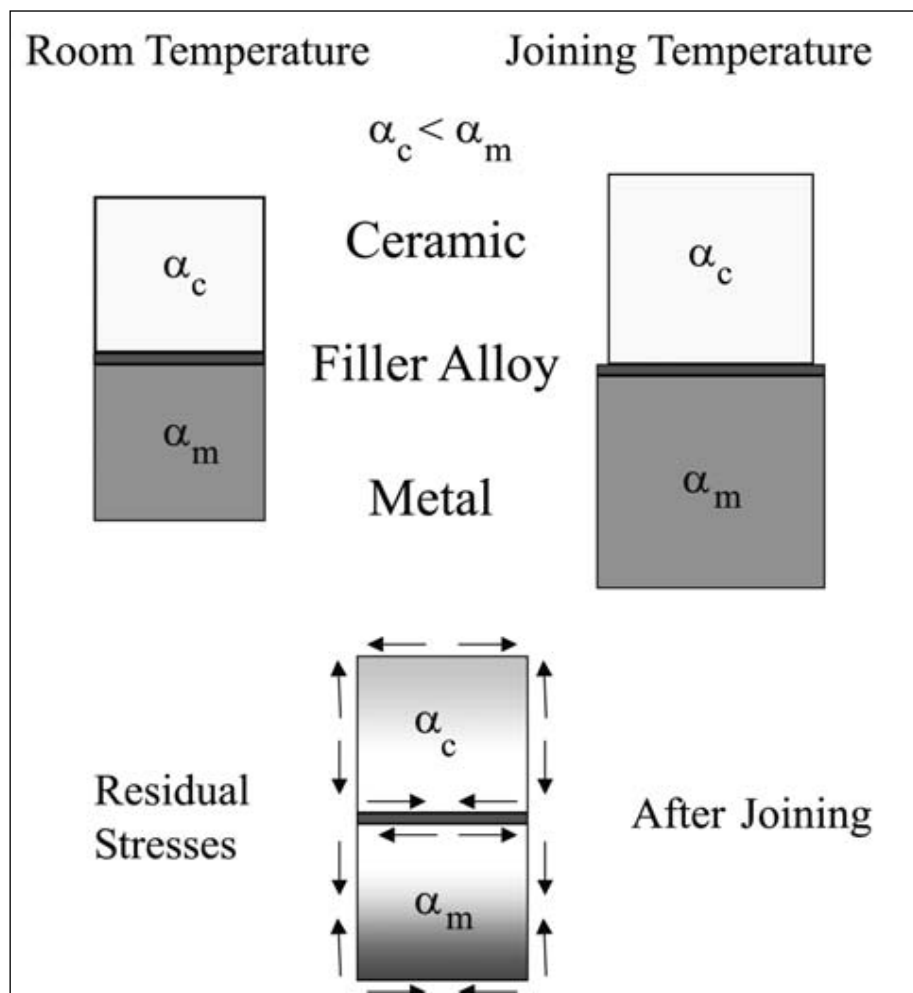


Figure 2-5 Schematic representation of residual stresses developed during joining process [36].

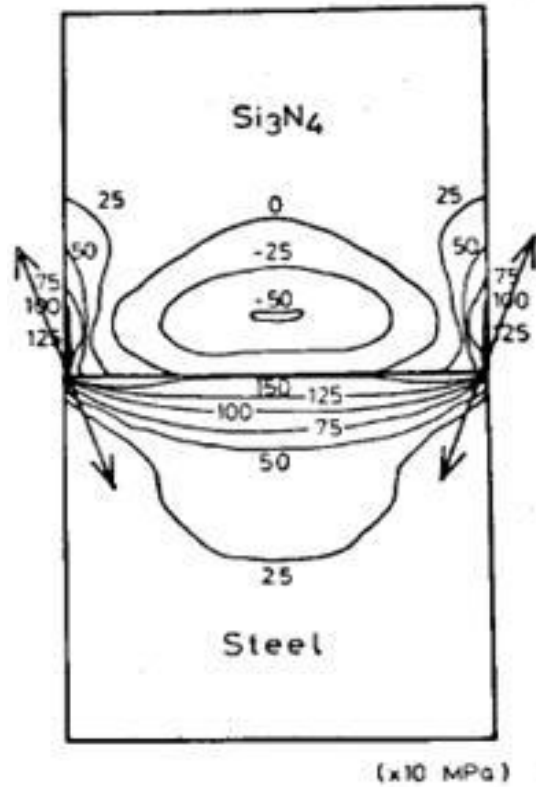


Figure 2-6 Contourmap of maximum principal stress calculated by FEM [66].

#### 2.6.1.1 Methods of reducing the residual stress

The magnitude of the residual stress was influenced by joint geometry, relative thickness of ceramic and metal, the ability of metal to relax stresses and temperature at which joint solidifies [40]. Suganuma in separate papers [68],[69], has investigated the influence of these parameters. In the former paper, Suganuma et al [68] had claimed that the maximum tensile stress in the silicon nitride was first increases with increases in the thickness of silicon nitride and slowly becoming constant, as seen on Figure 2-7. Hattali et al [70] also suggested that residual stress will increase if higher thickness of ceramic is employed. When investigating the effect of fabrication parameters in Alumina/Nickel alloy joints, using FEM, they had shown that the maximum residual stress in the ceramic will increase with increasing thickness of  $Al_2O_3$ .

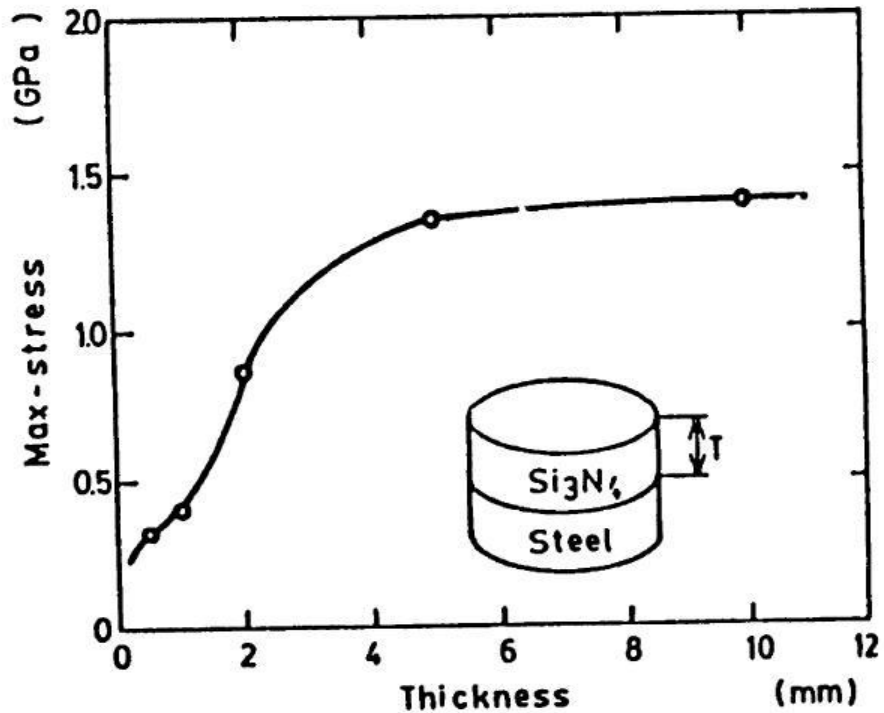


Figure 2-7 Thickness dependence on the maximum tensile stress in the silicon nitride/steel joint [68].

Through the later paper, Suganuma et al [69] had shown that the rectangular joint shape produce larger stress as compared to the cylindrical joint. In their work, they had studied the influence of shape and size on residual stress in the silicon nitride/Invar alloy joints obtained by brazing with aluminium as the brazing metal. The stresses distribution were found to be the same in both rectangular and cylindrical joint, however the magnitude were higher in the rectangular joint. Suganuma et al also suggested that increases in diameter will resulted in higher tensile stress in the cylindrical joint. They had claimed that the joint has two main ways of relieving the residual stress which are 1) the formation of a fine crack network in the reaction layer produced between aluminium and the Invar, and 2) the plastic deformation of the aluminium layer. These ways work very well for the smaller joint. The influence of the shape and size can be seen in Figure 2-8 and Figure 2-9.

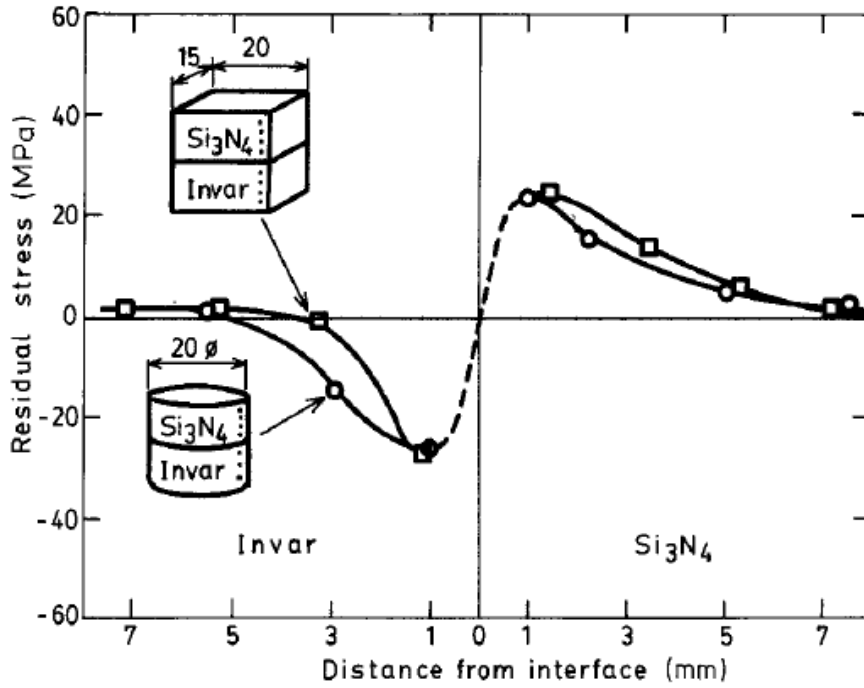


Figure 2-8 Effect of joint shape on the stress level of ceramic/metal joint [69].

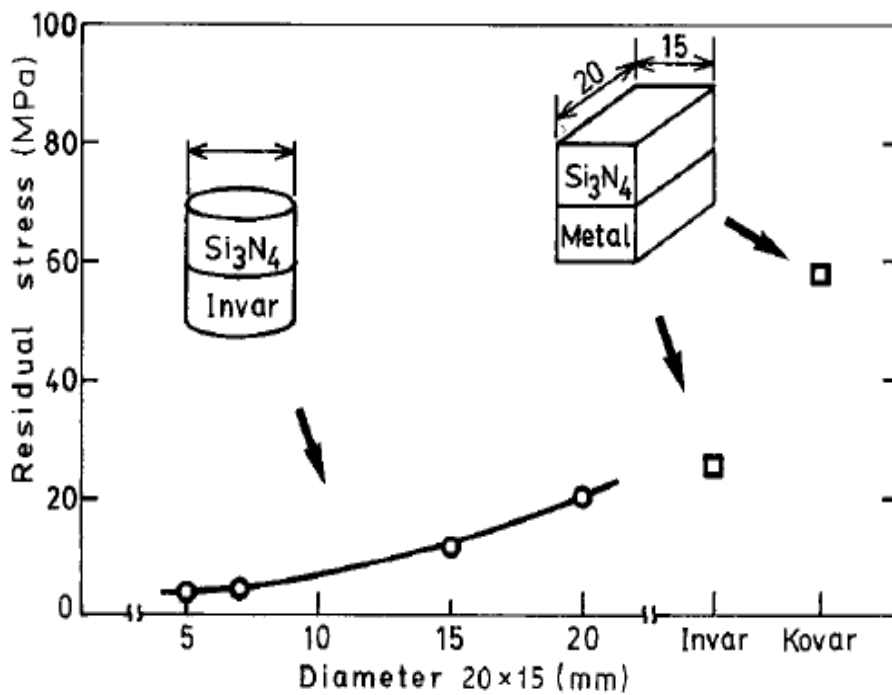


Figure 2-9 Effect of diameter on the magnitude of tensile stress in ceramic/metal joint [69].



Besides controlling the shape and size of the joint, it is certain that incorporating interlayer in between the ceramic and metal will reduce the tensile residual stress. The purpose of the interlayer is to reduce the thermal expansion mismatch between the two materials. Many researchers have looked into this and the summary of work done is given in Table 1-1.

The ability to compensate thermal expansion mismatch between the ceramic and metal is the vital problem in ceramic metal joining. The use of soft metals as the interlayer has been widely accepted in the ceramic metal joining. It was observed that the application of soft metals of high plastic deformability as interlayer materials will increase the efficiency of thermal stress relief [42].

Nevertheless, there are still weaknesses that need to be overcome when utilizing such single interlayer in the ceramic metal joint; as an exemplary case, copper interlayer has been said to provide maximum reduction of residual stresses, but their applicability in real systems is limited due to their low resistance to corrosion and oxidation at high temperatures [71]. In addition, Suganuma [12] had claimed that single interlayer cannot remove the residual stress effectively and would not resist to sudden temperature change or severe heat cycle since even soft metal plastic/creep deformation could not follow sudden temperature change. Thus, the use of multiple interlayers [51],[71] and functionally gradient material (FGM) [13],[72] were proposed.

Pietrzak et al. [72] described FGM as gradient materials that characterized by functional change in at least one of their properties. In the case of ceramic/metal joint, the most important is a change in physical, (i.e. thermal expansion coefficient  $\alpha$ ) and mechanical properties, by which the stress level in the joint is lowered. Suganuma [12] reported that the use of FGM is one of the effective methods in reducing the stress level in ceramic metal joint, however, the problem of incorporating FGM lies on the strength and reliability of the interlayer itself.

Table 2-1 Summary of interlayers for reducing thermal expansion mismatch in ceramic/metal joints. (I) Soft metal, (II) Composite, (III) Laminate (soft metal/low expansion & hard metal), and (IV) Crack layer. Source: Suganuma et al. [12]

<i>Group</i>	<i>Ceramic/Metal</i>	<i>Interlayer</i>	<i>Joining conditions</i>	<i>Strength</i>
(I)	Al <sub>2</sub> O <sub>3</sub> /Type 321 steel	Al	873 K, 50 MPa, 30 min	70 (t)
	TZP/Type 316 steel	Cu	1273 K, 1 MPa, 4 h	52 (b)
	MgO/Steel	Cu/Metal foam	1273 K – 1473 K*	33 (t)
	Al <sub>2</sub> O <sub>3</sub> /Steel	BA03	883 K, 10 MPa, 30 min	30 (t)
(II)	SiC/Al**	Cu-C fiber	1043 K (Al was joined at 823 K)*	-
	Al <sub>2</sub> O <sub>3</sub> /W	***	Al <sub>2</sub> O <sub>3</sub> -W	-
	Al <sub>2</sub> O <sub>3</sub> /Fe		Al <sub>2</sub> O <sub>3</sub> -Fe	-
	TiN/Mo		TiN-Mo	80 (t)
	Al <sub>2</sub> O <sub>3</sub> /Fe		FeO-Fe	-
	TZP/W		TZP-W	200 - 400 (b)
(III)	Al <sub>2</sub> O <sub>3</sub> /Type 405 steel		Nb/Mo	1673 K, 100 MPa, 30 min
	Al <sub>2</sub> O <sub>3</sub> /Type 316	Ti/Mo	1373 K, 9 MPa, 3 h	70 (t)
	Si <sub>3</sub> N <sub>4</sub>	/Steel	BA03/WC	200 (b)
	SiC			150 (b)
	Sialon			300 (b)
	Sialon/Steel	Type 304/WC steel	1373 K, 5 MPa, 1 h	150 (b)
	Si <sub>3</sub> N <sub>4</sub> /Type 405 steel	Fe/W	1473 K, 10 MPa, 30 min	60 (t)
	SiC	/ Super alloy	Ni/Kovar/Cu	100 (t)
	Si <sub>2</sub> N <sub>3</sub>			-
SiC/Type 316 steel	Ti/Mo	1083 K, 0 min*	50 (s)	
(IV)	Si <sub>3</sub> N <sub>4</sub> /Type 405	Al/Invar (cracking in intermetallic compound)	1073 K, 0.15 MPa, 7 min*	60 (t)

\* Brazing, the others are diffusion or eutectic joining

\*\* Soft metal with carbon fiber

\*\*\* Grading (cermet)

TZP : Tetragonal zirconia polycrystal

Suganuma and Okamoto [73] claimed that the following equations must be obeyed in order to reduce the magnitude of the stresses at the ceramic/metal interface:

$$\alpha_c \approx \alpha_I < \alpha_m, \quad (2-1)$$

for ceramic/interlayer I/metal joints

$$\alpha_c \approx \alpha_I > \alpha_{II} < \alpha_m, \quad (2-2)$$

for ceramic/interlayer I/interlayer II/metal joints

where;  $\alpha$ , C, I, II and m denotes thermal expansion coefficient, ceramic, first interlayer, second interlayer and metal respectively.

Employing multiple interlayer have directed to the use of soft metal/ low expansion & hard metal, commonly referred as laminate interlayer. Among the researchers who have looked into incorporating this type of interlayers are Suganuma et al. [72-74] and Kohno et al [76]. The former had introduced laminated interlayer of Nb/Ni for alumina/stainless steel joint while the latter had developed laminated interlayer of BA03/WC for three joints which are Si<sub>3</sub>N<sub>4</sub>/steel, SiC/steel and sialon/steel joint. Suganuma [12] reported that the laminate interlayer improves resistance to sudden temperature change. He explained that, since the movement of the soft metal is restricted with a ceramic and a low expansion/hard metal from both sides, it could deform easily following the shrinkage of the ceramic. Good plastic properties of the soft layer enable its easy strain while the tensile stresses being taken over and accumulated by the hard metal [38]. Furthermore, the harmful effect of the large expansion and contraction of the base metal is blocked by the hard metal layer.

The use of composite as the interlayer in the ceramic metal joint has also been evaluated by several researchers. Among the researchers whom have looked into the use of composite as the interlayer are Williamson et al [13]. Williamson et al. had incorporated a 2 mm thick 50 vol. % Ni-50 vol. % Al<sub>2</sub>O<sub>3</sub> homogeneous composite

interlayer into the  $\text{Al}_2\text{O}_3/\text{Ni}$  joint. Through the analysis, they had found that incorporating the composite interlayer into the ceramic/metal joint had surprisingly resulted in higher peak stresses as compared to the no-interlayer joint. It was also observed that the magnitude of plastic strain when the composite interlayer used was approximately one fourth of the magnitude in the no-interlayer joint. The results illustrate the important trade-off between residual stress and plastic strain in joining applications. Additional simulations with increasing thickness of the composite interlayer resulted in reduction of the stress magnitude.

Wang et al. [77] had found that the peak stress values near the interface of  $\text{Al}_2\text{O}_3$ -Ni joint reduces by incorporating a composite layer. It was stated that the plasticity in the composite layer is expected to play an important role in controlling the tensile stress concentration located near the edges of the ceramic component, close to the interface.

Another type of interlayer used in the ceramic metal joint is the crack interlayer [78]. It was reported that the fine crack interlayers could produce a strong joint but in its application, the cracking layer must be sandwiched by ductile layers in order to prevent the growth cracks especially into a ceramic [12].

#### *2.6.1.2 Evaluation of the residual stress*

Different authors have studied the joining of ceramic and metal. A. Abed [79] had shown that on joining sialon to stainless steel, cracking in the ceramic occurs only after cooling from the joining temperature to room temperature. The results showed that there is a good interfacial bonding strength between the sialon and austenitic stainless steel but it is not good enough to accommodate residual stress and avoid fracture.

Hussain [80] had shown that formation of a ductile layer in the steel adjacent to the interface of sialon-ferritic stainless steel that allowed good joining to be achieved. The coefficient of expansion of this layer is intermediate between those of sialon and steel. The author claimed that the ductile layer can relieve the thermal stresses during cooling and the compositional changes lead to the difference in coefficient of

expansion between sialon and ferritic stainless steel becoming smaller, thus, helps in further reducing the thermal stress.

There are several methods that can be used to determine the stress level and its distribution in the ceramic/metal joint. It can be obtained by means of experimental work e.g., strain gauge, X-ray diffraction, neutron diffraction and indentation fracture method. Strain gauge is a destructive method while the others are non-destructive. X-ray diffraction is far more employed than neutron diffraction due to the experimental availability. A disadvantage associated with the method consists in the limited penetration of the radiation into the material. Stress analysis is limited to shallow depths and bulk stresses cannot be assessed. Neutron diffraction on the other hand provides full penetration but requires longer data collecting periods and a neutron source [16],[36].

According to Travessa et al. [51], once the bonding is obtained, the strength of the joint is primarily dependent on the residual stresses at the interface. These stresses, originated from the thermal expansion mismatch between the metallic and the ceramic substrates and constructed during the cooling down from the bonding temperature, were first quantified by analytical method such as research works by Lorenzo Martin et al. [81] and Virkar et al. [82] which had shown that for a perfectly joined interface, the average residual stresses generated in the layers, as shown in Figure 2-10, A and B can be given as:

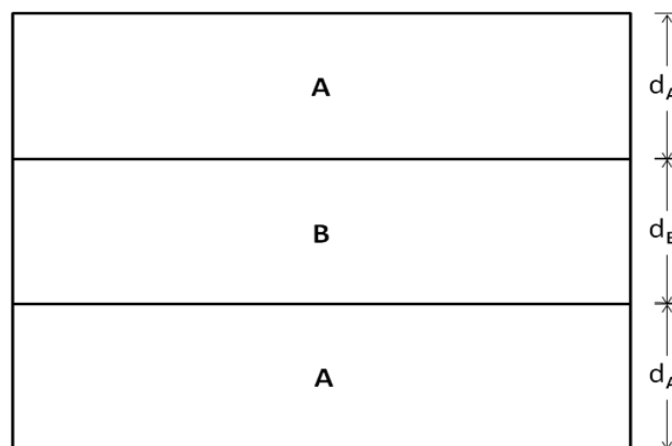


Figure 2-10 Schematic of the layered structure.

$$\alpha_A = \frac{-E_A E_B d_B \Delta \varepsilon_o}{(1-\nu)(2E_A d_A + E_B d_B)} \quad (2-3)$$

$$\alpha_B = \frac{2E_A E_B d_A \Delta \varepsilon_o}{(1-\nu)(2E_A d_A + E_B d_B)} \quad (2-4)$$

$E_A$ ,  $E_B$  are Young's modulus for materials A and B respectively,  $\nu$  is the Poisson's ratio while  $\alpha_A$ ,  $\alpha_B$  are the coefficient of thermal expansion (CTE) for materials A and B respectively.  $\Delta \varepsilon_o$  is the difference in the strain between the two layers and can be given in terms of the CTE of the two materials ( $\Delta \alpha$ ) as well as the cool down temperature range ( $\Delta T$ ) over which the stresses are generated:

$$\Delta \varepsilon_o = \Delta \alpha \Delta T = (\alpha_B - \alpha_A) \Delta T \quad (2-5)$$

From Equation 2-3, assuming  $E_A = E_B$ , surface compressive stress in outer layer A can be given as:

$$\sigma_c = -\frac{d_B E \Delta \varepsilon_o}{(1-\nu)(2d_A + d_B)} \quad (2-6)$$

where  $(2d_A + d_B)$  the total thickness of the layered composite. Assuming that the failure occurs at the outer surface A, fracture stress can be given simply as:

$$\sigma_f = \sigma_f^o - \sigma_c \quad (2-7)$$

where  $\sigma_f^o$  is the fracture stress for monolithic material A, and  $\sigma_c$  is the compressive stress in material A given by (2-6). Upon substitution,

$$\sigma_f = \sigma_f^o + \frac{d_B E (\alpha_B - \alpha_A) \Delta T}{(1 - \nu)(2d_A + d_B)} \quad (2-8)$$

Later, finite element method began to be applied not only to quantify the residual stresses, but also to describe the stress field.

## 2.7 Finite Element Method (FEM)

An effective approach to predict and analyze the magnitude and distribution of the residual stresses along a joint based on the particular properties of the materials to be joined is the FEM. FEM is reported to be simpler, faster and much cheaper than the experimental techniques. In addition, 2- or 3-dimensional stress maps can be obtained via FEM [36].

Commercial finite element software, ANSYS, will be employed in this research work to evaluate the residual stresses developed during cooling of the sialon/AISI 430 ferritic stainless steel joint. Pepper and Heinrich [83] have described FEM as follow:

The finite element method is a numerical technique which gives approximate solutions to differential equations that model problems arising in physics and engineering. As in simple finite difference schemes, the finite element method requires a problem defined in geometrical spaces (or domain) to be subdivided into a finite number of smaller regions (a mesh). In finite differences, the mesh consists of rows and columns of orthogonal lines; triangles or quadrilaterals can be used in two dimensions, and tetrahedrons or hexahedrons in three dimensions. Over each finite element, the unknown variables (e.g., temperature, velocity, etc.) are approximated using known functions; these functions can be linear or higher-order polynomial expansions that depend on the geometrical locations (nodes)

used to define the finite element shape. In contrast to finite difference procedures (conventional finite difference discretizations, as opposed to the finite volume method, which is integrated), the governing equations in the finite element method are problem domain. As a consequence of these operations, a set of finite linear equations is obtained in terms of a set of unknown parameters over each element. Solution of these equations is achieved using linear algebra techniques [83].

Simulation of cooling process of the ceramic/metal joint requires the need to solve heat-transfer equations during the iterative process. Heat transfer is a branch of engineering that deals with the transfer of thermal energy from one point to another within a medium or from one medium to another due to the occurrence of a temperature difference [84]. There are three modes of heat transfer i.e, conduction, convection and radiation.

Conduction is defined as the transfer of heat within a medium due to a diffusion process. The Fourier heat conduction law states that the heat flow is proportional to the temperature gradient. The constant of proportionality depends, among other things, on the *thermal conductivity* of the material [84].

Energy transport affected by the motion of a fluid is known as the convection heat transfer. The convection heat transfer between two dissimilar media is governed by Newton's law of cooling. It states that the heat flow is proportional to the difference of the temperatures of the two media. The proportionality constant is called the *convection heat transfer coefficient* or *film conductance* [84].

Thermal radiation is defined as radiant energy emitted by a medium and is due solely to the temperature of the medium. Radiant energy exchange between surfaces or between a region and its surroundings is described by the Stefan-Boltzmann law, which states that the radiant energy transmitted is proportional to the difference of the fourth power of the temperatures of the surfaces. The proportionality parameter is known as the *Stefan-Boltzmann constant*.

However, the cooling process of a ceramic/metal joint often does not include the radiation heat transfer. Thus, the assumption for heat transfer problem only involves



conduction and convection heat transfer. Since the three-dimensional problems whose geometry and loading are symmetrical about an axis can be analyzed using two-dimensional axisymmetric elements, the following finite element discussion will be based on the formulation of axisymmetric heat transfer problem.

According to Kulkarni et al. [15], for a heat transfer problem, it can be assumed that at any point of the body, the rate of heat transfer by conduction into a unit volume plus of heat generation rate in the unit volume is equal to the rate of change of thermal energy stored within the volume. Alternatively,

Rate of heat transfer by conduction + rate of heat generation = rate of change of thermal energy

Applying the principle of the conservation of energy, the heat transfer within the materials can mathematically be expressed as [85]:

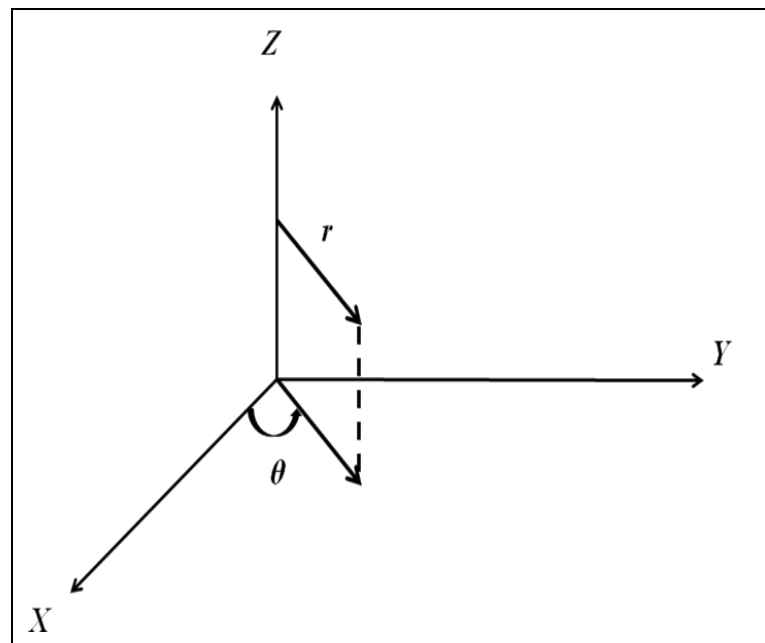


Figure 2-11 Axisymmetric formulation of a three-dimensional problem

$$\frac{1}{r} \frac{\partial}{\partial r} \left( k_r r \frac{\partial T}{\partial r} \right) + \frac{1}{r^2} \frac{\partial}{\partial \theta} \left( k_\theta \frac{\partial T}{\partial \theta} \right) + \frac{\partial}{\partial z} \left( k_z \frac{\partial T}{\partial z} \right) + q' = \rho c \frac{\partial T}{\partial t} \quad (2-9)$$

where  $k_r$ ,  $k_\theta$  and  $k_z$  represent the thermal conductivities in  $r$ -,  $\theta$ - and  $z$ - directions,  $q$  is the heat generation per unit volume,  $\rho$  is the density,  $c$  represents the specific heat and  $t$  is the time. For axisymmetric situations, there is no variation of temperature in the  $\theta$ - direction, and assuming thermal conductivity is constant ( $k_r = k_\theta = k_z$ ), Equation (2-9) reduces to

$$\frac{k}{r} \frac{\partial}{\partial r} \left( r \frac{\partial T}{\partial r} \right) + k \frac{\partial^2 T}{\partial z^2} + q = \rho c \frac{\partial T}{\partial t} \quad (2-10)$$

From the above equation we can obtain the temperature distribution in a body as a function of time.

Dissipation of heat takes place at the free surface via free convection. Rate of heat dissipation via convection ( $q$ ) is given by Newton's law of cooling [86][15].

$$q = hA(T - T_\infty) \quad (2-11)$$

where  $h$  = convection heat transfer coefficient,  $A$  = surface area,  $T$  = surface temperature,  $T_\infty$  = temperature of the surrounding fluid.

According to Kulkarni et al [15], thermal stresses were computed in the structural part of the analysis based on the temperature profile obtained from the thermal analysis. The thermal stresses were calculated using the principle of virtual work, which states that a very small change in the internal strain energy must be compensated by an equal change in the external load [87-91]. The external load in this case would be thermal load. Thus, the governing equation to calculate thermal stresses is given by [88]:

$$[K]\delta = F \quad (2-12)$$

where  $[K]$  = stiffness matrix,  $\delta$  = nodal displacement due to temperature change,  $F$  = thermal force. The total thermal force ( $F$ ) is given by the summation of the thermal forces acting on each element [88]:

$$F = \int [B]^T [C][B]\alpha\Delta T dV \quad (2-13)$$

where  $[B]$  = strain-displacement matrix,  $[C]$  = elasticity matrix,  $\alpha$  = coefficient of thermal expansion of a material for a given element,  $\Delta T$  = difference between the initial and final temperatures.

The corresponding thermal stresses are then calculated by the following equation [88]:

$$\sigma_{th} = [C]\varepsilon_{th} \quad (2-14)$$

where thermal strain is given by [88]:

$$\varepsilon_{th} = [B]\delta = [B][K]^{-1} F \quad (2-15)$$

Thus, the expression for the thermal stresses becomes [88]:

$$\sigma_{th} = [C][B][K]^{-1} F \quad (2-16)$$

Based on the governing equations presented, it was observed that the solution of thermal stress development is achieved using thermal and stress numerical analyses. Results from the heat transfer analysis are fed through to the appropriate stress analysis [92].

### 2.7.1 Review on Past Research Works of FEM in Ceramic/Metal Joint

Until recently, extensive studies had been carried out to study the residual stresses of ceramic-metal joints using FEM. Suganuma et al. [66],[75] in their series of research work in 1984 and 1985 by finite element analytical model, had shown that in joining dissimilar materials, there is formation of axial tensile stresses near the free surfaces of the materials with lower thermal expansion coefficient. The stresses that developed during cooling formed adjacent to the interface. In the former work, FEM also applied to select the suitable interlayer materials for optimum diffusion bonding of Al<sub>2</sub>O<sub>3</sub>/ferritic steel joint. The thickness of interlayer consisted of Nb, Mo, Ti, or Al<sub>2</sub>O<sub>3</sub>-50 vol. % Fe cermet was varied between 0.2 to 2 mm. The joint was cooled from 702°C and assumed to be pure elastic. It was observed that the tensile residual stress decreases as the interlayer thickness increases. Nb was found to be the most suitable interlayer for the Al<sub>2</sub>O<sub>3</sub>/ferritic steel joint as the thermal expansion coefficient of the Nb is almost similar to the alumina. They have come out with the countermap of maximum residual stress of Si<sub>3</sub>N<sub>4</sub>/steel joint, shown in Figure 2-6, in the latter work. The residual stress distribution, obtained by FEM, was a result of cooling from 800°C to room temperature fully elastically.

Kurita and Yoneda [3] , in 1993, had employed 2- and 3-dimensional FEM to evaluate residual stress in Si<sub>3</sub>N<sub>4</sub>/S45C joint. The results then compared with the XRD. It was observed that the residual stress values measured by XRD were closer to the values calculated by 3-dimensional FEM than the 2-dimensional FEM. It was also found that stress concentration occurred in the interfacial region and as the distance from the interface increased, both the stress values calculated by the 2-dimensional

and 3-dimensional FEM's agreed and decreased to zero. The maximum tensile stress was found occurred at the corner of the silicon nitride near the interface on the surface of the specimen.

Williamson et al. [13] , in 1995, had computed residual stresses and strains that developed in a joined  $\text{Al}_2\text{O}_3$ -Ni specimen during cooling from the fabrication temperature of  $827^\circ\text{C}$ . The numerical solution was obtained using the ABAQUS computer program. Spatially uniform cooling was assumed and the ceramic/metal joint was assumed to be perfectly bonded at the interface. The analysis was an elasto-plastic in which the  $\text{Al}_2\text{O}_3$  was treated as pure elastic while plasticity permitted within the Ni and any interlayer materials. The concept of stress and strain control via interlayers was studied. Simulations were performed for a sharp interface (no interlayer), a 2 mm thick compliant interlayer (simulating a braze alloy), a 2mm thick 50 vol. % Ni-50 vol. %  $\text{Al}_2\text{O}_3$  and an 8 mm thick linearly-graded FGM interlayer. Graded interlayers were treated as a series of perfectly bonded composite interlayers and each interlayers was assigned with different material properties. It was found that the stress distributions are highly dependent upon the interlayer properties. They also claimed that stress reductions are only predicted when the interlayer is highly compliant i.e. low yield strength material exhibiting ductility, or when an optimized i.e. thicker interlayer and nonlinear composition profile FGM is utilized. The results of utilizing composite interlayer have been discussed previously. Similar to the composite interlayer, increasing thickness of FGM also resulted in reduction of the stress level. In addition to reducing the magnitude of the peak stress, the graded interlayer also found effective in diminishing stress gradients and edge-induced shear stresses.

Soon-Bok and Jong-Ho [18] , in 1997, also utilize FEM to study the residual stress distribution of  $\text{Si}_3\text{N}_4$  and S45C (carbon steel). Two joints were considered which are  $\text{Si}_3\text{N}_4/\text{S45C}$  and  $\text{S45C}/\text{Si}_3\text{N}_4/\text{S45C}$  joint. The analysis was performed using ABAQUS code and temperature was allowed to drop from  $527^\circ\text{C}$  to  $27^\circ\text{C}$ . From the analysis, it was observed that the maximum residual stress of the  $\text{Si}_3\text{N}_4/\text{S45C}$  joint was lower that the  $\text{S45C}/\text{Si}_3\text{N}_4/\text{S45C}$  joint.

Raevska [93] , in 1998, had also used FEM in the effort of reducing the residual stresses developed in the ceramic metal joint.  $\text{Al}_2\text{O}_3$ -alloy covar were modelled and the effect of joint design, number of material couples, the interlayer and its thickness and the application of pressure during cooling were investigated. The specimens were allowed to cool from the temperature of  $1200^\circ\text{C}$  to room temperature. Through the analysis, Raevska suggested that the replacement by symmetrical joints, with axis of symmetry lies in the metal, is an opportunity for reducing the undesirable tensile stresses in the ceramic component on a ceramic-metal joint. It was observed that the tensile stresses reduce with the increases of number of sets of similar ceramic metal joints. It was also suggested that increasing thickness of the interlayer must be handled with care as it may impose negative effect on the joint strength. Raevska had also found that the magnitude of the stresses can be reduced by the application of pressure during cooling of the joint.

Abed et al. [94] , in 2001, had examined distribution of residual stresses in sandwich-like joint of sialon and austenitic stainless steel i.e., sialon-steel-sialon. The analysis was carried out using the finite element software ANSYS and the model was treated as pure elastic. Cooling was allowed from the fabrication temperature of  $1250^\circ\text{C}$ . They had found that the residual stress was distributed symmetrically in the sandwich-like joint. Another conclusion drawn was that the increasing thickness of the steel interlayer will produce higher magnitude of axial and radial stress. The FEM analysis was made based on the result of their experimental work i.e., reaction layers were included in the analysis. As a result, FEM also used to determine the material properties of the reaction layers.

Another research work that concentrated on the residual stress distribution in the ceramic-metal joint was carried out by Zhang et al [43] in 2002, also utilizing FEM. Residual stresses and strains that developed in the  $\text{Al}_2\text{O}_3$ -SS304 specimen, with Ni as the interlayer, as it is cooled from the fabrication temperature of  $1300^\circ\text{C}$  to room temperature of  $30^\circ\text{C}$  were studied. The effect of the interlayer thickness also investigated. Through the research, they had concluded that the ceramic parts near to the interface have high residual stress and are prone to cracking. The FEM results obtained were consistent with the fractographic analysis of the bending specimen.

Zhang also claimed that the magnitude of the residual stresses decreases with increases of the interlayer thickness.

Travessa et al. [51] also in 2002 had utilized FEM to evaluate the magnitude of the stresses by incorporating various interlayers, i.e., Ti, Ni, Cu and Mo. The thickness of the interlayers were varied between 0.1 and 0.5 mm. Bonding was performed at various temperature and time where the former ranging from 700 to 1000°C and the latter ranging from 15 to 180 minutes. From the analysis, it was concluded that the most important features in selecting the interlayer is the ductility of the material. This was proven as FEM resulted in the very similar residual stress distribution and magnitude when Ti or Ni was employed as the interlayer material. Ti and Ni have considerable differences on thermal expansion coefficient and elastic modulus, however, their yield strength is very similar. Thus, the magnitude and distribution of the stresses is almost the same. It was also observed that the stresses were further reduced as more interlayers used. The reduction in the magnitude of the stresses was significant as Ti-Mo were used as the interlayers instead of only Mo. Travessa et al. claimed that the behaviour can be attributed to the plastic deformation of Ti.

The influence of an interlayer's construction and thickness on thermal residual stresses generated in ceramic-metal joints was carried out by Pietrzak et al. [72] in 2007. They first examined the stress level in directly jointed model of Al<sub>2</sub>O<sub>3</sub>-heat resisting steel and found that the maximum tensile stress i.e., axial stress concentrated in the ceramic. When introducing FGM into the Al<sub>2</sub>O<sub>3</sub>-heat resisting steel joint, it was found that the stress level decreases by 50% than the original magnitude. Pietrzak et al. also concluded that the application of a gradient material consisting of three layers is a satisfactory solution for the assumed bonding model and a further build-up of the gradient material by additional layers did not give significant amount of stress reduction. It was also recommended to use the thickest layer of FGM close to the ceramic. It was observed that the application of FGM not only reduces the stress level but also shifted the location of their maximal value from the surface deeper inside.

Shen et al. [95] , in 2009, had calculated the residual stress distribution in Al<sub>2</sub>O<sub>3</sub>-TiC/W18Cr4V diffusion bonded joints using FEM. They had found that the gradient

of the axial and shear residual stress are great near the joint edge and are flat near the center. They also found that the maximal value of the tensile axial stress is located at the ceramic side, near the edge.

Hattali et al. [70] , also in 2009, had evaluated the magnitude and distribution of residual stresses in alumina/nickel alloy joints in order to determine the optimum fabrication parameters so the joints can be used for high temperature applications. Elasto-plasto-creep models have been adopted using ABAQUS code. Fabrication temperature was set to 1150°C and spatially uniform cooling was assumed. The importance of the joint geometry i.e., ratio of the length of the contact area to the thickness of the nickel was observed in this paper. Results showed that the highest tensile stress appeared at the edge of the boundary and shear stress present at the ceramic side near the joint interface. Through the fractographic analysis of the shear specimen, it was observed that crack initiates at the edge of the interlayer and then changes its direction into the ceramic and propagates into the ceramic part near the interface. The results were compared with the X-ray measurement and indentation fracture method and shows good correlation.

As described above, it can be seen that most of the previous researchers have concentrated on employing either  $\text{Si}_3\text{N}_4$  or  $\text{Al}_2\text{O}_3$  as the material to be joined with metal. In this research work, different material i.e., sialon was chosen to be joined with metal. Sialon, a man-made ceramic, is a combination of  $\text{Si}_3\text{N}_4$  and  $\text{Al}_2\text{O}_3$  and is believe to exhibit greater properties than the constituent materials. So far, investigations have been confined to the magnitude and distribution of residual stresses as well as methods to reduce the stress level.

## **2.8 Chapter summary**

This chapter has presented the theoretical knowledge and literature review on the ceramic/metal joint.

The discussion in the chapter begins with a brief summary of the materials to be joined as well as the benefit gain from the joint, techniques to join the materials and the problem arise in joining the materials. The methods of evaluating the problem



were the presented with the support of the related preceding research works on the area.

The key to successful numerical analyses relies on the selection of materials properties, the proposed mechanisms for interface formation, and the development of elastic or elastic-plastic deformation models [16]. Ceramic metal joint was first modelled as pure elastic [96]. The accuracy of FEM results further improved as elasto-plastic behaviour of the metallic component started to be adopted in the model [13]. Further improvement in the accuracy of the result was made possible by taking into account the transient response of the materials evaluated.



## CHAPTER 3

### MATERIALS AND METHODOLOGY

As clearly discussed in chapter 2, it can now be clearly understood that the formation of residual stress in the ceramic/metal joint is critical to the joint reliability. Magnitude and distribution of residual stress in sialon/AISI 430 ferritic stainless steel joint as well as the effect of geometrical parameters on the stress level are presented in this study.

#### **3.1 Chapter overview**

This chapter deals with the problem description and justification on method chosen to conduct the research. It concerns primarily on the materials selected and how the analysis were done.

Properties of the materials involved in the analysis were presented in this chapter. Methodology of utilizing FEM to solve the problem was addressed by discussing the details on the assumptions made in the analysis, geometry employed, element type chosen to represent the materials, meshing and description of the model.

Furthermore, the verification methods use to check the accuracy of the FEM model was also described in detail this chapter.

#### **3.2 Research procedure**

This project was started with the literature review on the related topic in order to gain the main idea on how the projects were carried out previously. Literature review was used to learn how others have utilized FEM in determining residual stresses in the ceramic metal joint. Assumptions and methods employed in the previous research

works were studied thoroughly. Besides establishing the theoretical framework for this project, literature review also provided information on the state of research in this field.

The next step was data gathering which was also done through the literature review. Material properties of each material used in the project were collected.

The research was then followed by modelling and simulating the residual stress across the sialon/AISI 430 ferritic stainless steel joint using ANSYS. The analysis was carried out in three stages here, which are 1) pre-processor phase, 2) processor (solution) phase, and lastly 3) post-processor phase. The problem was defined in the pre-processor phase and solved in the solution phase. Results obtained were reviewed and analyzed in the post-processor phase.

The FEM results were then compared with the calculation and literature review. Conclusions based on the findings were made at the end of the research.

### **3.3 Materials**

The proceeding sections will discuss the materials modelled in this analysis. The model used represents a cylinder shape joint of sialon ceramic and AISI 430 ferritic stainless steel.

#### **3.3.1 Sialon**

Sialon was modelled with the dimensions of 20 mm in diameter and 4 mm in thickness. The properties, thermal expansion coefficient that varies with temperatures and compositions of the sialon are given in Table 3-1, Table 3-2 and Table 3-3 respectively. Thermal expansion coefficient and composition of sialon shown in Table 3-2 and Table 3-3 respectively were experimentally tested using dilatometer and X-Ray Fluorescence (XRF) at AMREC, Kulim.

Table 3-1 Material properties of the ceramic and metal employed [97],[98].

<i>Material</i>	<i>Sialon</i>	<i>AISI 430</i>
E (GPa)	290	200
$\nu$	0.23	0.27
$\sigma_y$ (MPa)		275
$\rho$ (kg m <sup>-3</sup> )	3240	7800
$\lambda$ (W m <sup>-1</sup> K <sup>-1</sup> )	21	26.1
$C_p$ (J kg <sup>-1</sup> K <sup>-1</sup> )	600	460

E, Young modulus;  $\nu$ , Poisson ratio;  $\sigma_y$ , yield strength;  $\rho$ , density;  $\lambda$ , thermal conductivity;  $C_p$ , specific heat.

Table 3-2 Temperature-dependent coefficient of thermal expansion ( $\alpha$ ) of sialon and AISI 430 ferritic stainless steel.

<i>Temperature (K)</i>	$\alpha_{sialon} (10^{-6} K^{-1})$	$\alpha_{AISI 430} (10^{-6} K^{-1})$
304	8.9	9.3
374	5	10
474	3.1	10.2
573	2.5	10.3
675	2.5	10.5
775	2.6	10.5
875	2.8	10.5
974	2.7	10.4
1075	2.5	10.7
1175	2.1	10.9
1275	1.8	10.7
1375	1.3	10.7
1474	-0.1	11.2
1570	-1.8	11

### 3.3.2 Ferritic stainless steel

The metal used in this work is AISI 430 ferritic stainless steel. AISI 430 ferritic stainless steel was in the thickness of 1.2 mm. The properties, , thermal expansion coefficient that varies with temperatures and compositions of the AISI 430 ferritic stainless steel are given in the Table 3-1, Table 3-2 and Table 3-3 respectively. Thermal expansion coefficient and composition of steel shown in Table 3-2 and Table 3-3 respectively were experimentally tested using dilatometer and Arc Spark at AMREC, Kulim.

Table 3-3 Chemical composition of sialon and AISI 430 ferritic stainless steel.

<i>Element</i>	<i>Sample Concentration (wt %)</i>	
	<b>Sialon</b>	<b>SS_AISI430</b>
Fe	NC	Remainder
Si	Remainder	0.227
Mn	NC	0.313
P	NC	0.026
Cu	NC	0.098
Ni	NC	0.115
Cr	NC	15.718
Mo	NC	0.130
Ti	NC	0.002
Y	NC	NC
Al	3.5707	NC
C	NC	0.062
S	NC	0.003
O	2.8656	NC
N	1.5755	NC

### **3.4 Finite element modelling**

In this research, commercial finite element software was employed to determine the magnitude and distribution of the residual stress in the sialon/AISI 430 ferritic stainless steel joint. The analysis was carried out using ANSYS 11 provided in the CAE/CFD lab of Universiti Teknologi PETRONAS.

The main steps involved in this ANSYS session consisted of the following:

1) Preprocessing Phase

- Create model geometry
- Define element type
- Define material properties
- Mesh the model
- Apply the appropriate loads and boundary condition

2) Solution Phase

- Compute the solution

3) Postprocessing Phase

- Review and analyze results

#### **3.4.1 Assumptions**

A few assumptions, based on Abed et al. report [94], were made in this analysis. These assumptions are:

- 1) No external mechanical load is applied and hence a residual stress field is created by the mismatch of thermal expansion coefficients alone.
- 2) There are perfect interfaces between the materials as the materials were assumed to be perfectly bonded at the temperature of 1200°C.

- 3) The sample shrinks freely in the x- and y-directions as to allowed free deformation of the materials.

Two mediums of heat transfer allowed in the analysis. Conduction is between the two materials while convection is between the materials and the environment. However, the convection was allowed only at the top and side surface of the joint. The bottom of the joint was assumed to be adiabatic since it was placed on the floor of the furnace during heating and cooling of the joint. The symmetry axis was default to adiabatic boundary conditions.

### 3.4.2 Geometry of the sialon/AISI 430 ferritic stainless steel joint

A cylindrical shaped AISI 430 ferritic stainless steel of 20 mm in diameter and 1.2 mm in thickness with 4 mm thickness of sialon on the top surface was considered. Figure 3-1 shows the schematic representation of the sialon/AISI 430 ferritic stainless steel joint.

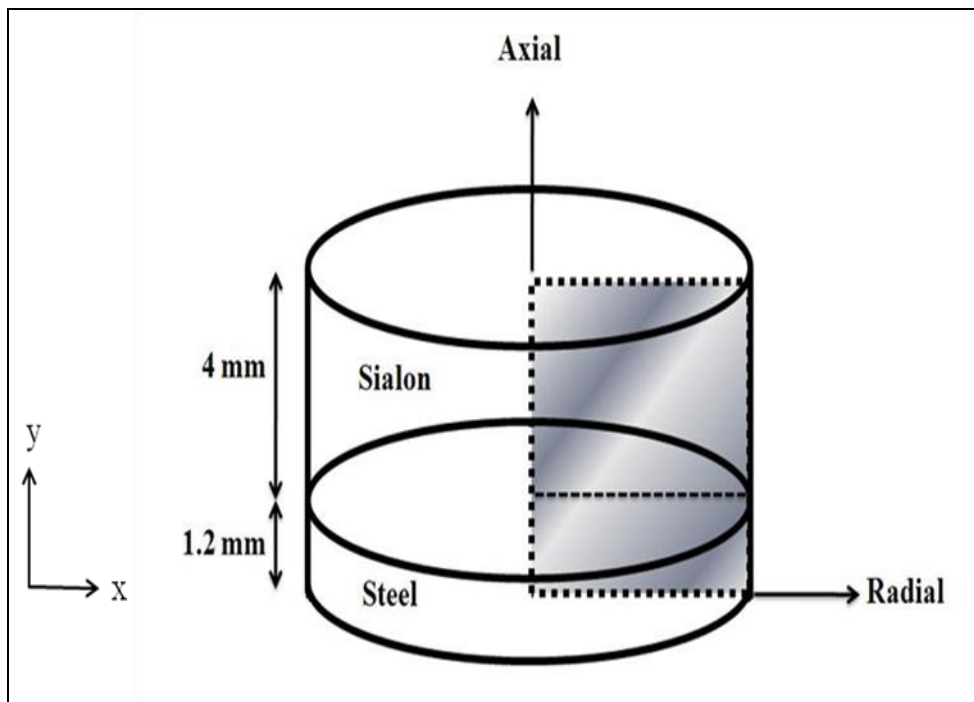


Figure 3-1 Schematic representation of the sialon/AISI 430 ferritic stainless steel joint



Since the model geometry is symmetrical in axial direction, the problem was analyzed as two-dimensional problem, as shown in Figure 3-2.

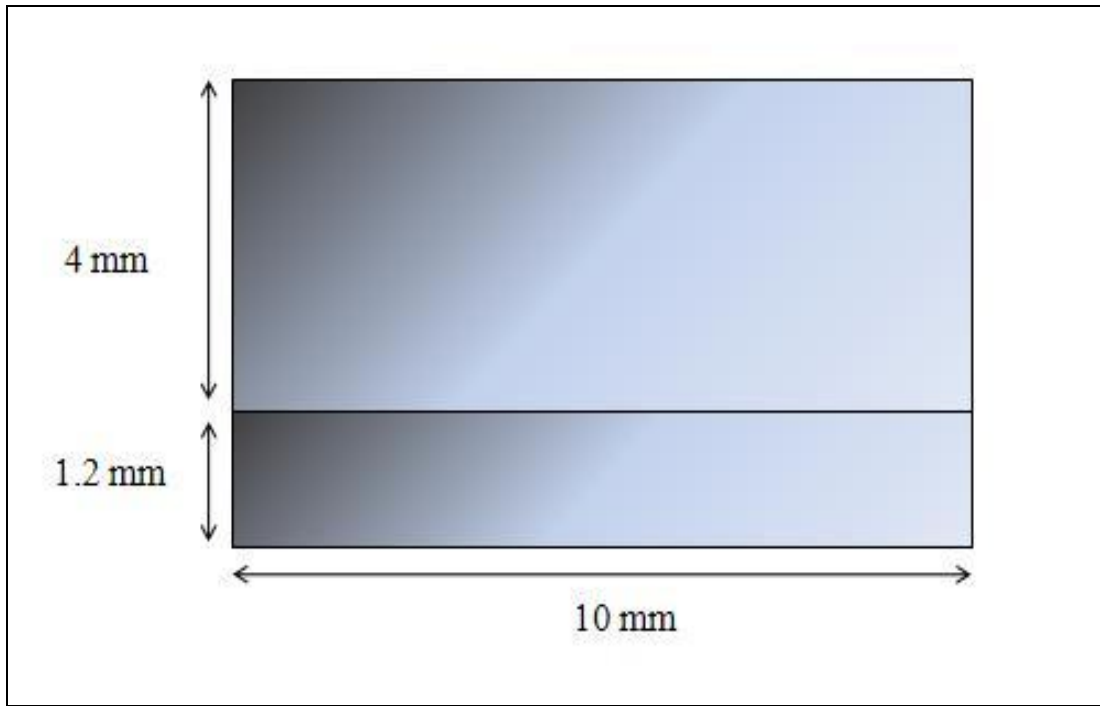


Figure 3-2 Schematic representation of the model geometry resulted from the geometric simplification, showing the dimensions used in the analysis

### 3.4.3 Selection of element type

Sequential coupled thermal- structural analysis was performed. The analysis was conducted in two steps. First, nodal temperatures were obtained from thermal analysis. The thermal result then applied as the load for the second step of the analysis, which was the structural analysis. Thermal stresses were computed in the second step of the analysis.

PLANE55 was chosen as element type for the thermal analysis. PLANE55 is a four node quadrilateral element used in modeling two-dimensional conduction heat transfer problems. The element has a single degree of freedom, the temperature. Convection or heat fluxes may be input at the element faces. Output data include

nodal temperatures and element data, such as thermal gradient and thermal flux components [85]. The geometry of PLANE55 is shown in Figure 3-3.

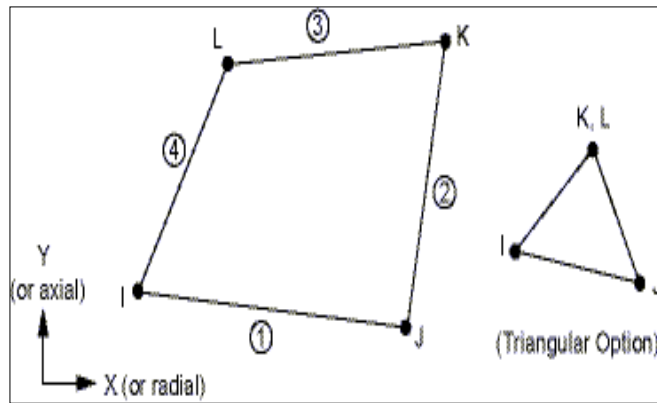


Figure 3-3 PLANE55 geometry

For the structural analysis, the four-node quadrilateral element PLANE42 has been used. PLANE42 is normally used in modeling solid problems. The element is defined by four nodes, with two degrees of freedom at each node, the translation in  $x$ - and  $y$ -directions. The element input data can include thickness if KEYOPTION 3 (plane stress with thickness input) is selected. Surfaces pressure loads may be applied to element faces. Output data include nodal displacements and element data, such as directional stresses and principal stresses [85]. The geometry of PLANE42 is shown in Figure 3-4.

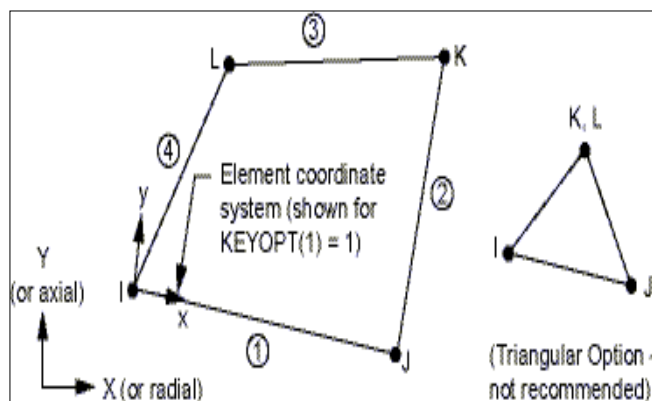


Figure 3-4 PLANE42 geometry

#### 3.4.4 Meshing of the model

The model was imparted with mapped meshing in a way that region near the joint interface and the free surface occupied with finer mesh. Element size of 0.05 was used throughout the analysis. The left boundary of the mesh corresponds to the symmetry axes were constrained in radial direction. All other boundaries remain free as to permit bending to occur during cooling. Details of meshing and constrains employed are shown in Figure 3-5. The problem was subdivided into 21105 nodes and 20800 elements.

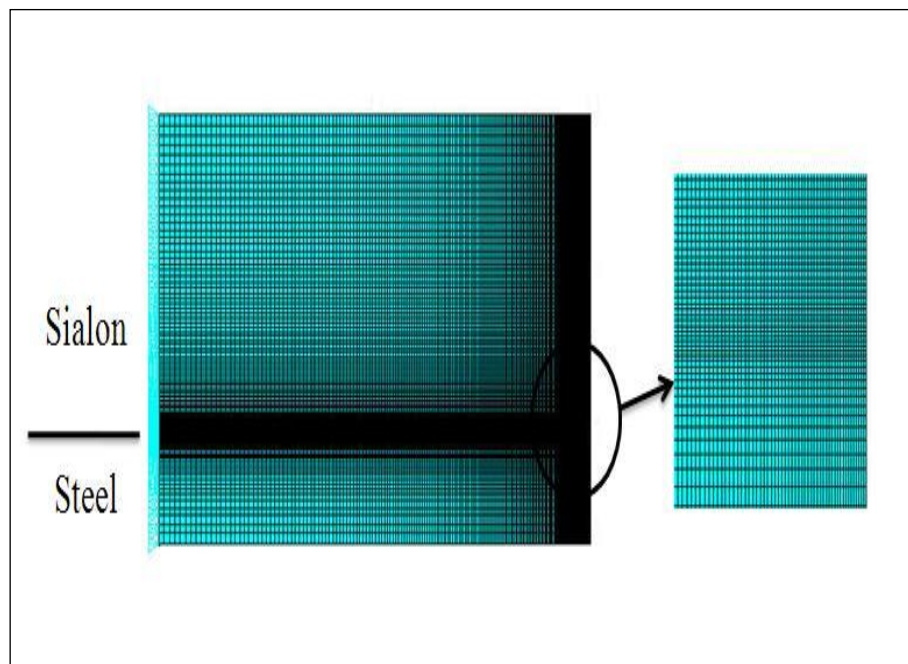


Figure 3-5 Details on meshing and constraints employed.

#### 3.4.5 Modelling of the sialon/AISI 430 ferritic stainless steel joint

For simplicity, the joint was first modeled as pure elastic to verify the effectiveness of the FEM. Furthermore, the calculation method that will be used to verify the FEM result did not take into account the plastic deformation of the metal.

For more accurate result, sialon was then treated as elastic while plasticity permitted within AISI 430 ferritic stainless steel. Elasto-plastic regime for the metal

which governed by von Mises yield and the associative Prandtl-Reuss flow rule were adopted. The equivalent Mises stress is given by the expression [99]:

$$\sigma_m = \sqrt{\frac{(\sigma_1 - \sigma_2)^2 + (\sigma_2 - \sigma_3)^2 + (\sigma_3 - \sigma_1)^2}{2}} \quad (3-1)$$

where  $\sigma_1$ ,  $\sigma_2$  and  $\sigma_3$  are principal stresses. When  $\sigma_m$  reaches the yield strength, the material begins to deform plastically.

The constitutive behavior of AISI 430 ferritic stainless steel was modeled using bilinear kinematic hardening i.e. the real stress-strain curves can be approximated by a series of straight lines. Transient thermal stress analysis was conducted for a total time of 14400s i.e. four hours. Transient thermal analysis determines the temperature distribution and other thermal quantities under conditions that vary over a period of time. Coefficient of thermal expansion (CTE), modulus of elasticity, poisson's ratio, density, specific heat, thermal conductivity as well as yield stress for AISI 430 ferritic stainless steel and sialon are given in Table 3-1 and Table 3-2.

Only thermal loading was employed to the model as sialon and stainless steel are assumed to be perfectly bonded at the interface at the fabrication temperature of 1200°C. Thus, stresses only developed during cooling down to room temperature. Modes of heat transfer applied in the analysis were conduction and convection. The convection heat transfer coefficient,  $h$ , used was that of still air. Figure 3-6 shows the representative finite element model for the problem.

### 3.4.6 Modeling the effect of geometrical paramaters

Thermal expansion coefficient mismatch effect in the ceramic/metal joint is a serious problem because even if a strong interface could be achieved, joints with large residual stress are easily broken [27]. The developments of residual stresses originated from the thermal expansion mismatch and induced during cooling down from the fabrication temperature strongly influence the joint integrity. Materials with low elastic modulus can accommodate strain and tend to deform under the influence of

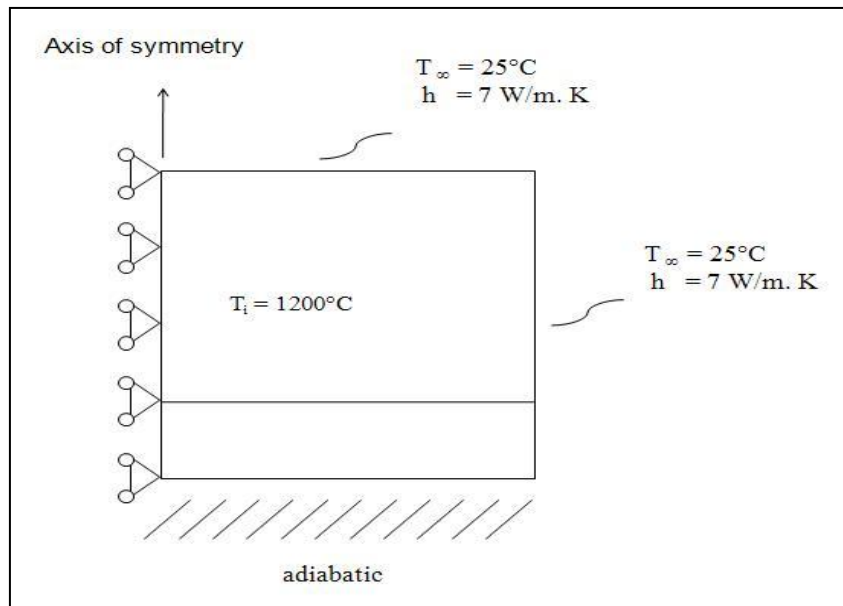


Figure 3-6 Schematic representation of boundary conditions.

these stresses. However, brittle material such as ceramic and glass will have a tendency to fracture.

Sialon, like any other ceramic can bear with compressive stress but not tensile stress. They tend to fracture under the influence of high tensile stress. Thus, in the effort of reducing the magnitude of the tensile stress, it is important to analyze the factors influencing these stresses. Suganuma, in his series of work [68],[69], has suggested that the magnitude of the residual stress depends on a number of aspects such as the thickness of the materials, diameter of the joint and joint design.

Further analyses were made to study the effect of each parameter on the magnitude of the stress by varying it, for example, thickness of sialon was varied, while fixing the other parameters constant i.e. diameter of the cylindrical joint is 20 mm and same joint design was used throughout the analysis.

When analyzing the effect of sialon thickness, the ratio of thickness of sialon to AISI 430 ferritic stainless steel,  $n$ , were varied from 0.8 to 12.5. ( $n$  is the ratio of thickness of sialon,  $h_{si}$ , to the thickness of stainless steel,  $h_{st}$ ;  $n = h_{si}/h_{st}$ ). Meanwhile, when analyzing the effect of the cylindrical diameter, the ratio of diameter to the thickness of the seal,  $R$ , were varied from 0.3 to 2. ( $R$  is the ratio of joint diameter,  $d$ , to the thickness of the seal,  $h$ ;  $R = d/h$  where  $h = h_{si} + h_{st}$ ).

Effect of joint design was studied by comparing the magnitude of maximum tensile stress developed in asymmetrical joint with symmetrical joint shown in Figure 3-7. The ratio of thickness of ceramic to metal,  $n$ , were varied from 1 to 10 in the analysis.

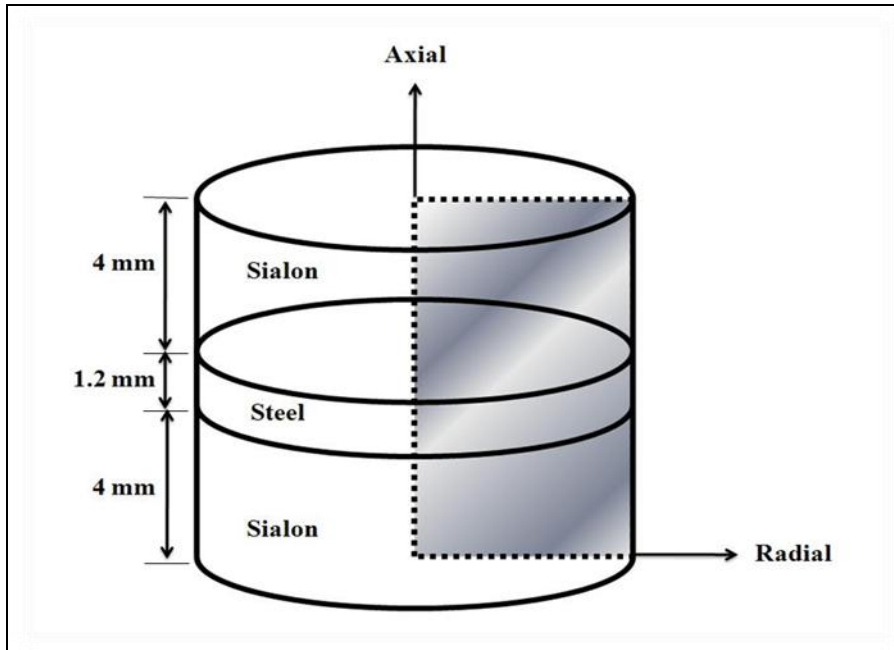


Figure 3-7 Schematic representation of symmetrical joint

Interlayer was incorporated in the sialon/AISI 430 ferritic stainless steel joint in the effort of reducing the tensile stress developed in the joint. The effect of interlayer and their thickness studied by treating the model as a series of perfectly bonded materials. Interlayer considered for the analysis were Cu, Ni, Ti and Mo. Since incorporating interlayer involve large amount of plastic deformation and require longer time, the analysis was done as steady-state. In the steady state analysis, the temperature distribution was assumed to be uniform, to avoid the need to solve a heat-transfer equation during the iterative process. The assumption is quite straightforward considering that cooling times are usually long enough based on the thermal diffusivity of metals and the relatively limited size of the joints [36]. The properties of the materials used were shown in Table 3-4. The interlayer was inserted in between of sialon and AISI 430 ferritic stainless steel, as shown in Figure 3-8. Thicknesses of the interlayer were varied from 0.5 mm to 1 mm.

Table 3-4 Material properties of the interlayer materials employed [51].

<i>Material</i>	<i>Cu</i>	<i>Ni</i>	<i>Ti</i>	<i>Mo</i>
$\alpha$ ( $10^{-6} \text{ K}^{-1}$ )	18.0	13.4	8.4	4.8
E (GPa)	125	200	110	275
$\nu$	0.34	0.31	0.34	0.29
$\sigma_y$ (MPa)	71	150	140	340
$\rho$ ( $\text{kg m}^{-3}$ )	8940	8890	4510	1020
$\lambda$ ( $\text{W m}^{-1} \text{ K}^{-1}$ )	153	88	17	138
$C_p$ ( $\text{J kg}^{-1} \text{ K}^{-1}$ )	380	460	528	251

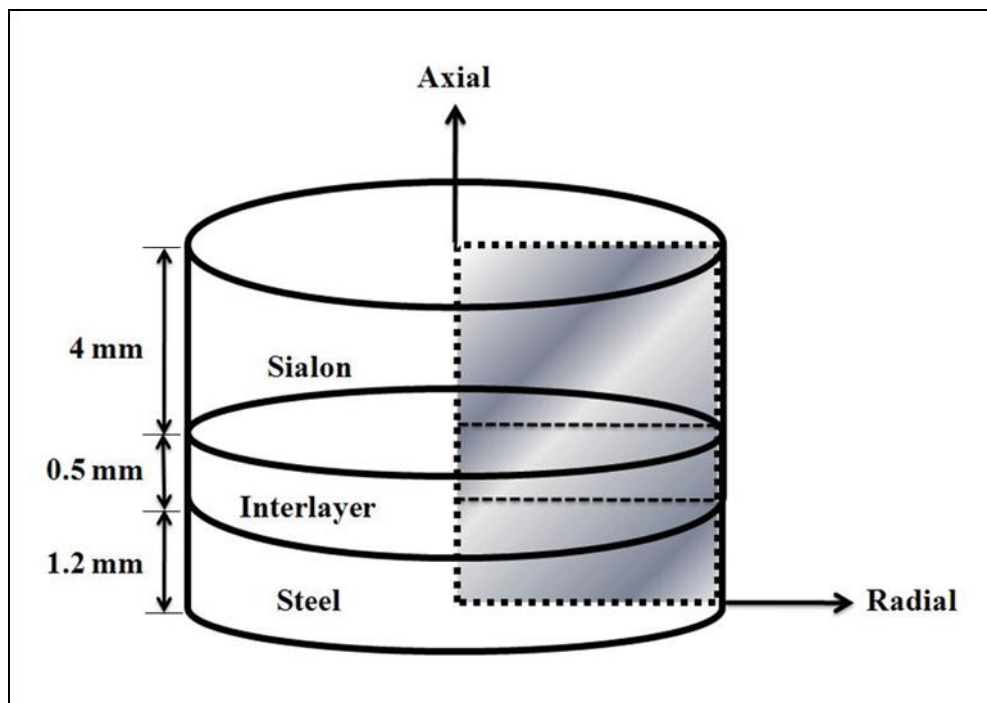


Figure 3-8 Schematic representation of the sialon/AISI 430 ferritic stainless steel joint with interlayer

### **3.5 Verification of the FEM analysis on the residual stress generated in sialon/AISI 430 ferritic stainless steel joint**

Verification of the FEM was conducted in order to verify the accuracy of the finite element model. The verification was performed by two methods which are by stress equation and comparison with literature review.

#### **3.5.1 Verification by using stress equations**

The calculation was made using the equations described in the literature review [81],[82] discussed on pages 33 and 34. The verification by calculation was made for the symmetrical joint shown in Figure 3-6 as to match the model used by the stress equations, shown in Figure 2-10. Model was treated as perfectly elastic. The analysis was carried out as steady-state analysis i.e. the results were not varied with time.

Equations (2-3), (2-4) and (2-5) discussed on page 33 and 34 were used in this analysis. In this calculation, A and B in the equations were referred as sialon and AISI 430 ferritic stainless steel, respectively. Calculation was carried out by substituting all of the dimensions and properties of sialon and AISI 430 ferritic stainless steel, given in Table 3-1, into the equations. The calculation results were then compared with the FEM results.

#### **3.5.2 Verification by using literature review**

Verification was made by substituting the properties used by Travessa et al [51] into present FEM input file. Result obtained was then compared with result shown by Travessa et al. in their paper. Travessa et al. had used FEM to evaluate the residual stress state in  $Al_2O_3$ /AISI 304 joint with various interlayers. For this verification, the interlayer chosen is Ti. The properties of materials used in this analysis are shown in Table 3-4 and 3-5. Figure 3-9 shows the schematic representation of the model used for the verification. Model represents 5 mm  $Al_2O_3$  perfectly joined to 5 mm AISI 304 steel using 0.5 mm Ti interlayer. The cylindrical joint modelled had a diameter of 10 mm. FEM calculation was made to obtain the residual stresses that developed in the



joint as it is being cooled down from the fabrication temperature of 800°C to room temperature of 25°C.

Table 3-5 Material properties of the components used in the comparison of present FEM with Travessa et al.'s work.[51].

<i>Material</i>	<i>Al<sub>2</sub>O<sub>3</sub></i>	<i>AISI 304</i>
$\alpha$ ( $10^{-6}$ K <sup>-1</sup> )	7.8	17.2
E (GPa)	380	193
$\nu$	0.23	0.34
$\sigma_y$ (MPa)		206
$\rho$ (kg m <sup>-3</sup> )	3900	7900
$\lambda$ (W m <sup>-1</sup> K <sup>-1</sup> )	24	16
$C_p$ (J kg <sup>-1</sup> K <sup>-1</sup> )	784	500

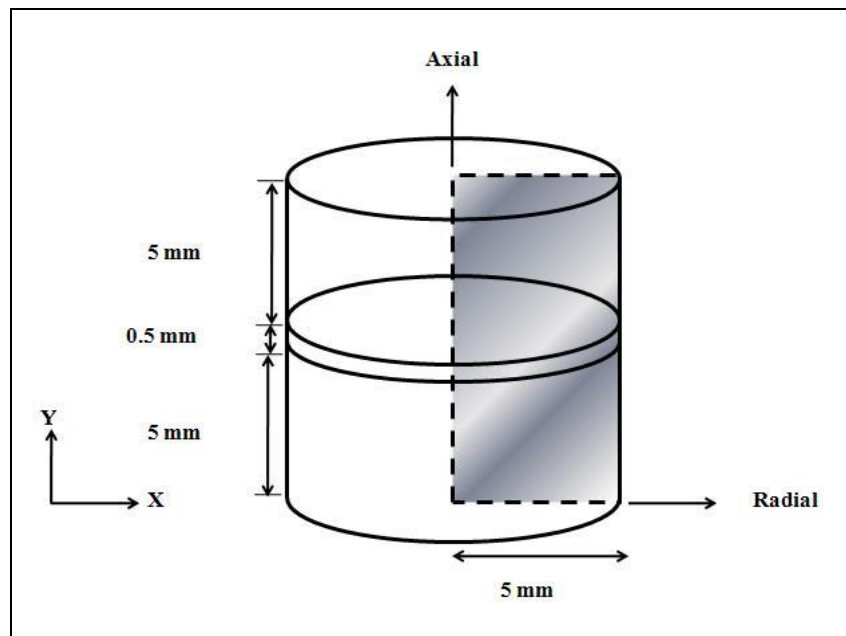


Figure 3-9 Schematic representation of the Al<sub>2</sub>O<sub>3</sub>/AISI 304 steel joint with Ti interlayer

Verification was also performed by comparing with Zhang et al.'s work [43]. Zhang et al. had performed finite element analysis using ANSYS to evaluate the effect of residual stress on the strength of an alumina-steel joint. The material properties employed in the analysis are listed in Table 3-6. The joint modeled was of Al<sub>2</sub>O<sub>3</sub> and AISI 304 with the same dimensions, 12 mm x 20 mm with 0.125 mm Ni interlayer. Figure 3-10 shows the schematic representations of the joint modeled.

Table 3-6 Material properties of the components used in the comparison of present FEM with Zhang et al.'s work [43].

<i>Temperature</i>		<i>&lt;400</i>	<i>400-</i>	<i>600-</i>	<i>800-</i>	<i>1000-</i>	<i>1200-</i>
<i>°C</i>			<i>600</i>	<i>800</i>	<i>1000</i>	<i>1200</i>	<i>1300</i>
<i>Al<sub>2</sub>O<sub>3</sub></i>	$\alpha$ ( $10^{-6}$ , °C)	8.002	8.578	9.154	9.73	10.306	10.594
	E (GPa)	372	372	372	372	372	372
	v	0.27	0.27	0.27	0.27	0.27	0.27
<i>AISI 304</i>	$\alpha$ ( $10^{-6}$ , °C)	20.187	21.147	22.107	23.067	24.027	24.507
	E (GPa)	210	179	170	160	150	142
	v	0.29	0.29	0.29	0.29	0.29	0.29
<i>Ni</i>	$\alpha$ ( $10^{-6}$ , °C)	15.45	16.55	17.65	18.75	19.85	20.4
	E (GPa)	204	190	174	158	144	136
	v	0.31	0.31	0.31	0.31	0.31	0.31

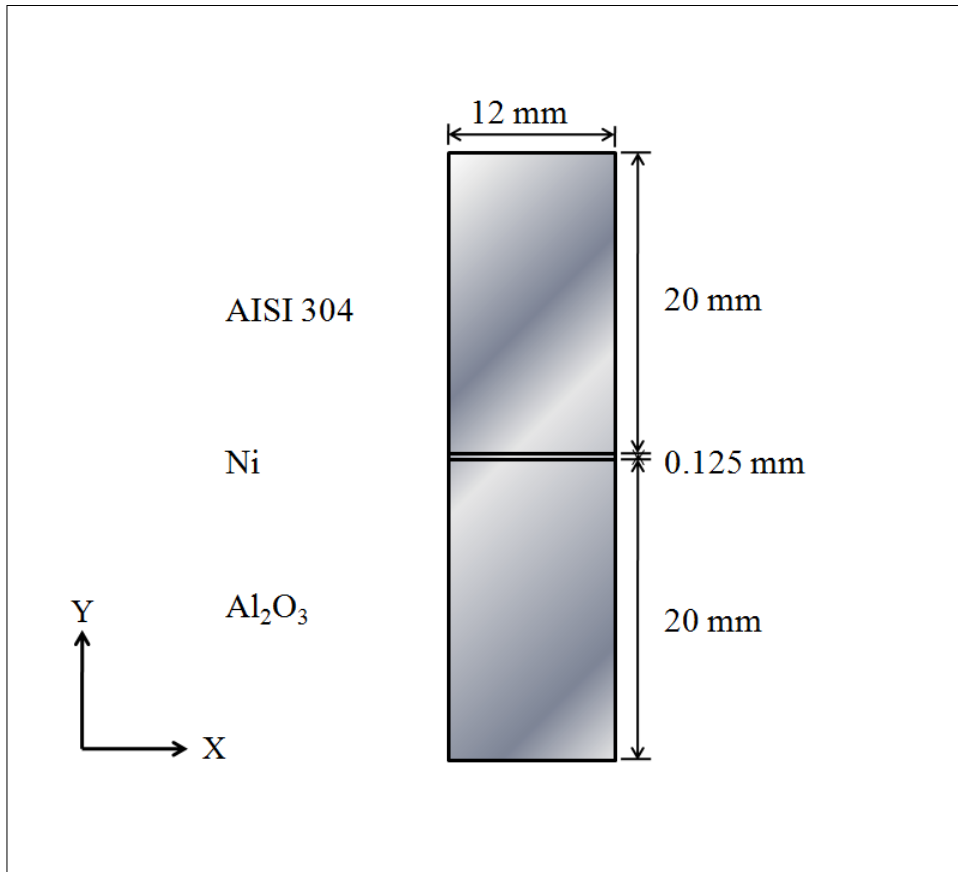


Figure 3-10 Schematic representation of the Al<sub>2</sub>O<sub>3</sub>/AISI 304 steel joint with Ni interlayer

### 3.5.3 Error Analysis

Error was computed using the percent formula as follow:

$$\% \text{ error} = \frac{\text{actual result} - \text{theoretical}}{\text{theoretical}} \times 100 \quad (3-2)$$

### **3.6 Chapter Summary**

This chapter presented the materials and whole methodology involve in this research work.

The chapter begins with a simple review of the research procedure and goes on with the properties of the materials employed in the analysis. Thorough description of utilizing FEM to tackle the problem was then addressed. The use of FEM has enabled the problem to be simplified into two-dimensional problem. The analysis was conducted as thermal-structural problem with plasticity and transient considered.

The verification methods were then presented in this chapter. FEM results will be compared with the stress equation and past work by other author. Details on how to conduct the comparison and calculation of the error were discussed.

## CHAPTER 4

### RESULT AND DISCUSSION

Residual stress developed in the ceramic/metal joint may causes deterioration of the joint strength and may even lead to the fracture of the joint. Thus, it is important to analyze the stress state in the joint.

This study presents the magnitude and residual stress distribution developed in the sialon/AISI 430 ferritic stainless steel joint. The effect of geometrical parameters on the stress level also evaluated as to find the optimum parameters to fabricate the ceramic/metal joint. These findings can be served as a valuable framework in designing the ceramic/metal joint.

#### **4.1 Chapter overview**

This chapter entails the results and discussions of the analysis on the stresses of sialon to AISI 430 ferritic stainless steel joint. A preliminary analysis was performed considering both materials as ideally linear-elastic components. The analysis was conducted to check the applicability of FEM using ANSYS to model and simulate the stress distribution across the ceramic/metal joint.

The analysis was verified using calculation as shown in literature review. Another verification which includes plasticity also carried out by comparing with the literature review. The steel was treated as elasto-plastic material. Meanwhile, plasticity was not allowed in the ceramic due to its brittleness i.e. failure without preceding plastic deformation. Magnitude and distribution of stress across the joint were discussed in details in this chapter. Method of reducing residual stresses were then described by concentrating on the geometrical specifications of the specimen i.e., thickness of sialon, diameter of the cylindrical joint, joint design as well as incorporation of interlayer.

## 4.2 Preliminary analysis

Preliminary analysis was conducted to validate the accuracy of the present FEM. there are two methods used to verify the FEM which are by using stress equation and also by comparing with the literature review. The former will be presented in section 4.2.1 while the latter will be discussed in section 4.2.2.

### 4.2.1 FEM vs. stress equation

In this section, residual stress that generated in the sialon/AISI 430 ferritic stainless steel symmetrically joint will be calculated by using FEM and equations 2-3, 2-4 and 2-5. The results obtained by both methods will be compared later and the percentage difference between the two results will be calculated.

#### *4.2.1.1 Result obtained by using FEM*

In this analysis, sample was cooled from the fabrication temperature of 1200°C to the room temperature of 25°C under the assumption that steel behave elastically without plastic deformation. Since plastic deformation will relieve stress concentrations within the ceramic part, it was expected that the FEM results would over estimate the residual stresses [42].

This preliminary analysis result was obtained and verified using analytical step discussed in literature review. Thus, the joint design considered was made matched to Figure 2-10, i.e. symmetrical joint. Thickness of sialons applied were 4 mm while thickness of steel was 1.2 mm. Diameter of the cylindrical joint was set to 20 mm.

This analysis was conducted in steady state and without variation in coefficient of thermal expansion of sialon and steel as to match the equations used for validation in section 4.2.1.2 later. The thermal expansion coefficient for sialon and steel are  $3.04 \times 10^{-6}$  and  $10.4 \times 10^{-6}$  respectively.

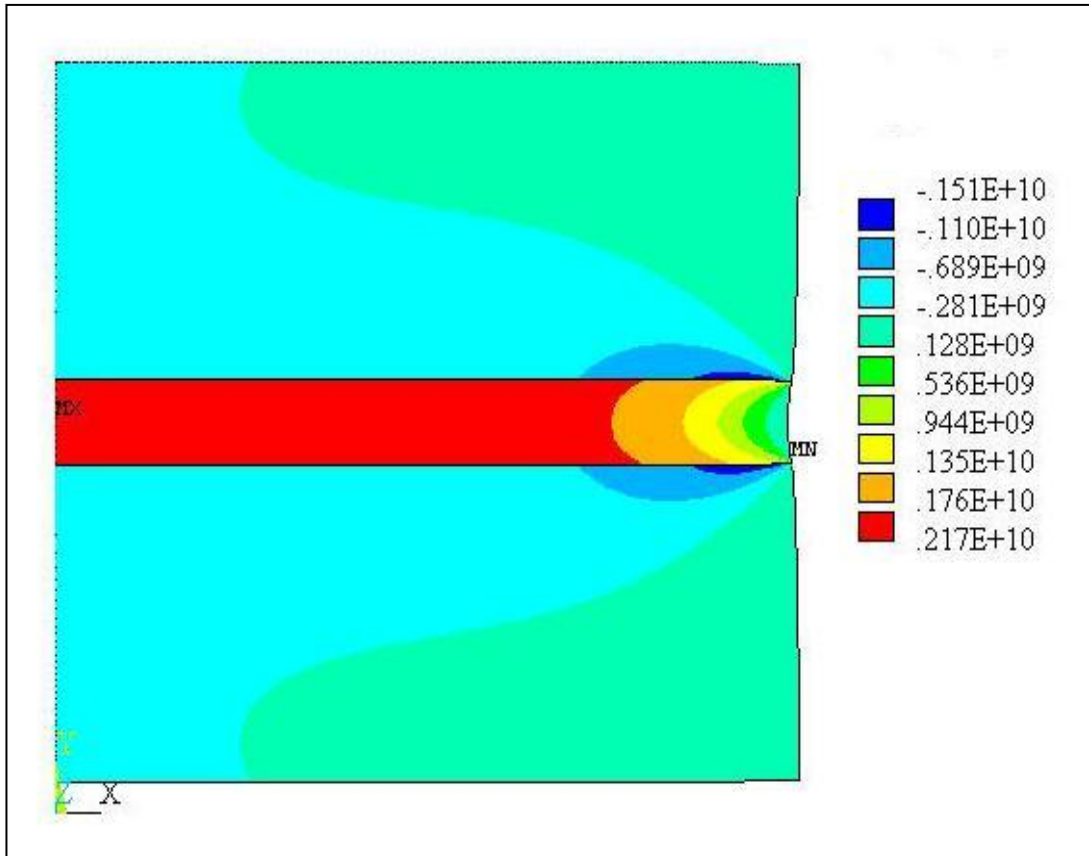


Figure 4-1 Radial stress distribution in fully elastic sialon/AISI 430 ferritic stainless steel joint

Figure 4-1 shows the radial stresses distribution of the sialon/ fully elastic AISI 430 ferritic stainless steel joint. It can be seen that the majority region in sialon experienced compressive stresses while steel on the other hand experienced tensile stresses. The stresses developed in the sialon were in the range of - 1510 MPa to 128 MPa. The average residual stress developed in the sialon region is - 281 MPa. The negative sign indicates that the stress acting in the compressive mode.

Meanwhile, stresses in the AISI 430 ferritic stainless steel were dominated by the tensile stress in the range of 128 to 2170 MPa. The average residual stress in the AISI 430 ferritic stainless steel was 1965 MPa acting in the tensile mode.

#### 4.2.1.2 Result obtained by using stress equation

Calculations were made in order to verify the results obtained via FEM. The equations used was provided and explained in the literature review and methodology section [81]. The properties employed in the calculations are shown in Table 3-1.

a) *Average stress in sialon*

After substitution in the equations (2-3) and (2-5);

$$\Delta\varepsilon_o = (10.4 \times 10^{-6} - 3.04 \times 10^{-6})(1473 - 298)$$

$$\Delta\varepsilon_o = 8.648 \times 10^{-3}$$

$$\sigma_{sialon} = \frac{-(300 \times 10^9)(200 \times 10^9)(0.0012)(8.648 \times 10^{-3})}{(1 - 0.22)((2)(300 \times 10^9)(0.004) + (200 \times 10^9)(0.0012))}$$

$$\sigma_{sialon} = -302 \text{MPa}$$



b) *Average stress in AISI 430 ferritic stainless steel*

After substitution in the equations (2-4) and (2-5);

$$\sigma_{steel} = \frac{(2)(300 \times 10^9)(200 \times 10^9)(0.004)(8.648 \times 10^{-3})}{(1 - 0.27)((2)(300 \times 10^9)(0.004) + (200 \times 10^9)(0.0012))}$$

$$\sigma_{steel} = 2154 \text{ MPa}$$

#### 4.2.1.3 Comparison between FEM and stress equation

As can be seen from Table 4-1, the percentage error of FEM results were 6.9% for average residual stress in sialon and 8.8% for average residual stress in steel. The small percentage error in the FEM results indicated that the FEM can be adopted in analyzing the magnitude of stress in ceramic/metal joint.

Table 4-1 Comparison of FEM and analytical results

Material	FEM result, MPa	Analytical result, MPa	Percentage error, %
Sialon	- 281	- 302	6.9
AISI 430	1965	2154	8.8

Although the results from FEM did not quantitatively 100% in agreement with the results obtained via calculation, it still can provide a simple and valuable framework for predicting the magnitude of stress in the ceramic metal joint.

As plastic deformation of steel was not accounted in this analysis, the stresses developed in the joint were extremely higher than the actual internal stress. However, this type of analysis can still be used as a simple guideline in evaluating the stress distribution in the ceramic/metal joint. Many researches e.g., Zhang et al. [43] , Shen et al. [95] and Abed at al. [94] in fact have utilized this simple elastic method to evaluate the state of stress in the ceramic/metal joint system.

#### **4.2.2 Past model vs. present model**

The comparisons were made between the present model and Travessa et al.'s model [51] as well as between the present model and Zhang et al.'s work [43]. Comparisons were made in terms of the distribution of the stress and also the magnitude of the stress generated. Percentage difference was calculated using the maximum tensile stress generated in both models.

Elasto-plastic analysis was carried out in this verification. AISI 430 ferritic stainless steel was treated as elasto-plastic while plasticity was not allowed in the sialon due to its brittleness.

Figure 4-2 and Figure 4-3 shows the axial stress distribution in the  $Al_2O_3$ /AISI 304 steel joint with Ti as the interlayer. The former was obtained from Travessa et al.'s work while the latter was obtained in the present work. It can be seen that the result obtained in the present work was in good agreement with the literature review, confirming the accuracy of the present work. Not only the stress distribution is almost identical, the stress magnitude only differs by 3.9%. The maximum tensile axial stress found by previous work was 207.9 MPa while the maximum tensile axial stress found via present work was 216 MPa.

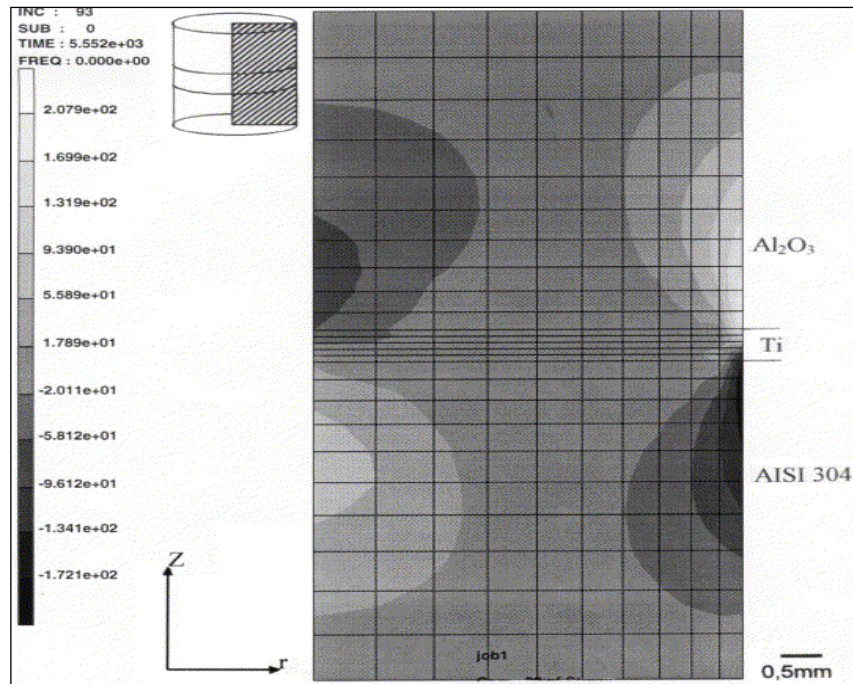


Figure 4-2 Axial residual stress distribution (in MPa) across Al<sub>2</sub>O<sub>3</sub>/AISI 304 steel joint with Ti interlayer [51].

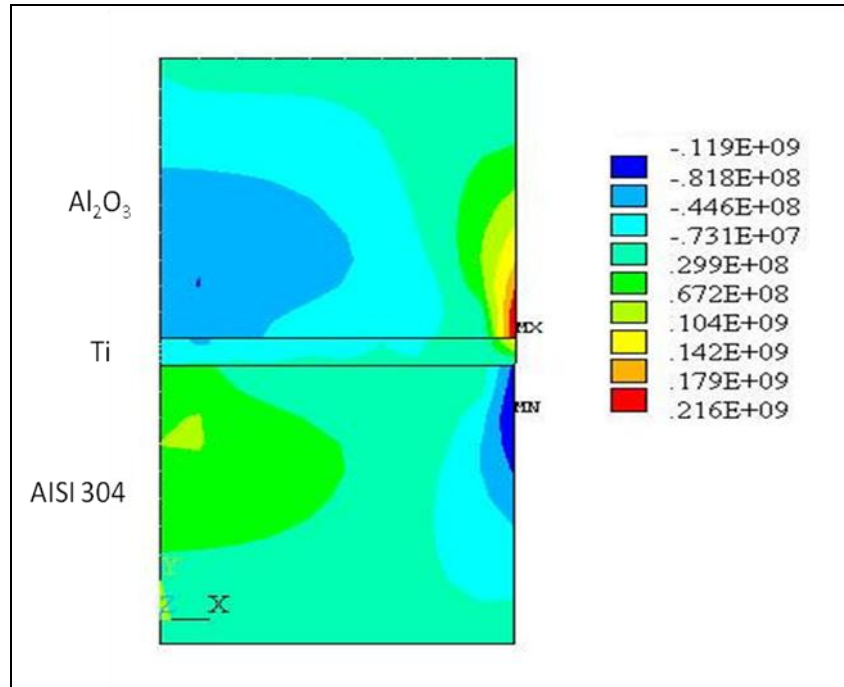


Figure 4-3 Present result of axial residual stress distribution in Al<sub>2</sub>O<sub>3</sub>/AISI 304 steel joint with Ti interlayer.

Figure 4-4 (a) shows the axial stress distribution in Al<sub>2</sub>O<sub>3</sub>/Ni/AISI 304 joint, obtained by Zhang et.al while Figure 4-4 (b) shows the axial stress distribution on the same joint obtained by using present FEM model. Result shows that the stress distribution across the joint obtained by both FEM model are identical. The maximum axial tensile stress obtained by Zhang et al. was 2090 MPa while the magnitude obtained by present FEM model was 2100 MPa. The magnitude of stress obtained by present FEM model only differs by 0.48% than the Zhang et al.'s model.

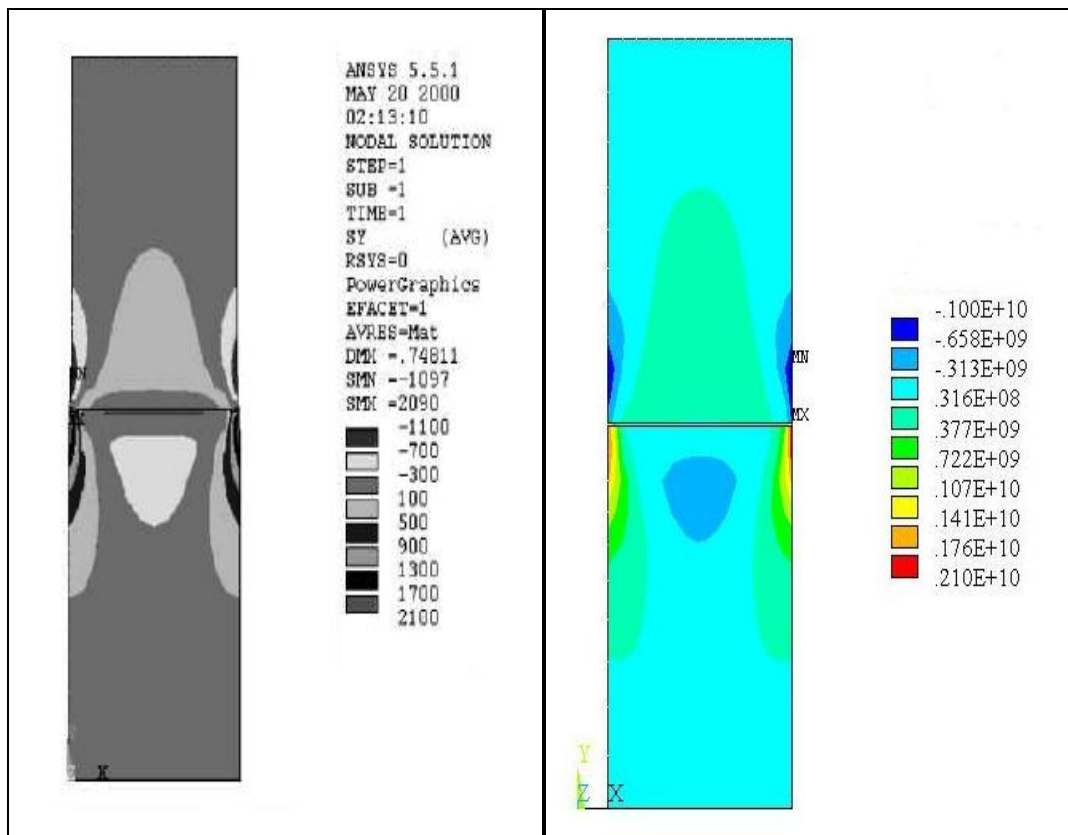


Figure 4-4 (a) Axial residual stress distribution across Al<sub>2</sub>O<sub>3</sub>/Ni/AISI 304 steel joint by Zhang et al.'s work [43], (b) Axial residual stress distribution across Al<sub>2</sub>O<sub>3</sub>/Ni/AISI 304 steel joint by present FEM model.

### 4.3 Elasto-plastic analysis

Transient elasto-plastic analysis was performed to provide more accurate values of stresses developed in the ceramic/metal joint. Since plastic deformation can relieve residual stresses concentration in the joint, it was expected that the magnitude of stresses obtained in this analysis will be lower than the elastic analysis.

#### 4.3.1 Magnitude and distribution of residual stress

Only four stresses i.e. radial, axial, shear and von Mises stress were evaluated since the distribution of the hoop stress is similar to that of the radial stress [20]. The residual stresses components resulting from the FEM are obtained in the following directions as shown in Figure 4-5; 1) radial stress,  $\sigma_x$ , corresponding to the stress value along the radial direction, 2) axial stress,  $\sigma_y$ , component that refers to stress profile through the thickness, and 3) shear stress,  $\tau_{xy}$ , components that acts along the tangential direction [100].

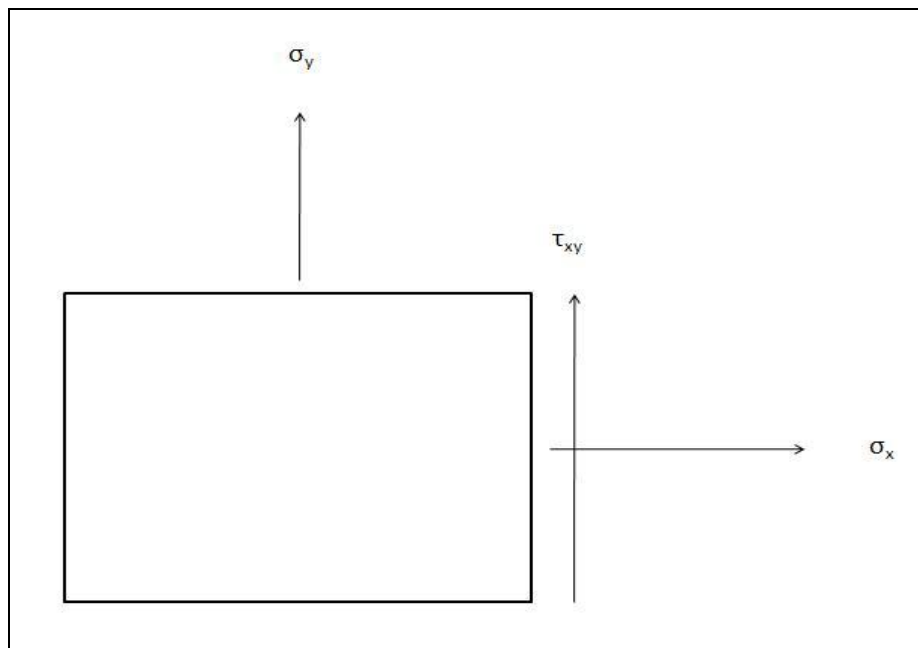


Figure 4-5 Plane state of stress.

The stresses were evaluated during cooling down of the sialon/AISI 430 ferritic stainless steel joint from the fabrication temperature of 1200°C to room temperature. Figure 4-6 illustrates the temperature profile, showing that the ceramic/metal joint achieved room temperature after four hours of cooling. Temperature and time shown in Figure 4-6 are in Kelvin and second respectively.

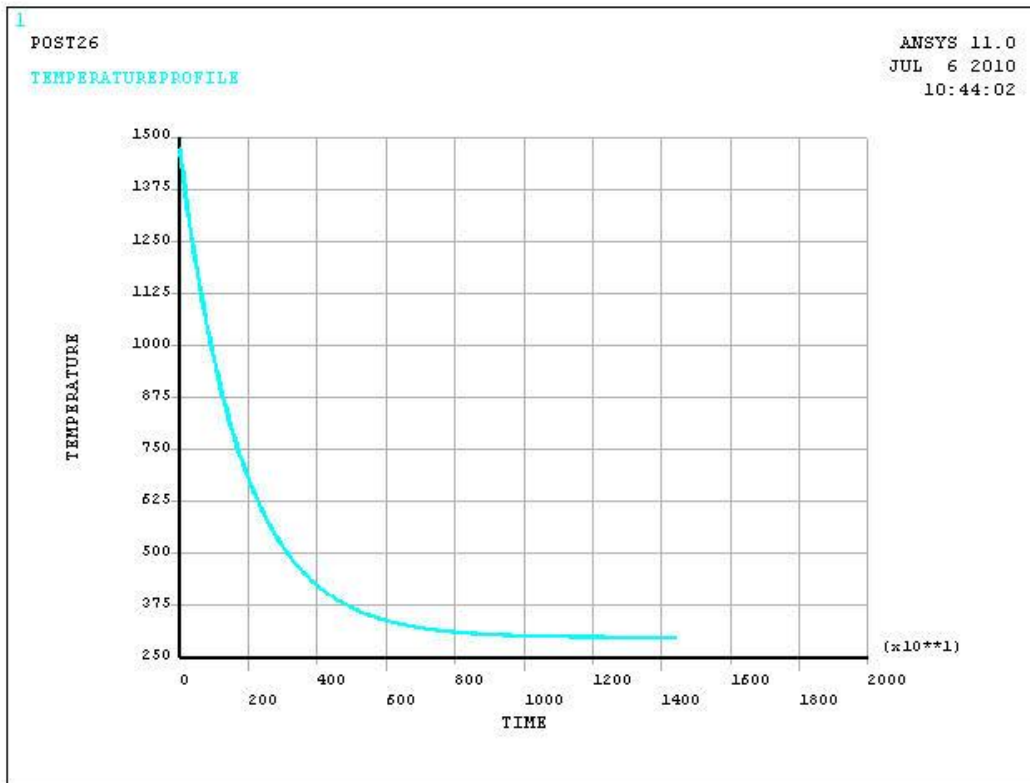


Figure 4-6 Temperature profile of the cooling process

Figure 4-7 shows the von mises stress distribution across the ceramic/metal joint. As can be seen from Figure 4-7, the maximum von Mises stress was found at the expected location which is at the edge of sialon. The maximum tensile stress is equal to 192 MPa. The magnitude of the maximum tensile stress is far more than exceeding the fracture stress of sialon, which is 825 MPa. Thus, it can be concluded that this sialon/AISI 430 ferritic stainless steel with the dimensions as modelled can be obtained without any fracture in the ceramic.

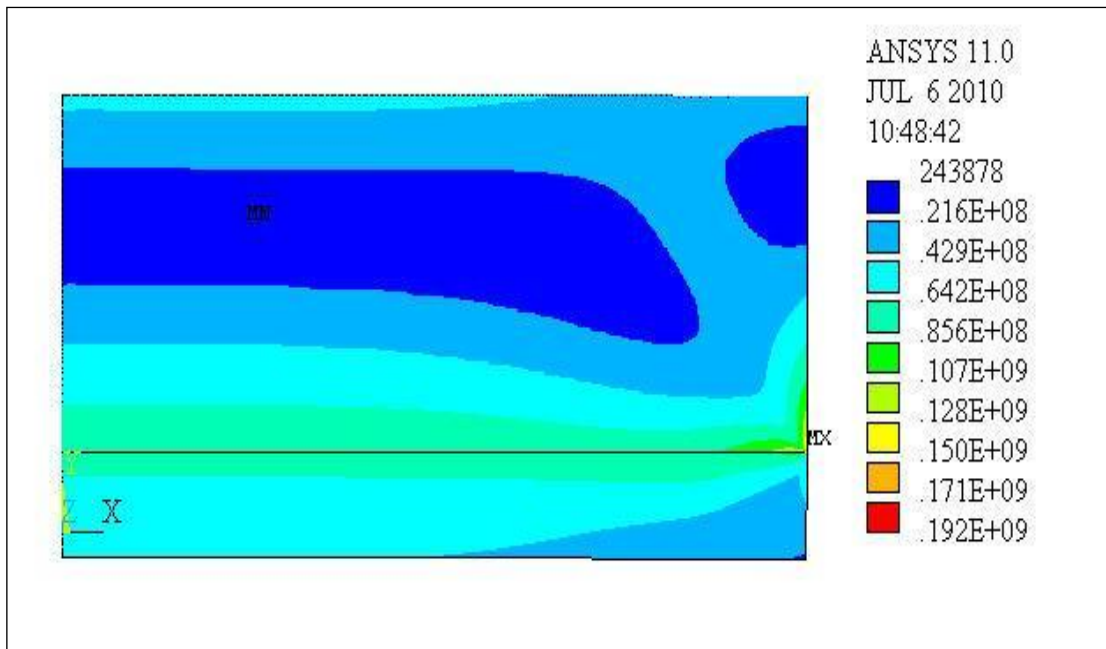


Figure 4-7 Von Mises stress distribution across the sialon/AISI 430 ferritic stainless steel joint.

Fig 4-8 shows the  $\sigma_x$  distribution near the sialon/AISI 430 ferritic stainless steel joint interface. It can be seen that, near the joint interface, sialon experienced compressive stresses while steel experienced tensile stresses. This is due to the thermal expansion mismatch of AISI 430 ferritic stainless steel and sialon. AISI 430 ferritic stainless steel with higher CTE contracted more during cooling of the joint from the joining temperature. However, its contraction was restrained by its bonding to sialon, thus resulting in compressive stresses on the ceramic side. Compressive stress is beneficial for the joint since compressive stress can improve the strength of the joint. Meanwhile, AISI 430 ferritic stainless steel reacted to that tendency, trying to extend the interface, yielding the concentration of tensile stresses, especially near the interface [36].

It can be seen that  $\sigma_x$  in AISI 430 ferritic stainless steel becoming tensile as approaching the joint interface while sialon ceramic on the other hand becoming compressive as moving closer to the interface. The maximum compressive radial stress in the sialon is equal to 90 MPa. The tensile radial stress on the free surface of sialon reaches 50 MPa. The maximum tensile radial stress of 72 MPa occurs in AISI 430 ferritic stainless steel.

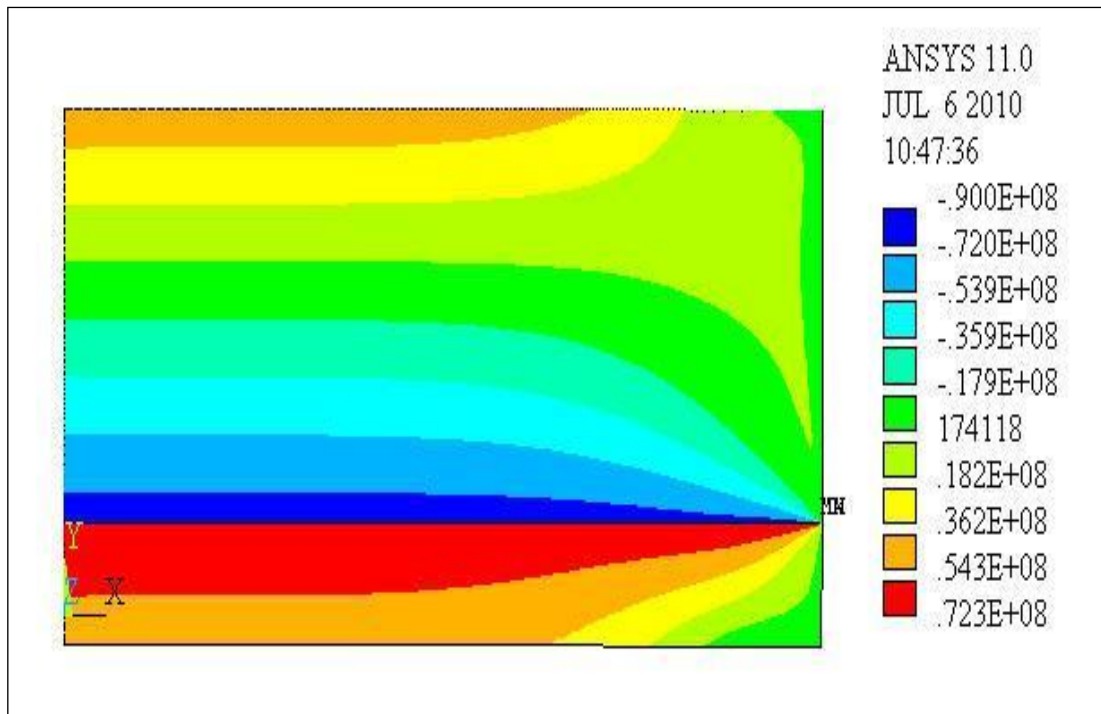


Figure 4-8 Radial stresses distribution across the sialon/AISI 430 ferritic stainless steel joint.

With regards to specimen failure during cooling, the large tensile stresses within the ceramic near the radial free surface appear to be the most significant [13]. This observation is consistent with the  $\sigma_y$  stresses distribution obtained by FEM, as showed in Figure 4-9. Figure 4-10 shows the close up view of the location of the maximum tensile stress. As can be seen from Figure 4-10, the maximum tensile axial stress is located at the free surface of sialon, very near to the joint interface. The location of the maximum tensile axial stress is at the same location found by von Mises stress distribution, claiming that this point bear the highest tensile stress in the joint. This tensile stress causes considerable decrease in the strength of the sialon and is belief to be the crack initiation point if any fracture occurs in the sialon/AISI 430 ferritic stainless steel joint. Hattali et al. [70] had reported that ceramic parts near the interface have high tensile residual stress and are prone to cracking. The cracks initiated at the edge will downgrade the ceramic properties and may even lead to fracture. The compressive stresses shown developed in AISI 430 ferritic stainless steel might be due to the effect of yielding of the steel [70].



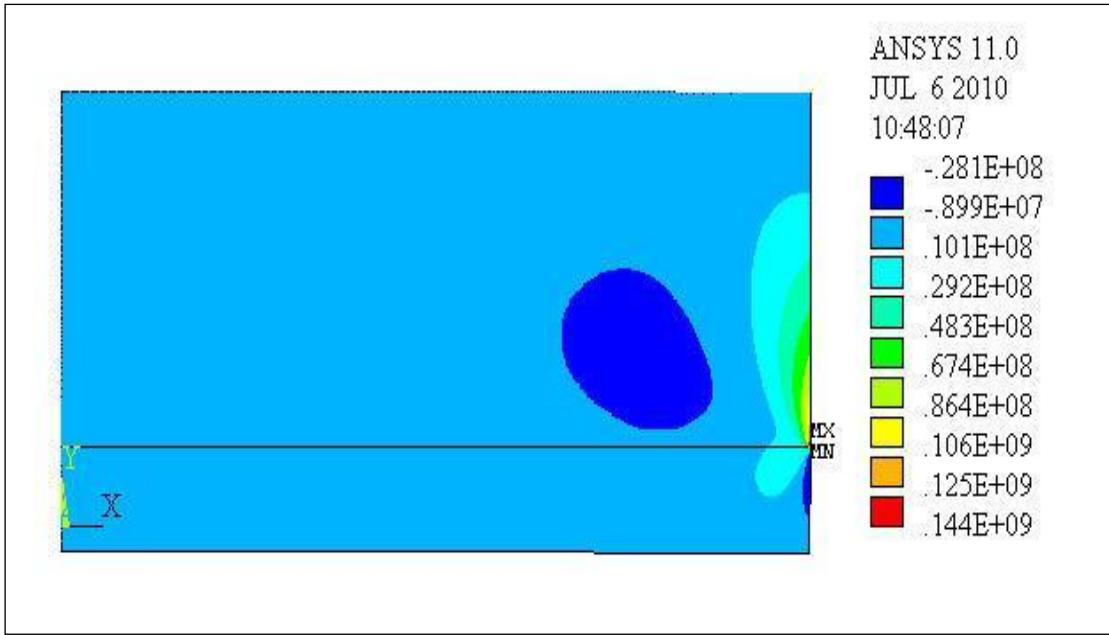


Figure 4-9 Axial stresses distribution across the sialon/AISI 430 ferritic stainless steel joint.

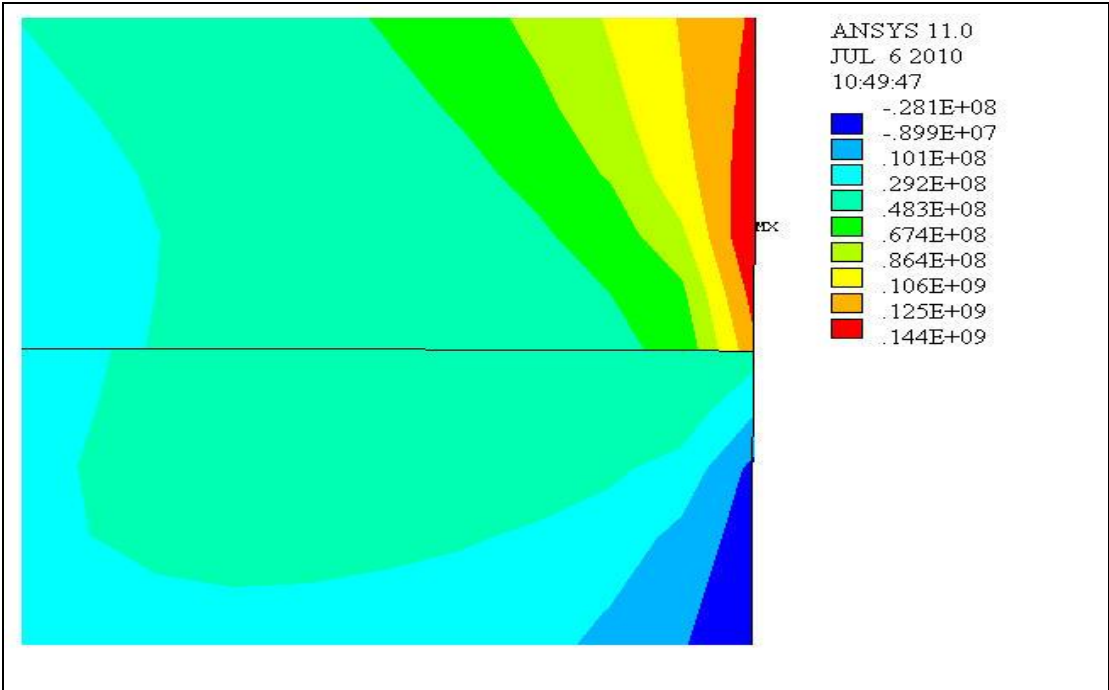


Figure 4-10 Close up view of axial stress distribution, showing the location of maximum tensile stress

It was observed that the amplitude of  $\sigma_y$  vanishes as moving further away from the joint interface and that, near the joint interface,  $\sigma_y$  were tensile in sialon while compressive in steel. The maximum axial stress was of 144 MPa located on the free surface of sialon, around 0.025 mm from the joint interface.  $\sigma_y$  was compressive in nature on the AISI 430 ferritic stainless steel side.

Suganuma [12] had stated that concentration of residual stress becomes severer as closing to the interface. The pattern of  $\tau_{xy}$  distribution for the sialon/AISI 430 ferritic stainless steel joint shows in Figure 4-11 agrees reasonably well with the statement. It can be seen in Figure 4-11 that the  $\tau_{xy}$  distribution concentrated on and near the interface of the joint. Figure 4-12 shows the close up view of the shear stress distribution. It was observed that large tensile shear stress developed around the interface.

The  $\tau_{xy}$  in both sialon and AISI 430 ferritic stainless steel were vanish as moving further away from the interface. The maximum shear stress here reaches 47 MPa, located on the joint interface, around 0.05 mm from the free surface.

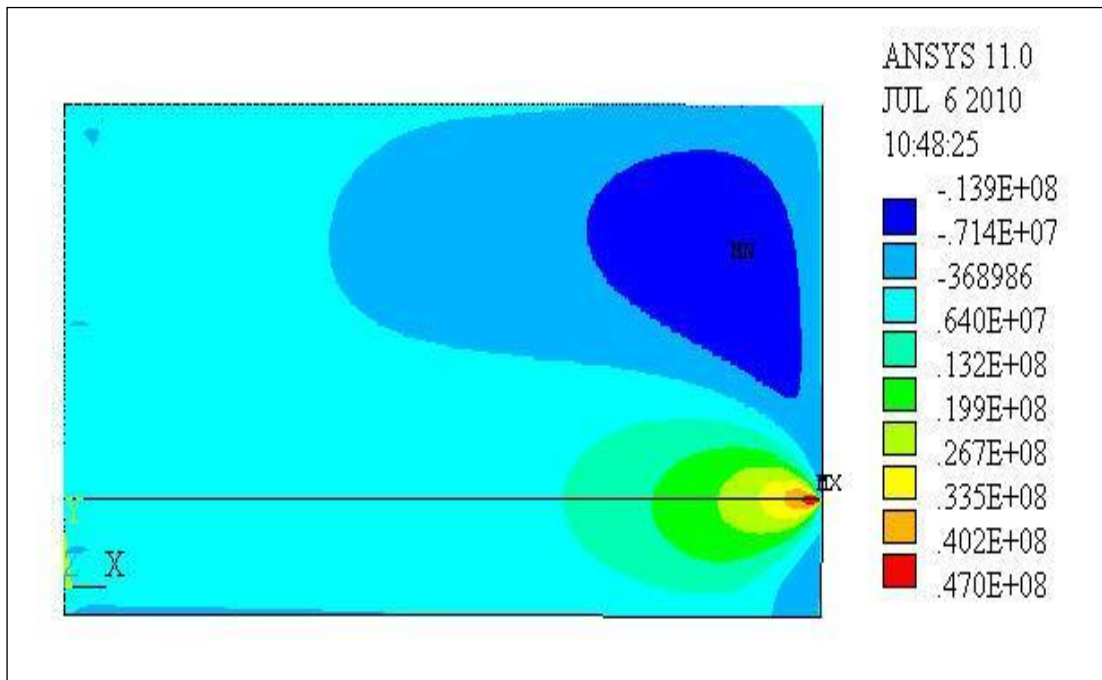


Figure 4-11 Shear stress distribution across the sialon/AISI 430 ferritic stainless steel joint.

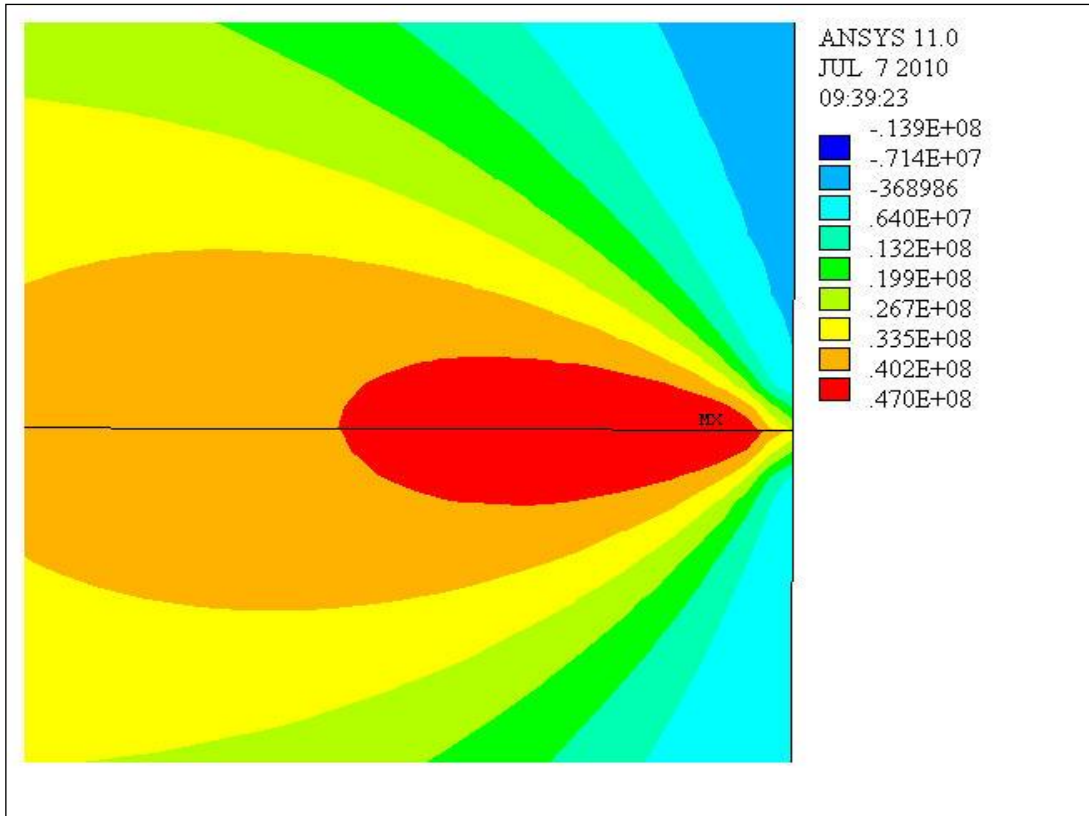


Figure 4-12 Close up view of shear stress distribution.

The shear stresses distribution shown in Figure 4-12, in combination with the maximum tensile  $\sigma_y$  located at the free radial surface of sialon, shown in Figure 4-10, clearly depicted the typical “concave/convex” fracture that occur in the ceramic metal joint when subjected to the application of force, such as the one shown in Figure 2-3.

Figure 4-13 shows the principal stress distribution in the sialon/AISI 430 ferritic stainless steel joint. Note that the pattern of principal stress distribution produced in the sialon/AISI 430 ferritic stainless steel joint are the same as the principal stress distribution in  $\text{Si}_3\text{N}_4$ /steel joint shown by Suganuma et al. [66] in Figure 2-6. It was observed that the magnitudes of residual stresses changes greatly near the edge and free surface of the ceramic/metal joint but flat at the other area, as can be seen from The distributions suggest that the edge and free surface were more vulnerable to fracture or failure.

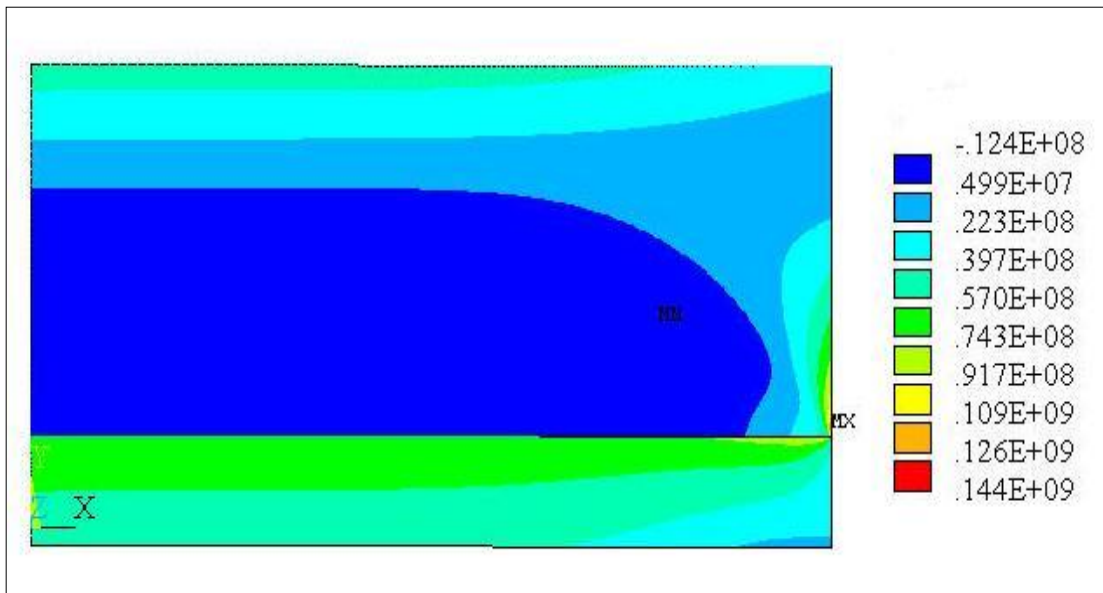


Figure 4-13 Principal stress distribution across the sialon/AISI 430 ferritic stainless steel joint.

#### 4.4 Effect of geometrical parameters

The effect of tensile residual stress in the sialon/AISI 430 ferritic stainless steel joint was clearly understood. The presence of the residual stress may cause fracture in the ceramic/metal joint and make it unsuitable to be adopted in structural application. The need to reduce the magnitude of the residual stress requires the need to understand the effect of each parameter on the stress level.

The goal of this part was to be able to understand the influence of a few factors on the magnitude of residual stress developed in the sialon/AISI 430 ferritic stainless steel joint. There were four factors evaluated, which are; 1) Effect of varying thickness of sialon, 2) Effect of varying diameter of the cylindrical joint, 3) Effect of employing sandwich-like joint design, and 4) The effect of interlayer and their thickness.

#### 4.4.1 Effect of thickness of sialon

The analysis was done by varying the thickness of sialon while fixing the other parameters constant. The ratio of thickness of ceramic to thickness of steel,  $n$ , were varied from 0.8 to 12.5.

Figure 4-14 shows the effect of increasing the thickness of sialon on the maximum tensile  $\sigma_x$ ,  $\sigma_y$  and  $\tau_{xy}$ . It can be seen from Figure 4-14 that increasing the ratio of thickness of sialon to steel will causes  $\sigma_x$  at the free surface of sialon firstly increases and further decreases later.  $\sigma_x$  was found increasing from 41 MPa at  $n$  equals to 0.8 to 54 MPa at  $n$  equals to 2.5. The magnitude was then decreases to nearly zero with additional ratio of thickness of sialon to steel. Mencik [101] reported that the decreases of radial stresses at the high thickness of ceramic probably due to the bending-induced stress relaxation. The bending effect was insignificant for thin ceramic joining due to their very low stiffness [101]. Figure 4-14 provided evident for the statement where  $\sigma_x$  were found higher at the lower thickness of ceramic. The bending effect however was well pronounced as the ratio of thickness of the ceramic to the steel increases. When higher thickness of ceramic was employed, larger bending curvature in the ceramic-metal joint occurs. Hence, the increase of thickness of ceramic results in considerable bending-induced stress relaxation and consequently lower stress in the ceramic [76-78].

On the other hand, different plot was observed for the  $\sigma_y$ . The larger bending curvature were first causes the tensile  $\sigma_y$  at the edge of sialon to increase with increasing ratio of thickness of the ceramic to the steel and remain constant later. As discussed previously, the bending effect was negligilbe at lower joint thickness, thus resulting in increases of stress level with increases thickness of sialon from 100 MPa at  $n$  equals to 0.8 to 149 MPa at  $n$  equals to 7.5. The magnitude of the stress remain constant later with the further increases in ratio of thickness of sialon to steel. The constant magnitude of stress at the higher ration of thickness of sialon to steel might also be due to the bending-induced stress relaxation. This pattern of stress confirms the suggestion of other author [68].

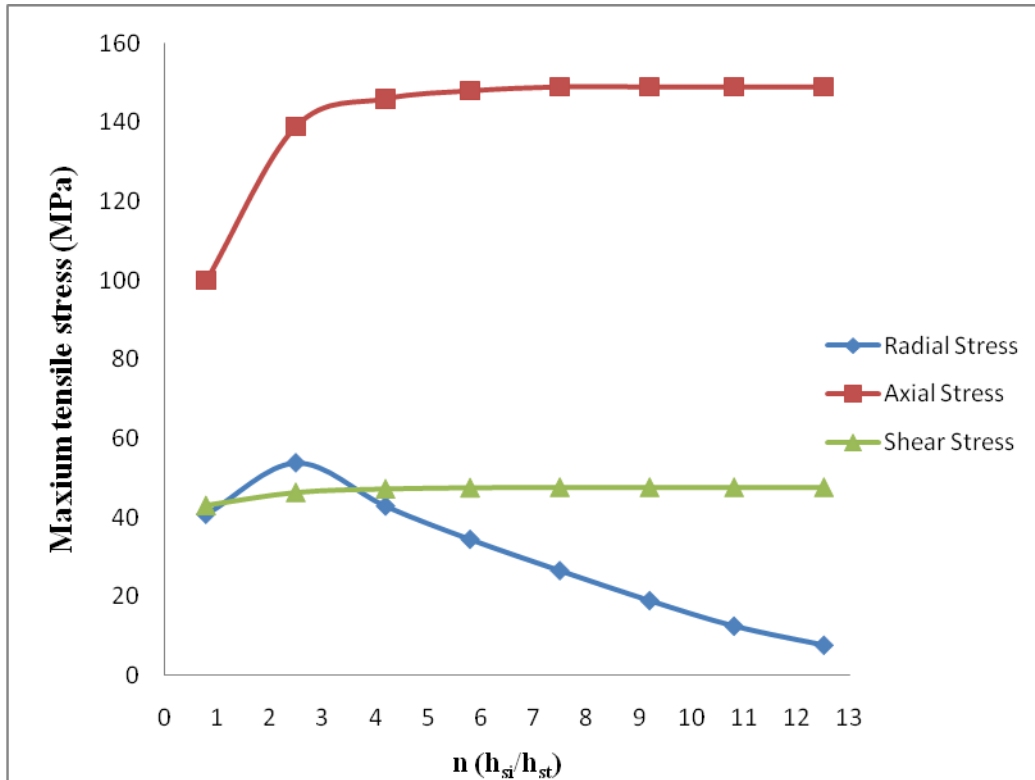


Figure 4-14 Effect of increasing the thickness of sialon on the axial stress level of the ceramic

Although  $\tau_{xy}$  produce the same plot as  $\sigma_y$ , it was not very sensitive to the additional ratio of thickness of sialon to steel. The stress was observed slightly increase from 43.1 MPa at  $n$  equals to 0.8 to 47.7 MPa at  $n$  equals to 7.5 and remain constant later.

Suganuma et al. [68] had investigated the effect of thickness on the joint strength by experimental work. Shear testing performed on silicon nitride/stainless steel diffusion bonded joints with various thickness showed that the joint strength decreased as thickness of the ceramic increased. The result obtained by Suganuma et al. was consistent with the FEM results. As residual stresses was seen increases with thickness of ceramic, the joint with higher thickness of ceramic was more detrimental to fracture and have poor joint strength.

#### 4.4.2 Effect of joint diameter

Figure 4-15 shows the effect of varying diameter of the cylindrical joint. In the analysis,  $R = h/d$  were varied from 0.3 to 2.  $R$  is the ratio of thickness of the seal ( $h = h_{si} + h_{st}$ ) to diameter of the cylindrical joint ( $d$ ).

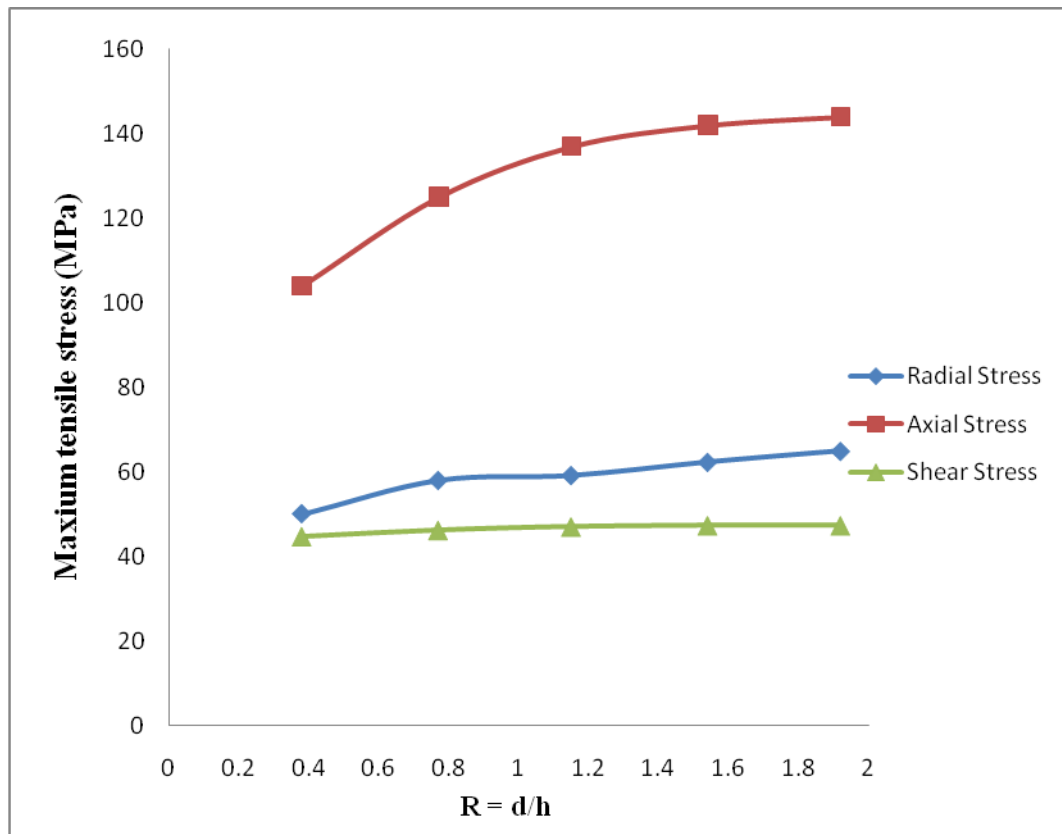


Figure 4-15 Effect of diameter on the stress level in the ceramic.

It can be seen that increases in the diameter of the joint resulted in increases in magnitude of the tensile  $\sigma_x$  and  $\sigma_y$ . On the other hand,  $\tau_{xy}$  were not sensitive with the increasing diameter, i.e. almost no changes observed in their magnitude. The increasing of  $\sigma_x$  and  $\sigma_y$  with increasing diameter might be due to the lesser effect of plastic deformation of metal. Suganuma's et al. [69] had concluded that wider rectangular bond face or increasing diameter for cylindrical joint should produce larger residual stress. It was reported that plastic deformation of the metal is one way of relieving the residual stress. However, this way works very well only for the smaller joint. Thus, larger joint size will accommodate higher residual stress.

### 4.4.3 Effect of joint design

Figure 4-16 shows the effect of joint design. Two designs were considered i.e., asymmetrical and symmetrical joints. Asymmetrical joint consist of sialon directly joined to AISI 430 ferritic stainless steel while symmetrical joint consist of steel sandwiched between two sialons i.e., sialon-AISI 430 ferritic stainless steel-sialon. The ratio of thickness of ceramic to thickness of steel,  $n$ , were varied from 1 to 10.

It can be seen from Figure 4-16 that stresses in asymmetrical joint are higher than the symmetrical joint. The increasing of stress magnitude at the lower  $n$  of asymmetrical joint explained that the bending effect is negligible for thin ceramic joining, as discussed earlier. However, the bending effect is significant as the  $n$  increasing, and inducing reduction in magnitude of the stresses in the ceramic-metal joint. This reduction of stresses can be seen from  $n$  equal to 3 for asymmetrical joint.

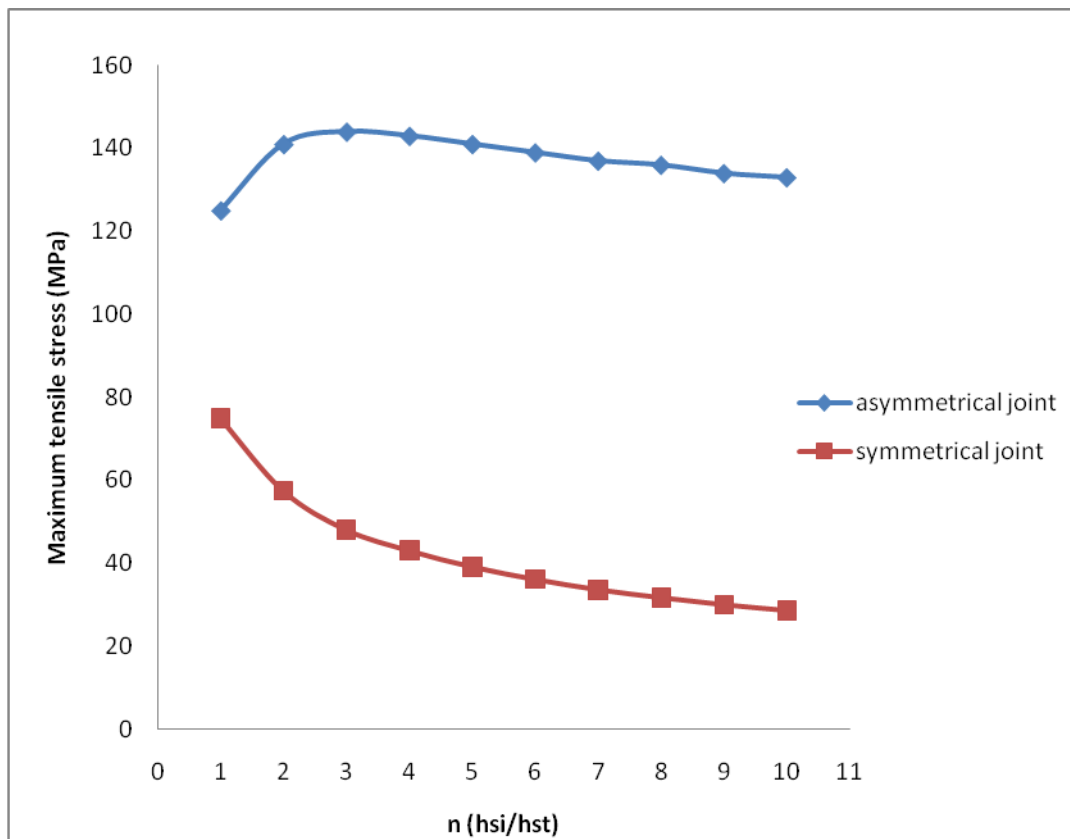


Figure 4-16 Effect of joint design on the magnitude of maximum tensile stress developed in the sialon/AISI 430 ferritic stainless steel joint.



As shown in Figure 4-16, stress in asymmetrical joint are higher than the symmetrical joint for all ratio. Thus, it can be concluded that employing the symmetrical joint can reduce the magnitude of the stresses. The results are in agreement with the suggestion of other authors [40],[104],[105],[93].

The increase in joint reliability when the sandwich-like joint is considered probably due to the bending movement of the metal is eliminated and that the stresses are distributed equally between the two ceramic faces [40]. Schwartz [40] reported that the deformation of metal reduced when symmetrical joint design employed. The reduction of deformation was because the shrinkage of the steel during cooling of the joint was restrained from both sides by the hard sialons, thus reducing the stress level produced in the joint.

The stresses distribution for symmetrical joint can be seen from Figure 4-17 to Figure 4-19. The stress distributions shown are for the  $n$  equal to 3, where thickness of ceramic is equal to 4 mm and thickness of steel is equal to 1.3 mm. It can be seen that the residual stresses distributed symmetrically in the sandwich-like joint. These results are consistent with the suggestion of Abed et al [94].

Stresses were found distributed symmetrically in each type of stresses and most of the sialons region experienced compressive or lower tensile stresses distribution while steel on the other hand experienced tensile stress. As compared to the asymmetrical joint, the radial stresses distributed more uniformly in the symmetrical joint design.

Figure 4-17 shows the distribution of radial stress in the sialon/AISI 430 ferritic stainless steel, symmetrically joint. The maximum tensile stress of found in the sialon was only around 7.06 MPa. The maximum compressive stress experienced was of about 81 MPa. As in asymmetrical joint, the metal also experienced tensile radial stress in this symmetrical joint. The magnitude of the tensile stress in the steel was found increasing from 72.3 MPa to 117 MPa. Tensile stress in steel however was not of a big problem since the stress can be consumed by plastic deformation and the fact that metal is tougher than the ceramic.

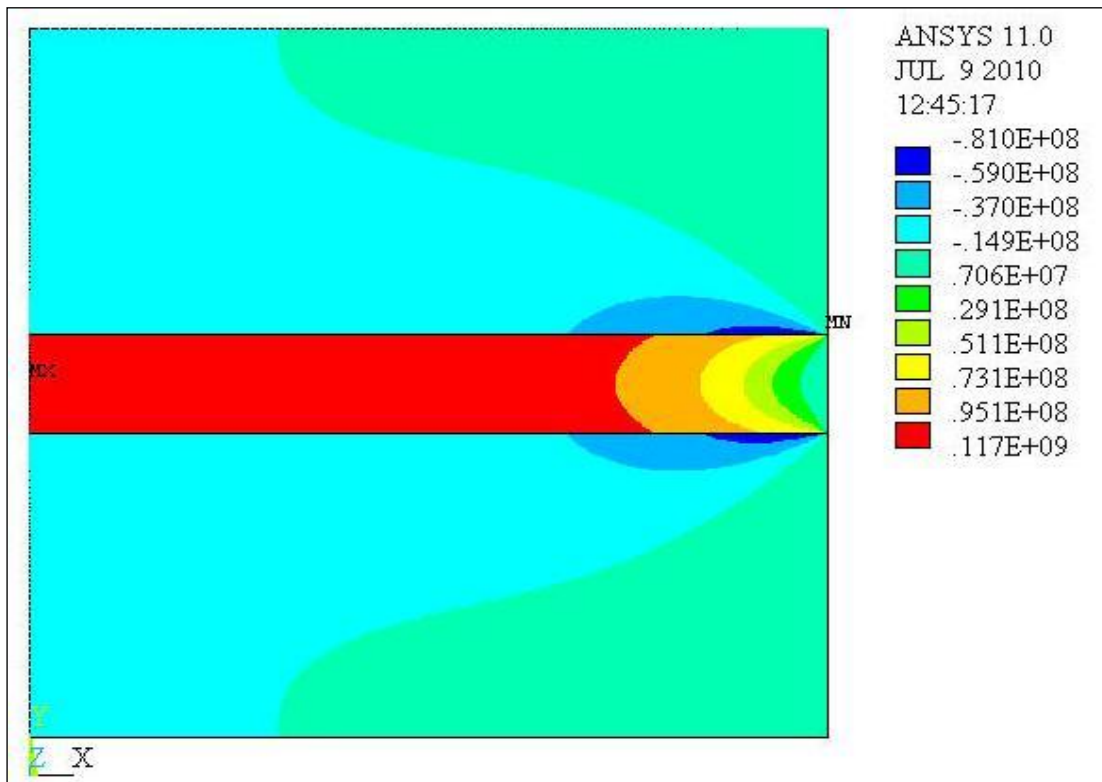


Figure 4-17 Radial stress distribution in symmetrical joint

Figure 4-18 shows the distribution of axial stress in the ceramic/metal symmetrically joint. The maximum tensile stress was reduced from 144 MPa in the asymmetrical joint shown in Figure 4-9 to 48 MPa when symmetrical joint adopted. The location of the maximum tensile stress remains the same. It can be seen that the magnitude of the stress in the symmetrical joint were flat across the joint but changes drastically to maximum at the joint edge. The result was consistent with the suggestion of Shen et al [95]. Furthermore, it was proven that the magnitude of maximum tensile stress in the symmetrical joint was lower than the asymmetrical joint by almost 70% reduction.

Figure 4-19 shows the shear stress distribution in the sandwiched joint. Similar to axial stress, distribution of shear stress also concentrated at the joint edge, very near to the interface. Uniform stress distribution was observed at the other area. The maximum shear residual stresses at the two sialon/AISI 430 ferritic stainless steel interfaces are nearly equal in magnitude but with reverse directions. So when external shear force is applied on the joint, the fracture easily occurs on the interface [95].

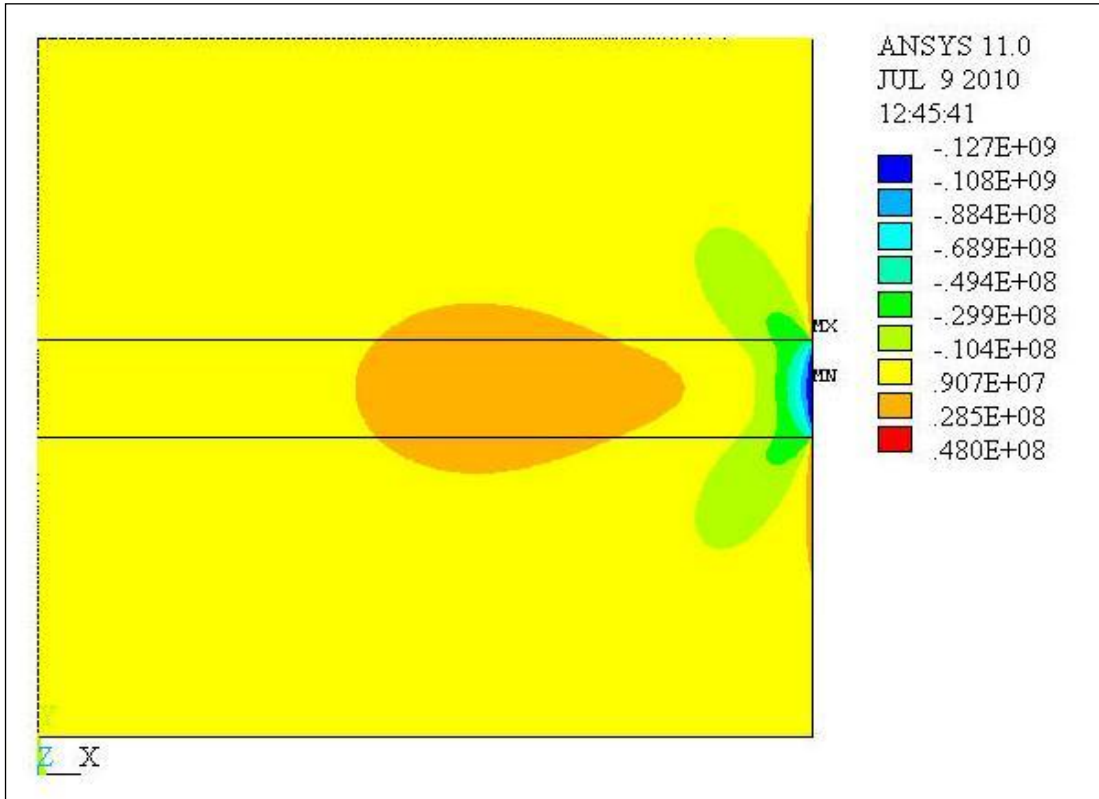


Figure 4-18 Axial stress distribution in symmetrical joint

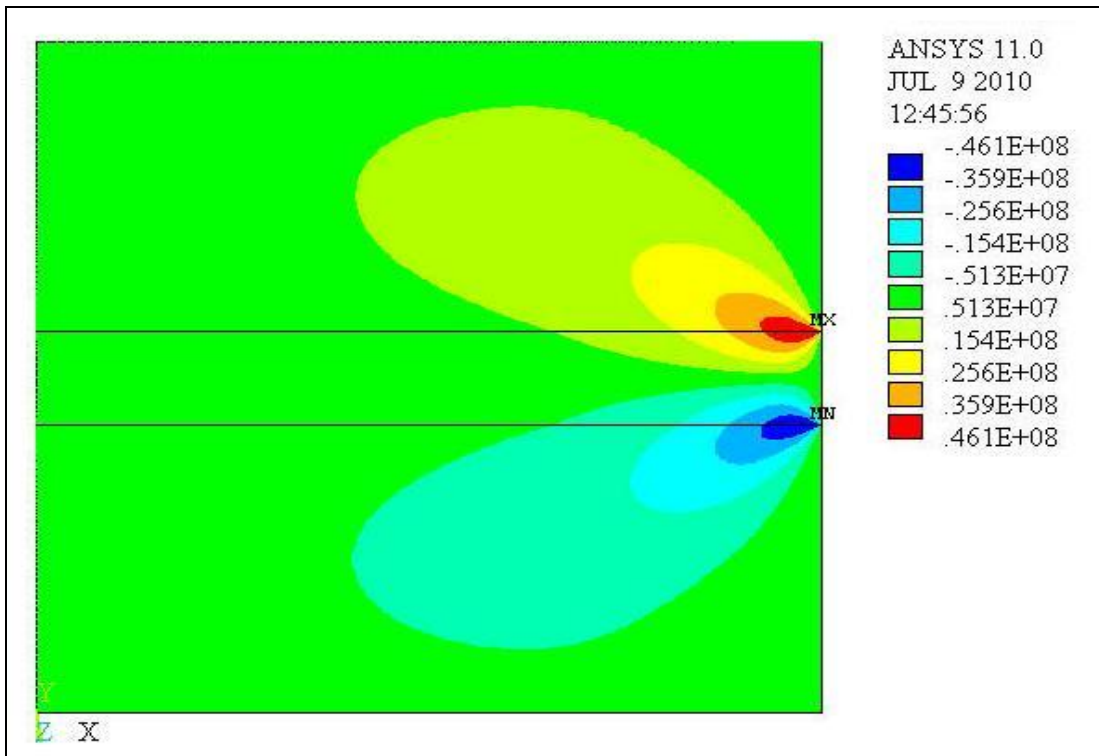


Figure 4-19 Shear stress distribution in symmetrical joint

#### 4.4.4 Effect of interlayer

It has been long established that incorporating interlayers will reduce the tensile residual stress in the ceramic/metal joint. In this section, the effect of interlayers and their thickness were examined. The interlayers evaluated are Cu, Ti, Ni, and Mo. The data used in the analysis were shown in Table 3-1. The thickness of each interlayer was varied from 0.5 to 1.0 mm. Since the analysis was conducted as steady-state instead of transient analysis, the magnitude of stress are higher.

Figure 4-20 shows the effect of incorporating interlayer in the ceramic/metal joint. Based on the plot seen in Figure 4-20, it can be concluded that interlayer with lower yield strength is more effective in reducing the stress level. Cu with the lowest yield strength provides the highest stress reduction. This was caused by significant yielding of the Cu interlayer, i.e. the deleterious influence of the large thermal expansivity value for Cu was counteracted by its ability to yield and relax the thermal stresses generated during cooling of the joint [106]. Ti and Ni exhibit almost the same magnitude of thermal stresses since their yield strength value are of about similar. When the highest yield strength material, Mo, was incorporated into the joint, the maximum tensile stress developed in fact exceeded the magnitude of stress produced in sharp interface (no interlayer). This might be due to no significant yielding occur when Mo was utilized and consequently the tensile strength of the ceramic/metal joint should depend totally on the thermal expansivity [106].

Williamson et al. [13] also found that incorporating low yield strength compliant interlayer in between Ni-Al<sub>2</sub>O<sub>3</sub> joint resulted in significant stress reduction. Based on the observation, it can be concluded that the stress level depends primarily on the plasticity of the materials and that thermal expansion coefficient is the secondary. High ductility materials appear to be the most beneficial interlayer since extensive localized plasticity can be accommodated within the interlayer without generating high critical stresses [13].

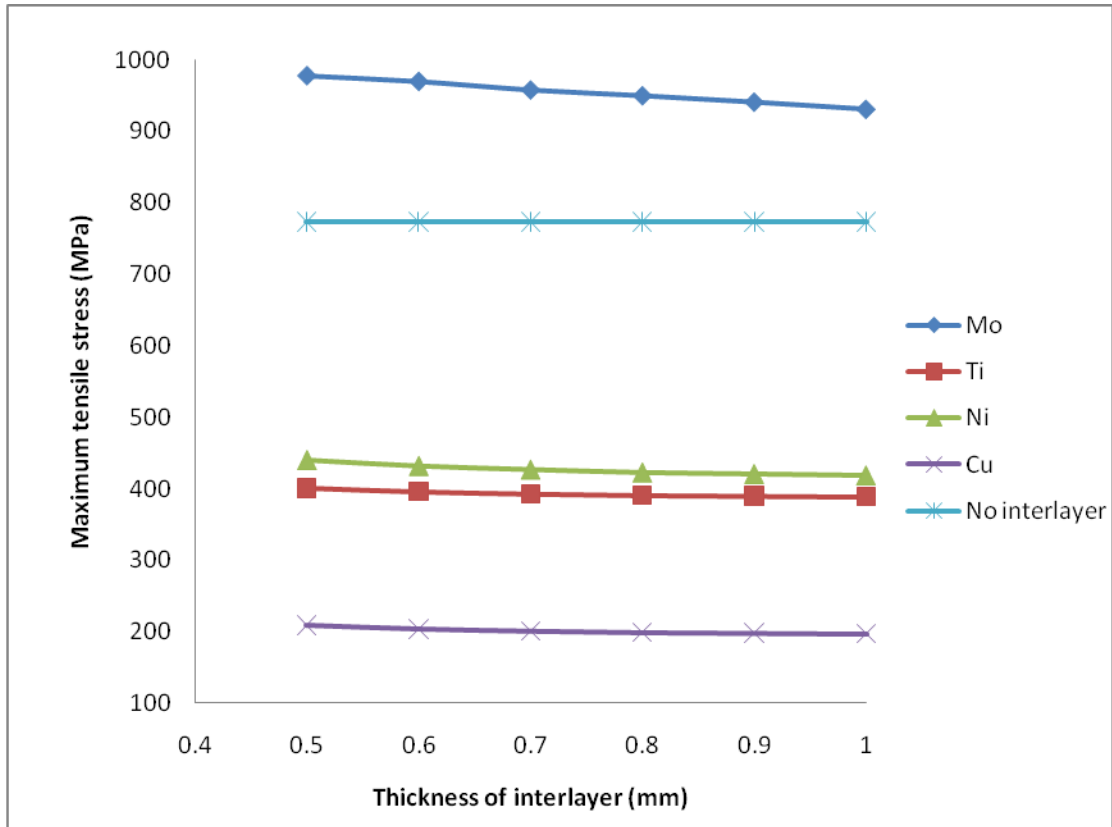


Figure 4-20 Effect of interlayer and their thickness on the maximum tensile stress developed during cooling of the sialon/AISI 430 ferritic stainless steel joint.

Figure 4-20 also shows that the magnitude of the maximum tensile stress decreases with increasing thickness of interlayer for all cases. Zhou et al. [106] indicated that the decreases of residual stresses with increases thickness of the interlayer occurred because the rigid restraint due to the higher yield strength steel substrate inhibited yielding of thin interlayers. When thickness of interlayer increases, the rigid restraint effect decreases and this allows interlayer material to yield and relax the thermal stresses generated during cooling of the ceramic/metal joint. This influence of thickness on the magnitude of stress produced during ceramic/metal joining was further explained by Zhou et al.[106] as follow:

The calculated thermal stresses produced during ceramic/metal bonding depend on whether the resulting thermal stress exceeds the yield point of the interlayer material. For fully elastic conditions, the thermal stress  $\sigma$  is determined by the well known relation:

$$\sigma = \Delta\alpha\Delta T + \frac{E_I E_{II}}{E_I + E_{II}} \quad (4-1)$$

where  $\Delta\alpha$  is the difference in thermal expansion coefficient,  $\Delta T$  is the temperature change and  $E_I$  and  $E_{II}$  are the elastic modulus of the metal and ceramic. When the thermal stress in the metal exceeds its yield strength, the determining equation for thermal stress is

$$\sigma = \sigma_{Iy} + (E_{Ip} \Delta\alpha\Delta T) \quad (4-2)$$

where  $E_{Ip}$  is the linear strain hardening coefficient and  $\sigma_{Iy}$  is the yield strength of the metal. In equation 4-1, the thermal expansivity mismatch term has the dominant effect on the thermal stress level produced during joining. When a low yield strength interlayer such as Cu is used, equation 4-2 indicates that the yield stress of the interlayer plays a dominant role [106].

#### **4.5 Chapter summary**

Findings of the research work were presented in this chapter. The chapter begins with the verification of the FEM model employed in the research work. The magnitude and residual stress distribution across the sialon/AISI 430 ferritic stainless steel joint presented and discussed. It was found that the stress distribution across the joint was in good agreement with previous research work by other author.

The effect of geometrical parameters on the residual stress level was then presented and possible reasons for the findings were addressed. It was observed that changes in any of the parameters will affect the magnitude of stress developed in the ceramic/metal joint.

## CHAPTER 5

### CONCLUSION AND RECOMMENDATIONS

Advanced ceramics are candidate materials for structural applications requiring high degrees of wear and corrosion resistance, often at elevated temperatures. Joints are produced to enhance the performance and applicability of materials. While the joints between similar materials are generally made for manufacturing complex parts and repairing components, those involving dissimilar materials usually are produced to exploit the unique properties of each constituent in the new component [107].

In the present work, sialon ceramic has been diffusion bonded to AISI 430 ferritic stainless steel. However, the most serious problem in successful joining of this dissimilar material is the thermal residual stresses. Thus, the residual stresses that generated in sialon/ AISI 430 ferritic stainless steel joint during cooling down from the fabrication temperature were predicted by the numerical model proposed.

#### **5.1 Chapter Overview**

This chapter summarize the findings of this research by providing overall conclusion of the thesis and suggestion for future research. The objectives of the research, outlined in chapter 1, are reviewed and their achievement addressed.

#### **5.2 Conclusion**

This study was taken with the objectives of evaluating the residual stress distribution in the sialon/AISI 430 ferritic stainless steel joint and the effect of the parameters involved on the residual stress level. Based on the analysis done and discussed, the following conclusions can be deduced;

1. It was found that sialon experienced compressive stresses in radial direction but tensile in axial direction. On the other hand, AISI 430 ferritic stainless steel experienced tensile stress in radial direction but compressive in axial direction. Maximum tensile stress found located on the free radial surface of sialon, close to the joint interface.
2. Increasing thickness of sialon firstly resulted in increasing magnitude of the axial stresses and later remaining constant with further increasing thickness of the ceramic.
3. The magnitude of residual stresses in the joint increases as the diameter of the cylindrical joint increases.
4. Employing symmetrical i.e., sandwich-like joint can reduce the magnitude of the stresses.
5. The use of low yield strength interlayer produced lower residual stress in the sialon/AISI 430 ferritic stainless steel. Cu was found to be the most effective interlayer for the joint due to its yielding which relaxed the residual stress produced. Increases in thickness of interlayer causes further decreases in the residual stress level.

FEM had resulted in a very satisfactory description on magnitude and distribution of stresses in the ceramic/metal joint. Therefore numerical simulation can be used for assessing residual stress in ceramic/metal joint, as a guide in component fabrication and as a framework for predicting the fracture. This method can be used as an alternative for trial and error experimental work as it is more time saving and reducing material consumption.

### **5.3 Recommendations**

It is recommended to make further analysis on the state of stress in the sialon/AISI 430 ferritic stainless steel joint. For further refinement of this numerical analysis, it is



suggested that the creep effects and viscoplastic relief of the metal are taken into consideration. Although the joint survive the cooling stage, their capability to be applied as structural applications is restricted due to the tensile residual stresses in the joint. Thus, more reliable method in reducing the magnitude of the stress should be explored.

Experimental works based on the numerical result can also be done on this sialon/AISI 430 ferritic stainless steel joint. For further stress analysis, X-ray method is recommended since this method is non-destructive. Since the joint strength is strongly related to the thermal residual stress, mechanical testing can be performed on the ceramic/metal joint to find correlation between the strength and residual stress.

Tensile test, bend test and shear test are said to be the most popular method for measuring the mechanical strength of the ceramic/metal joint [12].

#### **5.4 Chapter Summary**

This chapter draws the conclusions and identifies some improvement that could be made for further analysis.

The chapter begins with the summary of the research work and addressing the important findings obtained throughout the analysis. The contribution of this research work to the real life application was then mentioned. Recommendations based on numerical and experimental work was proposed at the end of the chapter.



## REFERENCES

- [1] C.B. Carter and M.G. Norton, *Ceramic materials*, Springer, 2007.
- [2] M.W. Barsoum, *Fundamentals of ceramics*, CRC Press, 2003.
- [3] M. Kurita and K. Yoneda, "Three-dimensional FEM residual stress analysis for ceramic-metal joint plate," *Transactions on Engineering Sciences*, vol. 2, 1993.
- [4] A. Tomsia, "Ceramic/metal joining for structures and materials," *Le Journal de Physique IV*, vol. 03, 1993, p. 10 pages.
- [5] D.W. Richerson, *Modern ceramic engineering*, CRC Press, 2006.
- [6] D. Richerson, *Modern ceramic engineering*, New York, USA: Marcel Dekker, 1992.
- [7] K. Suganuma, "Reliability factors in ceramic/metal joining," *Mater. Res. Soc. Symp. Proc. 314*, 1993, pp. 51-60.
- [8] Y. Katano, M. Ando, T. Itoh, and M. Sasaki, "Application of Ceramics to Turbocharger Rotors for Passenger Cars," *Journal of Engineering for Gas Turbines and Power*, vol. 115, Jan. 1993, pp. 9-16.
- [9] K. Katayama, T. Watanabe, K. Matoba, and N. Katoh, "Development of Nissan High Response Ceramic Turbocharger Rotor."
- [10] K. Matoba, K. Katayama, M. Kawamura, and T. Mizuno, "The Development of Second Generation Ceramic Turbocharger Rotor--Further Improvements in Reliability."

- [11] L. Sheppard, "Advances in automotive ceramics," *Am. Ceram. Soc. Bull.* 69, vol. 6, 1990, pp. 1011-1021.
- [12] K. Sukanuma, "Recent advances in joining technology of ceramics to metals.," *ISIJ International*, vol. 30, 1990, pp. 1046-1058.
- [13] R. Williamson, B. Rabin, and G. Byerly, "FEM study on the effects of interlayers and creep in reducing residual stresses and strains in ceramic-metal joints," *Composite Engineering*, vol. 5, 1995, pp. 851-863.
- [14] P. Charreyron, N. Bylina, and J. Hannoosh, *Fracture mechanics of ceramics*, New York: Plenum Press, 1986.
- [15] R. Kulkarni, K. Chawla, U. Vaidya, and J. Sands, "Thermal stresses in aluminum 6061 and nylon 66 long fiber thermoplastic (LFT) composite joint in a tailcone," *Journal of Materials Science*, vol. 42, 2007, pp. 7389-7396.
- [16] A.E. Martinelli, "Diffusion bonding of silicon carbide and silicone nitride to molybdenum," 1995.
- [17] J. Howe, *Intern. Mater. Rev.* 38, vol. 5, 1993, p. 257.
- [18] S.-B. Lee and J.-H. Kim, "Finite-element analysis and X-ray measurement of the residual stresses of ceramic/metal joints," *Journal of Materials Processing Technology*, vol. 67, May. 1997, pp. 167-172.
- [19] M.M. Schwartz, *Ceramic joining*, Materials Park, Ohio: ASM International, 1990.
- [20] H. Liu, J. Tao, Y. Gautreau, P. Zhang, and J. Xu, "Simulation of thermal stresses in SiC-Al<sub>2</sub>O<sub>3</sub> composite tritium penetration barrier by finite-element analysis," *Materials & Design*, vol. 30, Sep. 2009, pp. 2785-2790.
- [21] W.D. Kingery, H. Bowen, and D. Uhlmann, *Introduction to ceramics*, New York: Wiley, 1976.
- [22] M. Bengisu, *Engineering ceramics*, Springer, 2001.

- [23] R.J. Hussey, B. Hussey, and J. Wilson, *Advanced Technical Ceramics Directory and Databook*, Springer, 1998.
- [24] H. Mandal and D.P. Thompson, "New heat treatment methods for glass removal from silicon nitride and sialon ceramics," *Journal of Materials Science*, vol. 35, Dec. 2000, pp. 6285-6292.
- [25] Y. Oyama and O. Kamigaito, *Jpn. J. Appl. Phys.* 10, 1971, p. 1637.
- [26] K. Jack and W. Wilson, *Nature (London)* 238, 1972, pp. 28-29.
- [27] Y. Oyama, *Jap. J. Appl. Phys.* 11, 1972, pp. 15-72.
- [28] K. Jack, *J. Mater. Sci.* 11, 1976, pp. 1135-1158.
- [29] F. Cardarelli, *Materials Handbook*, Springer, 2008.
- [30] Srinivasan, *Engineering Materials And Metallurgy*, Tata McGraw-Hill, .
- [31] R.E. Smallman and R.J. Bishop, *Modern physical metallurgy and materials engineering*, Butterworth-Heinemann, 1999.
- [32] S. Kalpakjian and S.R. Schmid, *Manufacturing engineering and technology*, Prentice Hall, 2000.
- [33] K. Suganuma, "Joining technology for ceramic/metal composite structure," *Ceramic microstructures*, Springer, 1998.
- [34] U.S. Congress, Office of Technology Assessment, *Strategic materials: technologies to reduce US import vulnerability*, Washington, DC, 1985.
- [35] R.W. Messler, *Joining of materials and structures*, Butterworth-Heinemann, 2004.
- [36] R.M.D. Nascimento, A.E. Martinelli, and A.J.A. Buschinelli, "Review Article: recent advances in metal-ceramic brazing," *Cerâmica*, vol. 49, 2003.
- [37] M. Van der Voorde and M. Nicholas, *J. Am. Cer. Soc. Japan Int. Edit.* 99, 1991, pp. R-2.

- [38] A. Krajewski, "Joining of Si<sub>3</sub>N<sub>4</sub> to wear-resistant steel by direct diffusion bonding," *Journal of Materials Processing Technology*, vol. 54, Oct. 1995, pp. 103-108.
- [39] American Welding Society, *Welding Handbook*, 1978.
- [40] M.M. Schwartz, *Brazing*, Springer, 1995.
- [41] F. Bach, A. Laarmann, and T. Wenz, *Modern surface technology*, Wiley-VCH, 2006.
- [42] G. Elssner and G. Petzow, "Metal/ceramic joining.," *ISIJ International*, vol. 30, 1990, pp. 1011-1032.
- [43] J.X. Zhang, R.S. Chandel, Y.Z. Chen, and H.P. Seow, "Effect of residual stress on the strength of an alumina-steel joint by partial transient liquid phase (PTLP) brazing," *Journal of Materials Processing Technology*, vol. 122, Mar. 2002, pp. 220-225.
- [44] E. Yoshinori and K. Kazuo, "Evaluation of strength characteristics of ceramic/metal joints," *JSME International Journal*, vol. 35 (4), 1992, pp. 489-495.
- [45] A. Kodentsov, M. Rijnders, and F. van Loo, "Chemical Aspects of Metal-Ceramic Interactions," *Materials Science Forum*, vol. 207-209, 1996, pp. 69-78.
- [46] M.F. Ashby and K. Johnson, *Materials and design*, Butterworth-Heinemann, 2002.
- [47] Y. Zhang, D. Feng, Z. He, and X. Chen, "Progress in Joining Ceramics to Metals," *Journal of Iron and Steel Research, International*, vol. 13, Mar. 2006, pp. 1-5.
- [48] B. Stoop and G. Ouden, "Diffusion bonding of silicon nitride to austenitic stainless steel without interlayers," *Metallurgical and Materials Transactions A*, vol. 24, 1993, pp. 1835-1843.

- [49] B. Stoop and G. den Ouden, "Diffusion bonding of silicon nitride to austenitic stainless steel with metallic interlayers," *Metallurgical and Materials Transactions A*, vol. 26, Jan. 1995, pp. 203-208.
- [50] R. Polanco, A. De Pablos, P. Miranzo, and M.I. Osendi, "Metal-ceramic interfaces: joining silicon nitride-stainless steel," *Applied Surface Science*, vol. 238, Nov. 2004, pp. 506-512.
- [51] D. Travessa, M. Ferrante, and G. den Ouden, "Diffusion bonding of aluminium oxide to stainless steel using stress relief interlayers," *Materials Science and Engineering A*, vol. 337, Nov. 2002, pp. 287-296.
- [52] P. Hussain, A. Abdul Rani, A. Zainuddin, and W. Jaafar, "Physical, mechanical and chemical properties of the interaction between nitride and un-nitrided austenitic stainless steel to sialon."
- [53] K. Suganuma, "Interfaces and structural integrity of ceramic/metal joints," *Interfacial science in ceramic joining*, Springer, 1998.
- [54] A.K. Jadoon, B. Ralph, and P.R. Hornsby, "Metal to ceramic joining via a metallic interlayer bonding technique," *Journal of Materials Processing Technology*, vol. 152, Oct. 2004, pp. 257-265.
- [55] A. Foley, "Ceramic metal brazing in engine technology," *Materials for advanced power engineering 1994*, Springer, 1994.
- [56] Ç, G. am, Koç, and M. ak, "Progress in joining of advanced materials," *International Materials Reviews*, vol. 43, 1998, pp. 1-44.
- [57] F. Moret and N. Eustathopoulos, "Ceramic to metal direct brazing," *Le Journal de Physique IV*, vol. 03, 1993, p. 10 pages.
- [58] M. Lu and A.G. Evans, "Influence of Cyclic Tangential Loads on Indentation Fracture," *Journal of the American Ceramic Society*, vol. 68, 1985, pp. 505-510.
- [59] M. Hattali, S. Valette, F. Ropital, N. Mesrati, and D. Treheux, *J. Mater. Sci.* 44,

2009, pp. 3198-3210.

- [60] M. Vila, C. Prieto, P. Miranzo, M.I. Osendi, J.M.D. Río, and J.L. Pérez-Castellanos, "Measurements and Finite-Element Simulations of Residual Stresses Developed in Si<sub>3</sub>N<sub>4</sub>/Ni Diffusion Bonds," *Journal of the American Ceramic Society*, vol. 88, 2005, pp. 2515-2520.
- [61] Z. Zhong, Z. Zhou, and C. Ge, "Brazing of doped graphite to Cu using stress relief interlayers," *Journal of Materials Processing Technology*, vol. 209, Mar. 2009, pp. 2662-2670.
- [62] J. Schijve, *Fatigue of structures and materials*, Springer, 2001.
- [63] R. Nascimento, "Metalização Mecânica de Al<sub>2</sub>O<sub>3</sub> para Brasagem Metal/Cerâmica," in *Portuguese*, Brasil: D. Eng. Thesis, UFSC, 2001.
- [64] H. Kobayashi, Y. Arai, H. Nakamura, and T. Sato, "Strength evaluation of ceramic-metal joints," *Materials Science and Engineering: A*, vol. 143, Sep. 1991, pp. 91-102.
- [65] J.H. Kim and S.B. Lee, "Stress intensity factors and crack initiation directions for ceramic/metal joint," *Theoretical and Applied Fracture Mechanics*, vol. 30, Sep. 1998, pp. 27-38.
- [66] K. Suganuma, T. Okamoto, M. Koizumi, and M. Shimada, *Comm. Am. Ceram. Soc.*, vol. 12, 1985, p. 334.
- [67] A.V. Durov, B.D. Kostjuk, A.V. Shevchenko, and Y.V. Naidich, "Joining of zirconia to metal with Cu-Ga-Ti and Cu-Sn-Pb-Ti fillers," *Materials Science and Engineering: A*, vol. 290, Oct. 2000, pp. 186-189.
- [68] K. Suganuma, T. Okamoto, M. Koizumi, and M. Shimada, "Effect of Thickness on Direct Bonding of Silicon Nitride to Steel," *Journal of the American Ceramic Society*, vol. 68, 1985, pp. C-334-C-335.
- [69] K. Suganuma, T. Okamoto, M. Koizumi, and K. Kamachi, "Influence of shape and size on residual stress in ceramic/metal joining," *Journal of Materials*



*Science*, vol. 22, 1987, pp. 3561-3565.

- [70] M.L. Hattali, S. Terekhina, F. Ropital, N. Mesrati, and D. Tréheux, "Optimization of fabrication parameters of Alumina/Nickel alloy joints for high-temperature application," *IOP Conference Series: Materials Science and Engineering*, vol. 5, 2009, p. 012011.
- [71] J.-W Park, P.F Mendez, and T.W Eagar, "Strain energy distribution in ceramic-to-metal joints," vol. 50, Mar. 2002, pp. 883-899.
- [72] K. Pietrzak, D. Kalinski, and M. Chmielewski, "Interlayer of Al<sub>2</sub>O<sub>3</sub>-Cr functionally graded material for reduction of thermal stresses in alumina-heat resisting steel joints," *Journal of the European Ceramic Society*, vol. 27, 2007, pp. 1281-1286.
- [73] K. Suganuma and T. Okamoto, "Interlayer bonding methods for ceramic/metal systems with thermal expansion mismatches," *Fundamentals of diffusion bonding*, Amsterdam: Elsevier, 1987, p. 71.
- [74] K. Suganuma, T. Okamoto, M. Shimada, and M. Koizumi, *J. Nucl. Mater.*, vol. 133 & 134, 1985, p. 773.
- [75] K. Suganuma, T. Okamoto, and M. Koizumi, *Comm. Am. Ceram. Soc.*, vol. 67, 1984, p. 256.
- [76] A. Kohno, T. Yamada, and K. Yokoi, *J. Jpn. Inst. Met.*, vol. 49, 1985, p. 876.
- [77] X.L. Wang, B.H. Rabin, R.L. Williamson, H.A. Bruck, and T.R. Watkins, "Residual stress distribution in an Al<sub>2</sub>O<sub>3</sub>-Ni bonded with a composite layer," *Proceedings of the 1996 MRS Spring Meeting Apr 8-12 1996*, MRS, San Francisco, CA: 1996, pp. 177-182.
- [78] K. Suganuma, T. Okamoto, M. Koizumi, and M. Shimada, *J. Mater. Sci.*, vol. 22, 1987, p. 1359.
- [79] A. Abed, "Ph.D. Thesis."
- [80] P. Hussain and A. Isnin, "Joining of austenitic stainless steel and ferritic

- stainless steel to sialon,” *Journal of Materials Processing Technology*, vol. 113, Jun. 2001, pp. 222-227.
- [81] C. Lorenzo-Martin, D. Singh, J. Routbort, and G. Chen, “Residual stresses generated during joining of dissimilar alumina-zirconia composites by plastic deformation and its implications on mechanical properties,” *Materials Science and Engineering: A*, vol. 517, Aug. 2009, pp. 78-84.
- [82] A.V. Virkar, J.L. Huang, and R.A. Cutler, “Strengthening of oxide ceramics by transformation-induced stresses.,” *Journal of the American Ceramic Society*, vol. 70, 1987, pp. 164-170.
- [83] D.W. Pepper and J.C. Heinrich, *The finite element method*, Taylor & Francis, 1992.
- [84] J.N. Reddy and D.K. Gartling, *The finite element method in heat transfer and fluid dynamics*, CRC Press, 2001.
- [85] S. Moaveni, *Finite element analysis: theory and application with ANSYS*, Pearson Prentice Hall, 2008.
- [86] J. Holman, *Heat transfer*, New York: McGraw-Hill Inc., 1981.
- [87] ANSYS, *Release 8.0*, Canonsburg: ANSYS Inc., 2002.
- [88] M. Toparli, S. Sahin, E. Ozkaya, and S. Sasaki, “Residual thermal stress analysis in cylindrical steel bars using finite element method and artificial neural networks,” *Computers & Structures*, vol. 80, Sep. 2002, pp. 1763-1770.
- [89] R. Ghafouri-Azar, J. Mostaghimi, and S. Chandra, “Modeling development of residual stresses in thermal spray coatings,” *Computational Materials Science*, vol. 35, Jan. 2006, pp. 13-26.
- [90] G.A. Keramidas and E.C. Ting, “A finite element formulation for thermal stress analysis. Part I: Variational formulation,” *Nuclear Engineering and Design*, vol. 39, Nov. , pp. 267-275.
- [91] M. Sunar, B. Yilbas, and K. Boran, “Thermal and stress analysis of a sheet

- metal in welding,” *Journal of Materials Processing Technology*, vol. 172, Feb. 2006, pp. 123-129.
- [92] R.W. Lewis, K. Morgan, H. Thomas, and K. Seetharamu, *The Finite element method in heat transfer analysis*, John Wiley and Sons, 1996.
- [93] Raevska S., “Reduction of the stresses introduced during the diffusion bonding of dissimilar materials,” *Journal of Materials Processing Technology*, vol. 77, May. 1998, pp. 50-53.
- [94] A. Abed, P. bin Hussain, I.S. Jalham, and A. Hendry, “Joining of sialon ceramics by a stainless steel interlayer,” *Journal of the European Ceramic Society*, vol. 21, Dec. 2001, pp. 2803-2809.
- [95] X. Shen, Y. Li, U. Putschkov, J. Wang, and W. Huang, “Finite-element analysis of residual stresses in Al<sub>2</sub>O<sub>3</sub>-TiC/W18Cr4V diffusion bonded joints,” *Computational Materials Science*, vol. 45, Apr. 2009, pp. 407-410.
- [96] A. Foley and C. Winters, *British Ceram. Proceed*, 1989.
- [97] International Syalons, “Syalon 201 - An advanced silicon nitride ceramic,” [Online]. Available: <http://www.syalons.com/materials/syalon201/>, Apr. 2009.
- [98] efunda, “Stainless steel AISI Type 430,” [Online]. Available: [http://www.efunda.com/materials/alloys/stainless\\_steels](http://www.efunda.com/materials/alloys/stainless_steels), Apr. 2009.
- [99] M. Toparli, F. Sen, O. Culha, and E. Celik, “Thermal stress analysis of HVOF sprayed WC-Co/NiAl multilayer coatings on stainless steel substrate using finite element methods,” *Journal of Materials Processing Technology*, vol. 190, Jul. 2007, pp. 26-32.
- [100] X. Zhang, B. Xu, H. Wang, Y. Jiang, and Y. Wu, “Prediction of three-dimensional residual stresses in the multilayer coating-based systems with cylindrical geometry,” *Composites Science and Technology*, vol. 66, Oct. 2006, pp. 2249-2256.
- [101] J. Mencik, *Mechanics of components with treated or coated surfaces*,

Dordrecht: Kluwer Academic Publishers, 1995.

- [102] J.-. Jeong, S.-. Lee, W.-. Lee, Y.-. Baik, and D. Kwon, "Mechanical analysis for crack-free release of chemical-vapor-deposited diamond wafers," *Diamond and Related Materials*, vol. 11, Aug. 2002, pp. 1597-1605.
- [103] J. Haider, M. Rahman, B. Corcoran, and M. Hashmi, "Simulation of thermal stress in magnetron sputtered thin coating by finite element analysis," *Journal of Materials Processing Technology*, vol. 168, Sep. 2005, pp. 36-41.
- [104] V. Abramov, *Residual stresses and deformations in metals*, Moscow: GNTIML, 1963.
- [105] I. Metelkin, M. Pavlova, and N. Pozdeeva, *Joining ceramics with metals*, Moscow: Metallurgia, 1977.
- [106] Y. Zhou, F.H. Bao, J.L. Ren, and T.H. North, "Interlayer selection and thermal stresses in brazed Si<sub>3</sub>N<sub>4</sub> steel joints," *Materials Science and Technology*, vol. 7, Sep. 1991, pp. 863-868.
- [107] "ASTM C 1469-00: Standard test method for shear strength of joints of advanced ceramics at ambient temperature," *Annual Book of ASTM Standards*, United States: ASTM International, .

## LIST OF PUBLICATIONS

- [1] C.S.Hassan, P..Hussain and M.Awang.

Stress Analysis on Direct Joining of Sialon/AISI 430 Ferritic Stainless Steel  
Joint

*International Conference on Plant Equipment and Reliability, 2010.*

- [2] CS.Hassan, P..Hussain and M.Awang.

Stress Analysis on Direct Joining of Sialon/AISI 430 Ferritic Stainless Steel  
Joint

*Journal of Applied Science.*